

WATER COMBINATION BANDS AND MIXED SYSTEMS
AT THE OIL/WATER INTERFACE

by

REBECCA ALTMAN

A DISSERTATION

Presented to the Department of Chemistry and Biochemistry
and the Division of Graduate Studies of the University of Oregon
in partial fulfillment of the requirements
for the degree of
Doctor of Philosophy

June 2021

DISSERTATION APPROVAL PAGE

Student: Rebecca Altman

Title: Water Combination Bands and Mixed Systems at the Oil/Water Interface

This dissertation has been accepted and approved in partial fulfillment of the requirements for the Doctor of Philosophy degree in the Department of Chemistry and Biochemistry by:

Dr. James Prell	Chairperson
Dr. Geraldine Richmond	Advisor
Dr. Cathy Wong	Core Member
Dr. Ray Weldon	Institutional Representative

and

Andrew Karduna	Interim Vice Provost for Graduate Studies
----------------	---

Original approval signatures are on file with the University of Oregon Division of Graduate Studies.

Degree awarded June 2021

© 2021 Rebecca Altman
This work licensed under a Creative Commons
Attribution-NonCommercial-ShareAlike



DISSERTATION ABSTRACT

Rebecca Altman

Doctor of Philosophy

Department of Chemistry and Biochemistry

June 2021

Title: Water Combination Bands and Mixed Systems at the Oil/Water Interface

Surface chemistry is fundamental to life. The interface between oil and water is a unique environment home to vital chemical phenomena, from reactions occurring at our cell membranes to the functionality of industrial products we consume. Understanding the behavior of molecules at the surface between oil and water is necessary for building upon fundamental aspects of this ubiquitous surface; however, detailed investigations of the molecular level of the oil/water surface are limited due to experimental challenges of probing a buried interface. Vibrational sum frequency (VSF) spectroscopy is non-invasive surface specific nonlinear spectroscopic technique that can probe the population and orientation of molecular vibrations at interfaces. The work presented in these studies utilizes VSF and surface tensiometry methods to investigate two main areas of surface chemistry at the oil/water surface: 1) the presence and implications of weak VSF signal from combination bands of surface water molecules, and 2) intermolecular interactions between charged and nonionic surface adsorbates in polymer-surfactant and co-surfactant mixed systems.

These studies find the spectral presence of both the stretch + libration and bend + libration combination modes of interfacial water molecules are very sensitive to surface charge, as is expected from surface water vibrational responses. Due to the broad nature

of these modes, their presence in the surface water spectrum can have significant effects on the VSF analysis of C-H and C-D vibrational modes from surface adsorbates as their alkyl vibrational modes interfere with the signal from water combination bands. Studies investigating the surface structure of mixed systems containing nonionic polymer and charged surfactants reveal minimal interfacial interactions between charged surfactants with surface-active nonionic polymers; however, surface-inactive nonionic polymers, such as polyacrylamide, are synergistically drawn to the surface through charge-dipole interactions with charged surfactants. Studies investigating co-surfactant mixtures of nonionic Span-80 with anionic surfactants indicate competitive adsorption between the two surfactant species, as Span-80's attraction to the oil phase is stronger than any intermolecular interactions occurring between Span-80 and the anionic surfactants.

This dissertation includes both published and unpublished co-authored material.

CURRICULUM VITAE

NAME OF AUTHOR: Rebecca Altman

GRADUATE AND UNDERGRADUATE SCHOOLS ATTENDED:

University of Oregon, Eugene OR
California Polytechnic State University, San Luis Obispo CA

DEGREES AWARDED:

Doctor of Philosophy, 2021, University of Oregon
Bachelor of Science, Chemistry, 2016, California Polytechnic State University

AREAS OF SPECIAL INTEREST:

Chemistry Education
Surface Chemistry
Physical Chemistry

PROFESSIONAL EXPERIENCE:

Graduate Research Assistant, Department of Chemistry and Biochemistry,
University of Oregon, 2016-2021

Chemistry Instructor, Linn Benton Community College, 2021

Graduate Teaching Fellow, Department of Chemistry and Biochemistry,
University of Oregon, 2016-2017

Learning Assistant, Department of Chemistry and Biochemistry, California
Polytechnic State University, San Luis Obispo, 2014-2016

GRANTS, AWARDS, AND HONORS:

Graduate Teaching Award, Chemistry, University of Oregon, 2017

Outstanding Learning Assistant Award, California Polytechnic State University,
San Luis Obispo, 2016

Chemistry Faculty Scholarship, California Polytechnic State University, San Luis
Obispo, 2014

Frost Fellowship, Summer Research, California Polytechnic State University, San
Luis Obispo, 2014

Outstanding First Year Chemistry/Biochemistry Student Award California
Polytechnic State University, San Luis Obispo, 2013

PUBLICATIONS:

“Twist and stretch: Assignment and surface charge sensitivity of a water combination band and its implications for vibrational sum frequency spectra interpretations”, **R.M. Altman** and G.L. Richmond, *J. Phys. Chem. B Under Second Review*

“Coming to Order: Adsorption and Structure of Nonionic Polymer at the Oil/Water Interface as Influence by Cationic and Anionic Surfactants”, **R.M. Altman** and G.L. Richmond, *Langmuir* **2020** 36 (8) 1975-1984

“How Low Can You Go? Molecular Details of Low-Charge Nanoemulsion Surfaces”, A.P. Carpenter, **R.M. Altman**, E. Tran, and G.L. Richmond, *J. Phys. Chem. B* **2020** 124 (20), 4234-4245

“The Formation and Surface Stabilizing Contributions to Bare Nanoemulsions Created with Negligible Surface Charge”, A.P. Carpenter, E. Tran, **R.M. Altman**, and G.L. Richmond, *PNAS* **2019** 116 (19), 9214-9219.

“Come Together: Molecular Details into the Synergistic Effects of Polymer–Surfactant Adsorption at the Oil/Water Interface”, B.K. Schabes, **R.M. Altman**, and G.L. Richmond, *J. Phys. Chem. B* **2018** 122 (36), 8582-8590

ACKNOWLEDGMENTS

As I sit down to acknowledge all those who have made this accomplishment possible, I am deeply humbled. The past several years have held some of the greatest and some of the truly most challenging moments. It is all of you I have to thank for being my joy in the ups and my anchor through the downs. As I leave graduate school, it is not the degree I cherish, but the fact that this pursuit brought me closer to each of you.

I owe every step of this journey to my family. Mom and Dad, you are the reason I made it through. Mom, thank you for your hours of listening to my heart and for your profound care. I owe so much of my emotional and mental health to you. Dad, thank you for your example of gentleness and leadership, and for dropping everything to spontaneously take me snow shoeing and backpacking when I was at my utter wit's end. Ruth, I don't deserve how fiercely you love me. Brad, your deeply steadfast care and support have never failed to comfort me. Timmy, you are my heart- thank you for crying and laughing with me. And the deepest of thank you's to my grandparents, to whom I owe so much of my education. Grandpa, thank you for always being interested in what I'm studying... even when I don't talk about it. I've always immensely appreciated it.

To my Oregon family, thank you. You have made these past years joyful. To that cherished community group who took me under their wing when I was freshly moved to Oregon: you gave me roots. Thank you. To Megan, Emilie, and JJ- your beautiful hearts challenge and encourage me, I forever treasure and love you. Heidi and Taylor- you have been my lifeline. From our Wednesday morning pancakes to Tuesday night sush sesh, thank you for carrying me through with your gentleness. Andrew, I'm so thankful I didn't have to make it through this without you. Thank you for your gentle heart, for pushing

me to grow, and for being more excited about my own accomplishments than I allow myself to be. You helped me finish strong. And to a few more- Troxell, for your generosity and friendship. Becca, for the bike rides and solace in deep contemplations. Hope, for feeding me. All my other Valhalla Villa roomies, for reminding me there's more to life than graduate school. Elena, for your consistent friendship. The Lane 5 community and Megan for being my accountability and encouragement in physical health. Don and Laurie, for your immense generosity in housing and feeding me. Emilie, Dan, William, and Baby Roufs, for making me a part of your home. I love you all. You have made it difficult to ever leave Eugene.

And to my University of Oregon community- you are some of the best of the scientific community. Geri, I am very thankful to have had you as an advisor. Thank you for always supporting me, especially during this difficult last year. And thank you for always doing your best to make our lab a family. Priscilla, thank you for all your advice, friendly conversation, and everything else you do that us graduate students never recognize. Brandon, your advice and friendship guided me into becoming a successful graduate student, thank you. Andrew, your willingness to always chat regarding theory and experiments have been crucial to my progression as a scientist. Emma, thank you for your empathetic heart and your camaraderie through all the ups and downs. And to Evan, Konnor, Marc, and Ashley, who helped me survive being a graduate student in 2020.

I thank the University of Oregon and the U.S. Department of Energy for financially supporting this work.

For Dad, Mom, Ruth, Brad, and Timmy,
this would not have been possible without your continual love and support.

And for all my students,
you are the reason I started and the reason I finished.

TABLE OF CONTENTS

Chapter	Page
I. INTRODUCTION.....	1
II. BACKGROUND AND EXPERIMENTAL METHODS.....	4
Vibrational Sum Frequency Theory	4
Laser System and Experimental Setup	7
Spectral Fitting Procedure	9
Sample Preparation.....	10
Pendant Drop Surface Tensiometry.....	11
III. WATER COMBINATION BANDS AT THE OIL/WATER INTERFACE.....	13
The Water Stretch + Libration Combination Band	13
A) The neat water spectrum at the oil/water interface.....	14
B) Isotopic dilution studies of the water spectrum at the oil/water interface in the presence of surface charge.....	21
C) Combination band frequency shift upon surface charge	26
D) Implications for studying the C-H stretching region with VSF	28
The Water Bend + Libration Combination Band	31
A) Experimental considerations for detecting VSF signal in the C-D stretching region at the oil/water interface	33
B) Charge-dependence of the water bend + libration combination mode.....	34
C) C-D stretching VSF response in the water bend + libration region	35
IV. MIXED SYSTEMS AT THE OIL/WATER INTERFACE.....	39
Nonionic Polymer + Surfactant Systems.....	40
A) Nonionic polymers alone at the oil/water surface	40

Chapter	Page
B) Surface-active nonionic polymers with charged surfactants	44
C) Nonionic polymer PAM + charged surfactants	54
Nonionic Surfactant + Charged Surfactant Mixed Systems	67
A) Nonionic Span-80 surfactant with anionic SDS	69
B) Nonionic Span-80 surfactant with anionic AOT	77
V. CONCLUSIONS	88
APPENDICES	91
A. FIT PARAMETERS FOR SPECTRA OF WATER STRETCH + LIBRATION COMBINATION BAND SYSTEMS	91
B. FIT PARAMETERS FOR SPECTRA OF POLYACRYLAMIDE- SURFACTANT SYSTEMS	99
C. FIT PARAMETERS FOR SPECTRA OF SPAN-80 CO-SURFACTANT SYSTEMS	104
REFERENCES CITED	106

LIST OF FIGURES

Figure	Page
2.1 Depiction of VSF experimental set up	6
2.2 Schematic of laser system.	8
3.1 VSF spectra of neat H ₂ O/oil and D ₂ O/oil interface	14
3.2 VSF spectrum of neat H ₂ O/CCl ₄ surface with and without normalization of the calculated Fresnel factors	18
3.3 Isotopic dilution VSF spectra at the CCl ₄ /water neat surface	19
3.4 Isotopic dilution VSF spectra at the CCl ₄ /water surface with SDS and DTAB	22
3.5 VSF spectra with H ₂ O and D ₂ O blue of the free OH(D) in the presence of d-SDS and d-SDS + NaCl	25
3.6 VSF spectra of the CCl ₄ /D ₂ O interface with no surfactant and d-SDS	28
3.7 VSF spectra in the C-H region of Span-80 with d-SDS and with d-DTAB.....	30
3.8 IR transmittance spectrum through a CCl ₄ layer of ~3 mm thickness	33
3.9 VSF spectra of the H ₂ O bend + libration combination mode in the presence of h-SDS and h-DTAB	35
3.10 VSF spectra of d-SDS and d-DTAB in H ₂ O at the oil/water interface	36
3.11 VSF spectra of d-DTAB in D ₂ O and H ₂ O	37
4.1 VSF spectra of PVA at the CCl ₄ /D ₂ O interface	41
4.2 VSF spectra of PEG at the CCl ₄ /D ₂ O interface	42
4.3 VSF spectra of PVA at the CCl ₄ /H ₂ O interface in the H ₂ O vibrational region.....	43
4.4 VSF spectra of PAM at the CCl ₄ /D ₂ O interface.....	44
4.5 Chemical structures for DTAB and SDS.....	45

Figure	Page
4.6 VSF spectra of PVA at the CCl ₄ /D ₂ O interface with d-SDS and d-DTAB.....	46
4.7 VSF spectra of 0.015 mM PEG at the CCl ₄ /D ₂ O interface with d-SDS and d-DTAB	47
4.8 VSF spectra in PPP polarizations of PEG at the CCl ₄ /D ₂ O interface with d-SDS and d-DTAB	49
4.9 VSF spectra of 0.15 mM PEG at the CCl ₄ /D ₂ O interface with d-SDS and d-DTAB	50
4.10 VSF spectra of F127 at the CCl ₄ /D ₂ O interface with d-SDS	52
4.11 Chemical structures for SDS, DTAB, and CTAB.....	54
4.12 Surface pressure of PAM with DTAB, DTAB, and SDS.....	55
4.13 VSF spectrum of d-SDS at the CCl ₄ /D ₂ O interface with PAM.....	56
4.14 VSF spectrum of d-SDS at the CCl ₄ /D ₂ O interface in the carbonyl stretching region with PAM	58
4.15 VSF spectrum of d-SDS with NaCl at the CCl ₄ /D ₂ O interface with no polymer and with PAM	59
4.16 VSF spectrum of d-DTAB at the CCl ₄ /D ₂ O with PAM.....	60
4.17 VSF spectrum of d-DTAB at the CCl ₄ /D ₂ O with PAM in the carbonyl stretching region	62
4.18 A depiction of the structure of interfacial PAM with cationic surfactant	62
4.19 Electrostatic potential map of an acrylamide monomer	63
4.20 Time-dependent surface pressure and VSF spectra of PAM with DTAB at the oil/water interface	64
4.21 VSF spectra at the CCl ₄ /D ₂ O surface of d-CTAB with PAM.....	65
4.22 A depiction of the oil/water interface of PAM when alone and in mixed systems	66
4.23 Chemical structures of SDS, AOT, and Span-80	68

Figure	Page
4.24 VSF spectra of 0.025 mM Span-80 at 1 hour and 24 hours	69
4.25 VSF spectra of 0.025 mM Span-80 with d-SDS at 1 hour and 24 hours	72
4.26 VSF spectra and surface pressure for Span-80, SDS, and the mixed system.....	74
4.27 VSF spectra for three different preparation procedures of d-SDS with Span-80.....	76
4.28 VSF spectra of d-AOT with Span-80 with H ₂ O and D ₂ O	78
4.29 VSF spectra of d-AOT at the CCl ₄ /D ₂ O surface at 1 hour and 24 hours	79
4.30 VSF spectra in the carbonyl stretching region of d-AOT at the CCl ₄ /D ₂ O surface.....	81
4.31 VSF spectra of 0.1 mM Span-80 at 1 hour and 24 hours	82
4.32 VSF spectra in the carbonyl stretching region of Span-80 at the CCl ₄ /D ₂ O surface.....	83
4.33 VSF spectra of Span-80 with d-AOT at 1 hour and 24 hours	84
4.34 VSF spectra in the carbonyl stretching region of Span-80 with d-AOT	86

LIST OF TABLES

Table	Page
3.1 Mole fractions for the various H ₂ O:D ₂ O isotopic dilution ratios	19
4.1 Comparison of S.P. values and fit intensities at different polymer concentrations for mixed systems	63

CHAPTER I:

INTRODUCTION

Surfaces are essential to life. While many important events occur in bulk media—birds fly through air, fish swim in water—the point where those bulk phases meet creates a unique environment home to irreplaceable and life-changing phenomena. The health of our global environment is reliant on chemical reactions at the surface of atmospheric aerosols. The successful functioning of each cell in our bodies is determined by interactions occurring at its membrane surface. Advances in technology that make our lives so much easier (and more difficult) are built upon foundational surface properties of various materials. Whether we realize it or not, we interact with surface science every day, from the air we breathe to the products we buy.

Water is a crucial component to many of these interfaces. Its simplistic structure, yet intricate behavior is an essential driving force to countless surface processes.¹⁻⁶ Experimentally probing various vibrations of water molecules can provide insight into intermolecular interactions between molecules located at surfaces, which determine the overall properties and function of the surface. Specifically, the properties of the oil/water interface are vitally dependent on the behavior of surface water molecules, which impact the efficacy of numerous applications occurring at the interface between oil and water, such as oil spill dispersant remediation, pharmaceutical drug delivery systems, and the functionalization of polymer films.^{4, 7-11} The presence of additional surface-active molecules such as surfactants and polymers can alter the functionality of the interface as they interact with surface water molecules, providing desirable molecular structures and properties at the oil/water surface.

However, the surface of water can be extremely difficult to experimentally probe, especially at these buried interfaces. Some studies have opted to observe the behavior of molecules in bulk phases to then infer what may be happening at the surface, while other studies use computational methods to virtually simulate what is likely occurring at these difficult-to-observe interfaces.¹²⁻¹⁵ Several experimental methods such as surface tensiometry, ellipsometry, and neutron and x-ray scattering allow the detection of

properties of surfaces themselves, each with their own limitations.^{12, 16-17} However, the collective work of the scientific community to culminate the findings of studies utilizing all these methods can provide a detailed picture of the mysterious and notoriously complex world of surface science.

The studies presented in this work utilize surface tensiometry and vibrational sum frequency (VSF) spectroscopy experimental techniques to probe molecular systems at the oil/water interface. VSF spectroscopy is a surface-specific, non-invasive nonlinear spectroscopic experimental technique that provides information regarding the population and orientation of vibrational dipoles at an interface.¹⁸ The interfacial studies given here of the oil/water interface provide novel insight into two main areas of its surface chemistry: 1) fundamentally understanding the source of weak resonant responses in the surface water spectrum due to combination bands, and 2) probing intermolecular interactions between charged and nonionic surface adsorbates. Using VSF spectroscopy to observe the behavior of water molecules at the oil/water interface provides a crucial foundational understanding of the surface water vibrational spectrum and how it is altered by various surface adsorbates. Probing the molecular structure of surface adsorbates themselves provides insight into complex interactions between interfacial molecules in mixed systems at the oil/water surface. Specifically, molecular interactions between charged and uncharged surface species at the oil/water interface are determined in these studies through detailed analysis of the adsorbates' vibrational response in VSF spectra and surface pressure measurements of the mixed systems, providing fundamental insight into their roles in the industrial and environmental applications in which they are used.

Chapters II outlines the necessary background information and sum frequency generation theory for understanding the purpose and analysis of the studies included in this work. Chapter III investigates the fundamental behavior of specific vibrational responses from interfacial water molecules not yet reported at the oil/water interface, namely the stretch + libration combination mode and the bend + libration combination mode, also known as the "association band". The chapter also investigates significant implications of these water combination band responses for the analysis of VSF spectra. Chapter III contains material currently under second review for publication, with Dr. Geraldine Richmond as the principal investigator for the work. Chapter IV applies the

knowledge gained from the analysis of the surface water combination bands to investigate various mixed systems of nonionic and charged surface adsorbates at the oil/water interface. This chapter begins by investigating several mixed systems of nonionic polymers with charged surfactants and analyzes various intermolecular interactions responsible for the collective interfacial behavior of molecules in these mixed solutions. The chapter then focuses on co-surfactant mixed systems containing both nonionic and anionic surfactant species and investigates their possible competitive adsorption at the oil/water surface. Chapter IV contains published work with Dr. Geraldine Richmond as the principal investigator, as well as work that will be published with co-authors Evan Christoffersen and Konnor Jones who built upon the preliminary findings reported here of competitive adsorption between nonionic and anionic surfactants, with Dr. Geraldine Richmond as the principal investigator. Chapter V provides a conclusion of the studies presented in this work and summarizes their overall implications for the surface science community.

CHAPTER II:

BACKGROUND AND EXPERIMENTAL METHODS

Vibrational Sum Frequency Theory:

Spectroscopy probes interactions between light and matter. Vibrational spectroscopies can probe various molecular vibrations as molecules absorb photons of light with frequencies matching that of the molecular vibrations, usually in the infrared (IR) wavelength region. Commonly used linear IR spectroscopy methods can probe these molecular vibrations by detecting the transmission of a beam of photons through a sample of interest as the photon wavelengths vary. However, to spectroscopically detect molecular vibrations present at an interface instead of in bulk media, nonlinear spectroscopy techniques are required.

Vibrational sum frequency generation (VSF) is a second-order nonlinear process that probes molecular vibrations at an interface. Detailed descriptions of the theory behind VSF generation are described elsewhere, however a brief overview is provided here.¹⁸⁻²¹ To understand the origin of a VSF response, it is helpful to begin with a mathematical description of how molecules respond to incoming electric fields. The electron cloud of each molecule determines its response to the electric field of incident photons. As the incoming electric field interacts with the electrons surrounding the molecule, the molecule experiences an induced electric dipole response, given by

$$\boldsymbol{\mu} = \boldsymbol{\mu}_0 + \alpha \boldsymbol{E} \quad (1)$$

where $\boldsymbol{\mu}_0$ is the molecule's permanent dipole, α is its polarizability, and \boldsymbol{E} is the vector quantity describing the electric field. On a larger scale, when an aggregate of molecules experiences an incoming oscillating electric field, their collective response is given by the change in polarization, or dipole per unit of volume,

$$\boldsymbol{P} = \epsilon_0 \chi^{(1)} \boldsymbol{E} \quad (2)$$

where $\chi^{(1)}$ is the susceptibility describing the macroscopic average of all individual molecular polarizabilities (α). Equation 2 describes the linear first-order polarization response, however, if the magnitude of the incoming light's electric field increases, this response begins to include nonlinear contributions, as in equation 3,

$$\mathbf{P} = \varepsilon_0\chi^{(1)}\mathbf{E} + \varepsilon_0\chi^{(2)}\mathbf{E}^2 + \varepsilon_0\chi^{(3)}\mathbf{E}^3 + \dots \quad (3)$$

where $\chi^{(2)}$, $\chi^{(3)}$, etc. are the nonlinear second-, third-, and higher order susceptibilities. The corresponding nonlinearity of each individual molecule's response to the incoming field described by equation 4,

$$\boldsymbol{\mu} = \mu_0 + \alpha\mathbf{E} + \beta\mathbf{E}^2 + \gamma\mathbf{E}^3 + \dots \quad (4)$$

where β , γ , and likewise higher order variables in equation 4 are the nonlinear molecular hyperpolarizabilities.

Second-order nonlinear optical effects such as sum frequency generation are not allowed in centrosymmetric environments. An extended discussion of the origin of this selection rule is described elsewhere, although a brief discussion follows here.¹⁸⁻¹⁹ Because all directions are equivalent in a centrosymmetric environment, the second-order susceptibility tensor remains unchanged when there is a reversal of the axis, described mathematically as

$$\chi_{ijk}^{(2)} = \chi_{-i-j-k}^{(2)} \quad (5)$$

However, fundamental rules of tensors require the sign of the $\chi^{(2)}$ tensor to reverse upon this inversion in the axis directionalities, as

$$\chi_{ijk}^{(2)} = -\chi_{-i-j-k}^{(2)} \quad (6)$$

The only condition under which both equations 5 and 6 are satisfied is when the $\chi^{(2)}$ tensor for the centrosymmetric environment is equal to zero, indicating the molecular vibrations present in bulk media do not produce any VSF response. Interfaces, however, are inherently non-centrosymmetric, causing certain $\chi_{ijk}^{(2)}$ tensor elements to remain non-zero under symmetry and tensor rule considerations.¹⁸⁻¹⁹ This allows molecular vibrations present at an interface to be detected by VSF when other conditions, such as the ones described below, are met.

With this surface-specificity of VSF established, the second-order polarization response of molecules probed by VSF spectroscopy is thus described mathematically as in equation 7.

$$\mathbf{P}^{(2)} = \varepsilon_0\chi^{(2)}\mathbf{E}^2 \quad (7)$$

To experimentally produce a VSF response from molecules at a surface, a fixed visible and a tunable IR beam are overlapped in both space and time at an interface. These

pulsed lasers allow the detection of the second-order response of interfacial molecules (as depicted in Figure 2.1), causing the expression for the second-order polarization of a VSF process to be more accurately described by

$$\mathbf{P}^{(2)} = \varepsilon_0 \chi^{(2)} \mathbf{E}_{IR} \mathbf{E}_{vis} \quad (8)$$

The second-order nonlinear susceptibility, $\chi^{(2)}$, is the macroscopic average of the response of interfacial molecules undergoing a vibrational excitation,

$$\chi^{(2)} = \frac{N}{\varepsilon_0} \langle \beta \rangle \quad (9)$$

where N is the number of molecular vibrations being probed that are present at the surface and β is the second-order hyperpolarizability tensor describing the vibrational response of each individual molecule present (as seen in equation 4). The $\chi^{(2)}$ term is dependent on the average of the molecular hyperpolarizability tensors being probed, indicated by the brackets around the β term in equation 9. Thus, if the average orientation of a particular molecular vibration causes a net cancellation of the vibrational dipoles described in the β tensor being probed, no VSF signal will be detected even when the molecules are present at the surface. The dependence of $\chi^{(2)}$ on the number of molecular vibrations present at the interface, N , and the average of the molecular hyperpolarizabilities, $\langle \beta \rangle$, as shown in Equation 9 reveals the sensitivity of VSF signal to both the population and average orientation of molecular vibrations at the surface.

When the incident tunable IR beam reaches a wavelength resonant with a vibrational mode of a molecule present at the non-centrosymmetric environment of an

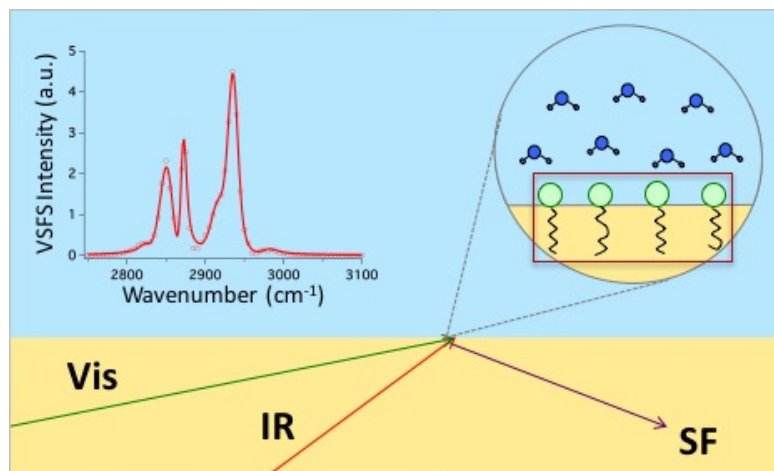


Figure 2.1: Depiction of a VSF experimental set up, where the aqueous phase is shown in blue and the oil phase is shown in yellow. To produce VSF spectra, the vis and tunable IR pulsed beams are overlapped in space and time at the interface to probe the $\chi^{(2)}$ response of interfacial molecules.

interface, the resulting VSF signal intensity is enhanced. This signal enhancement is also directly proportional to the intensity of both the incident IR and visible beams, as shown in equation 10.

$$I_{SF} \propto I_{IR} I_{vis} |\chi^{(2)}|^2 \quad (10)$$

The value of each molecular β response contributing to the macroscopic $\chi^{(2)}$ response is dependent upon both the Raman and IR transition moments of the vibrational mode.^{18-19, 21-22} Because the average of the molecular hyperpolarizabilities (β) of the interfacial molecules gives rise to the $\chi^{(2)}$ VSF response, β 's dependence on the IR and Raman transition moments reveal the VSF selection rule requiring a molecule's vibrational modes to be both IR and Raman active to produce VSF signal.

As VSF is known to be sensitive to the average orientation of vibrational dipoles, altering the polarization of the incoming IR and visible beams can probe the components of a molecule's vibrational dipole present in different orientations relative to the surface. A polarization scheme of SSP (sum frequency, visible, and IR beam polarizations, respectively) probes net vibrational dipoles perpendicular to the surface, whereas a polarization scheme of SPS probes those parallel to the surface. A polarization scheme of PPP probes vibrational dipoles with a net orientation either parallel or perpendicular to the surface.¹⁸ Other polarizations schemes, such as PSP, have been shown to selectively probe the vibrational response of chiral structures (either molecularly or macroscopically) at the surface.²³⁻²⁵ The studies described in this work utilize polarization combinations of SSP, SPS, PPP, and PSP to investigate the interfacial structure of surface molecules.

Laser System and Experimental Setup:

The visible and infrared beams needed to produce VSF signal are generated by an Ekspla SFG spectrometer with 30 ± 3 ps pulses at a repetition rate of 50 Hz. To generate the laser pulses, a master oscillator uses a photodiode through a gain medium to produce a beam mode-locked by a saturable absorber. This beam undergoes two amplification processes, both using Nd:YAG gain mediums, causing the wavelength of the amplified beam to be 1064 nm. The seed pulse then passes an array of optics that split the pulse into three beams: one remaining at 1064 nm, and the other two frequency-doubled by second harmonic generation (SHG) through KDP nonlinear crystals to produce 532 nm beams.

One of these 532 nm beams is directed to the interface and is used as the visible beam when producing VSF signal at the interface in the sample cell. The second 532 nm beam passes through an OPG and OPA, which includes nonlinear crystals and a diffraction grating that selectively tune the idler beam pulse. This pulse, combined with the remaining 1064 nm beam, undergoes difference frequency generation (DFG) in a silver gallium sulfide (AgGaS₂) crystal to produce the tunable infrared pulse (2 - 10 μm) incident to the interface sample, where it is overlapped with the 532 nm visible pulse in both space and time. As the VSF signal is produced from these overlapped beams at an interface of interest, a series of optics selectively filters out the unwanted wavelengths and polarizations of light, leading the sum-frequency signal beam to a monochromator and photomultiplier tube detector, where the VSF signal at each wavelength is recorded to produce a spectrum with a resolution of $\pm 3 \text{ cm}^{-1}$. A schematic of this experimental laser setup is shown in Figure 2.2.

The standard sum frequency cell setup used in these studies utilizes a bottom-up geometry where both the visible and tunable IR beams pass through a calcium fluoride window and ~3.5 cm of a carbontetrachloride (CCl₄) oil phase before reaching the CCl₄/water interface while overlapped in both space and time. The beam angles at the point of the interface allow for total internal reflection, which produces the maximum enhancement of sum frequency generation at the surface. Specifically, the 532 nm visible beam has an incident angle of 68 degrees with an average energy of ~4 μJ per pulse. The tunable IR beam has an incident angle of 76 degrees with an average energy of ~60 μJ

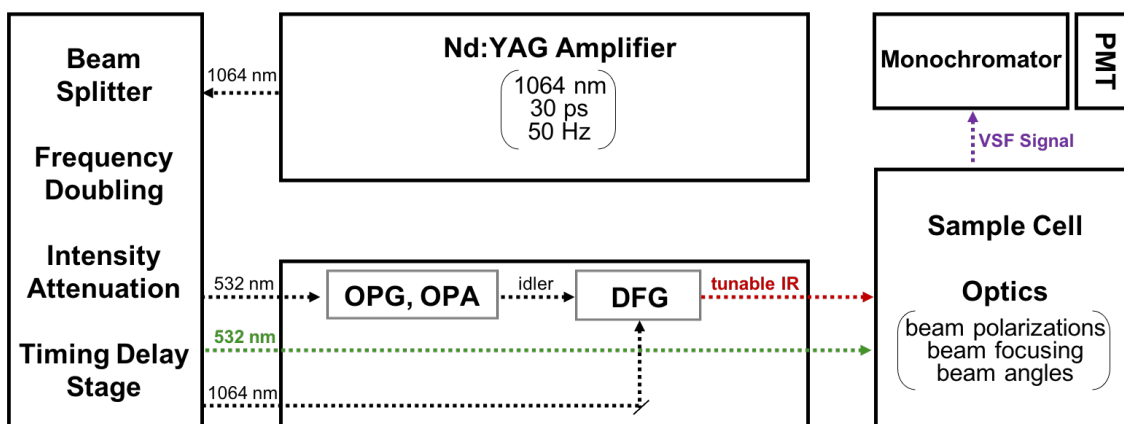


Figure 2.2: A schematic of the laser system used in these studies. Our setup includes an Nd:YAG gain medium to amplify a 1064 nm beam, which is split and frequency doubled before undergoing difference frequency generation (DFG) to produce the tunable IR beam incident on the interface.

per pulse in the wavelength region of 2800 – 3100 cm⁻¹. The energy of the tunable IR beam varies slightly depending on the chosen wavelength, and as such, all spectra presented here are normalized. To account for these any wavelength-dependent changes, as well as any IR absorption through bulk media, the VSF spectra are normalized to the nonresonant signal produced by a gold mirror suspended in CCl₄ at each corresponding wavelength in the spectral range of interest.²⁶ All spectra reported here are an average of at least three different spectra taken on separate days, each with an averaged 550 shots per point.

Spectral Fitting Procedure:

Because VSF spectroscopy is a nonlinear process, the vibrational modes probed at the surface and detected in the resulting spectrum can mix with each other to produce constructive and destructive interferences. Such mixing can occur between both resonant and nonresonant responses at the surface. Thus, it is important to mathematically fit the resulting VSF spectra to be able to quantitatively comment on specific spectral features. Fits to spectra in the studies presented here follow previous Richmond publications²⁷ where the procedure described by Bain et al²² fits line shapes to a convolution of a Gaussian and Lorentzian distribution (Equation 11), taking into account the homogenous broadening (Γ_L) caused by the nature of the vibrational transition as well as the inhomogenous broadening (Γ_v) caused by the molecular environment of the detected vibrational modes. Each peak is fit to five parameters: amplitude (A_v), phase (φ_v), Lorentzian linewidth (Γ_L), frequency (ω_v), and Gaussian linewidth (Γ_v).

$$|\chi^{(2)}(\omega_{SF})|^2 = \left| \chi_{NR}^{(2)} e^{i\varphi_{NR}} + \sum_v \int_{-\infty}^{\infty} \frac{A_v e^{i\varphi_v} e^{-[(\omega_L - \omega_v)/\Gamma_v]^2}}{\omega_L - \omega_{IR} - i\Gamma_L} d\omega_L \right|^2 \quad (11)$$

A series of spectra can be globally fit, where certain parameters known to remain constant between systems are fit simultaneously to each spectrum in the series. Mathematical fits to spectra included in this study were either individually or globally fit, the details and parameters of which can be found in the corresponding Appendices.

Sample Preparation:

The oil/water interface investigated by VSF spectroscopy and surface tensiometry in these studies utilized carbon tetrachloride (CCl_4) as the oil phase due to its transmission of the IR beam in the wavelength regions of interest. The CCl_4 was purchased from Sigma Aldrich (HPLC grade, 99.9%) and was twice distilled before use. The H_2O used in these studies was filtered to ultrapurity with a resistance of $18.2 \text{ M}\Omega \cdot \text{cm}$. The D_2O aqueous solvent used in these studies was purchased from Cambridge Isotope Laboratories, Inc. at 99.9% deuteration and was used as received. D_2O was used as the aqueous solvent in many of the VSF studies presented here to shift the water vibrational modes out of the region of alkyl vibrational modes ($2800\text{-}3000 \text{ cm}^{-1}$), so C-H stretches of interfacial surfactants and polymers could be observed. The specifications for each chemical used in the studies presented here follows.

Polyacrylamide (PAM) ($M_n = 40,000$) containing no amount of hydrolysis, poly(ethylene glycol) (PEG, $M_n = 4,600$), and poly(vinyl alcohol) (PVA, $M_n = 89,000\text{-}98,000$) with 99% hydrolysis were purchased from Sigma Aldrich. Pluronic F127, a block co-polymer with polyethylene oxide and polypropylene oxide monomers, was purchased from Thermo Fisher Scientific. The cationic surfactants dodecyltrimethylammonium bromide (DTAB) and cetrimonium bromide (CTAB) used in these studies were purchased from Acros Organics the highest purity possible (99+%). Their fully deuterated analogues ($\text{d}_{34}\text{-DTAB}$ and $\text{d}_{42}\text{-CTAB}$) were purchased from CDN Isotopes, both at the highest purity possible (98+%). Anionic sodium dodecyl sulfate (SDS) surfactant and its fully deuterated analogue ($\text{d}_{25}\text{-SDS}$) were purchased from Sigma Aldrich at the highest purities possible (99.0% and 98.0+%, respectively). Sorbitan monooleate (Span-80) was purchased from Sigma Aldrich. Dioctyl sulfosuccinate sodium salt, also known as sodium bis(2-ethylhexyl) sulfosuccinate, (AOT) was purchased from Sigma Aldrich at 99% purity. Its alkyl tail deuterated analogue, sodium bis(2-ethylhexyl- d_{17}) sulfosuccinate, (d-AOT) at 98% deuteration was purchased from Sigma Aldrich. All surfactants and polymers were used as received.

While some evidence suggests small amounts of dodecanol contaminants are found in commercial sources of SDS,²⁸⁻³⁰ it has been shown that dodecanol does not affect the surface properties of SDS at the oil/water interface due to its high solubility in

oil.³¹⁻³² While trace amounts of dodecanol may be present in the studies herein containing SDS surfactant, we attribute any interfacial effects from these samples as being induced by the SDS surfactant.

All glassware and VSF sample cells were extensively cleaned before use, by first soaking in a concentrated sulfuric acid bath containing NoChromix for at least 12 hours and subsequently placed in an ultrapure water bath for at least 12 hours. Stock solutions of all chemicals used in these studies were made and stored in acid-washed glassware. Unless otherwise stated, all VSF sample solutions of mixed systems containing two aqueous solutes (surfactants or polymers) were prepared by creating 5 mL samples of each surfactant/polymer at twice the desired concentration. These individually diluted solutions were then mixed together to create a 10 mL aqueous sample at the appropriate concentrations for each solute. Surface tensiometry samples were prepared similarly, but with a final volume of 5 mL. These mixed system aqueous solutions were used immediately after they were created.

Pendant Drop Surface Tensiometry:

Surface tension measurements utilized the pendant drop method on a KSV Instruments Attension Theta Optical Tensiometer. As molecules adsorb to an interface and alter the interactions between the surface species, the resulting surface tension changes. Surface tensiometry provides complimentary information to VSF data by allowing a quantitative measurement with implications regarding the amount of molecular adsorbates at the oil/water interface.^{26, 33-34}

For the pendant drop experimental method used here, a hook-needle containing the aqueous solution of interest was suspended in a cuvette containing the oil phase, CCl₄. Images of the droplet shape were taken in increments over time and fit to the Young-Laplace equation to obtain the surface tension value as molecules in the aqueous solution adsorbed to the surface. Measurements began immediately after the aqueous drop was formed in the oil and continued until equilibrium was reached, where the surface tension no longer changed.

Reported values of these experiments are often conveyed as a measure of surface pressure, which is obtained by subtracting the surface tension value for each aqueous

sample from the neat oil/water surface tension measurement. Thus, a neat CCl₄/water surface has a surface pressure value of 0 mN/m and aqueous solutions containing surface adsorbates cause an increase in the system's surface pressure over time as the molecules aggregate to the surface. The neat CCl₄/water surface tension value was taken before each sample run to ensure the cleanliness of the instruments, with an averaged value of 45 ± 1 mN/m.

CHAPTER III:

WATER COMBINATION BANDS AT THE OIL/WATER INTERFACE

This chapter contains work currently under publication review, with Dr. Geraldine Richmond as the principal investigator.

Understanding the vibrational spectrum of water at hydrophobic interfaces is necessary for investigating complex surface chemistry phenomena. However, spectral assignments of water modes at surfaces as studied by Vibrational Sum Frequency spectroscopy are often more nuanced than in linear spectroscopy. Previous studies investigating the water spectrum at hydrophobic surfaces have mainly focused on the region of the O-H stretch oscillators ($3000 - 3700 \text{ cm}^{-1}$), yet there are many other water modes detected by VSF at these surfaces that are consequential to understanding the water spectrum at hydrophobic interfaces.^{20, 35-42} The studies discussed in this chapter investigate the source and charge dependence of two water combination modes present in the VSF spectrum at the oil/water surface, and their implications for analyzing various regions of VSF spectra. The oil/water surface provides an ideal chemical system for investigating these modes, as the small nonresonant background at the oil/water surface does not obscure the VSF detection of weak resonant modes.

The Water Stretch + Libration Combination Band:

The studies presented in this section provide insight the source of a broad response in the surface water VSF spectrum that appears at energies slightly higher than the free OH at the oil/water interface. Isotopic dilutions of the aqueous solvent demonstrate this signal is due to a combination mode of the stretch and libration motions of interfacial water. This mode is found to be highly sensitive to surface charge. In addition to providing previously uninvestigated details of this response, the results reported here contain important implications for analyzing various chemical systems by VSF spectroscopy.

A) The neat water spectrum at the oil/water interface

The O-H stretch oscillators present at the bare oil/water surface have been studied in detail.^{35, 38, 43} However, previous investigation of the high energy region of the water spectrum of water stretch oscillators is limited, though questions regarding the source and behavior of VSF signal in these regions remain.⁴⁴⁻⁴⁷ This lack of previous investigation is likely due to the experimental difficulties in probing such weak signals that exist in this high-energy region. This study utilizes VSF spectroscopy to analyze resonant modes from interfacial water molecules in this vibrational region.

The VSF spectra of the high energy region for the bare water spectrum at the oil/water interface is shown in Figure 3.1 with aqueous phases of H₂O (red trace), and D₂O (circles trace). The spectral region shown probes the vibrational response from H₂O molecules, thus, D₂O resonant modes are not present in this region, as they redshift to lower wavenumbers upon deuteration. The straight fit line through the D₂O experimental data is the nonresonant signal at the oil/water interface, discussed later in further detail.

It is well understood from literature that the sharp feature in the H₂O spectrum at $\sim 3665\text{ cm}^{-1}$ in Figure 3.1 is free OH mode. This mode results from water molecules with one O-H oscillator protruding into the hydrophobic phase, unable to engage in hydrogen bonding with other water molecules. The free OH at the CCl₄/water interface is redshifted to a lower frequency than at the air/water interface, where it is found at 3702 cm^{-1} .^{36, 48}

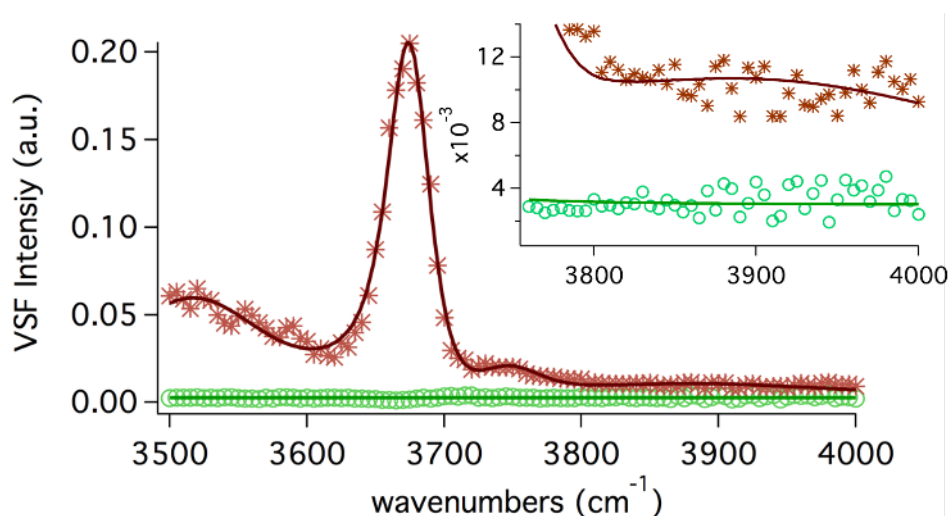


Figure 3.1: VSF spectra of the neat H₂O/oil (stars) and D₂O/oil (circles) interface. The sharp peak at $\sim 3665\text{ cm}^{-1}$ corresponds to the free OH mode. The weak signal in the $3800\text{-}4000\text{ cm}^{-1}$ region, proposed to be from the water stretch + libration combination band, is amplified in the inset. Lines are fits to spectra. The fit line in the D₂O/oil (circles) trace displays the experimentally determined nonresonant response for this system. Full fit parameters can be found in Appendix A, Table A.1.

This frequency shift is due to weak bonding interactions with the oil phase that are not present at the air/water interface.

The VSF signal at wavenumbers lower than the free OH ($3500\text{-}3650\text{ cm}^{-1}$) correspond to the O-H stretch oscillators of surface water molecules in coordinated hydrogen-bonding environments. Signal from these modes in VSF spectra are known to be very sensitive to surface charge.^{43, 49} We attribute the feature at $\sim 3744\text{ cm}^{-1}$, slightly blue of the free OH, to the asymmetric stretch of water monomers at the $\text{CCl}_4/\text{water}$ interface, as assigned in previous experimental and computational studies.^{35-36, 50}

The spectra of the H_2O and D_2O surfaces in the high energy region are shown in spectral inset of Figure 3.1, with a y-axis scale that allows the magnification of the weak signal detected. While the VSF signal in this region is certainly weak compared to the intensity of the free OH, it can be observed that the $\text{CCl}_4/\text{H}_2\text{O}$ spectrum (red stars trace) displays a higher signal intensity than that of the nonresonant signal detected at the $\text{CCl}_4/\text{D}_2\text{O}$ surface, indicating resonant signal contributions from water molecules are present in this region.

While this may be considered an unusual region to observe resonant signal from H_2O , as O-H stretching modes higher in energy than the water monomer O-H stretches are traditionally not expected, previous VSF studies have observed similar signal blue of the free OD for D_2O solutions, but have not attributed it to a specific assignment.⁴⁵⁻⁴⁷ However, literature of IR, Raman, and computational studies investigating the vibrational behavior of bulk liquid water and gas phase water clusters suggest signal detected in this region is likely due to a combination band of a water libration with a water stretch.⁵¹⁻⁶⁰ Specifically, previous gas phase studies attribute the source of this combination band to a water asymmetric O-H stretch being excited simultaneously with a low-frequency torsion libration.^{51-52, 55, 58} Water librations are detected at very low frequencies, which are extremely difficult to detect spectroscopically by VSF at an interface.⁶¹⁻⁶³ However, when one of these libration vibrations is excited simultaneously with a water stretching vibration to create a combination band, the frequency lies at energies slightly higher than where the free OH is found.^{51-52, 55-56} For the chemical systems investigated here at the liquid water surface, the O-H stretches of the hydrogen-bonded water molecules excited simultaneously with the libration motions causes the frequency of the resulting

combination mode to appear at energies to the blue (higher) than the free OH at the oil/water interface.^{43, 52, 56, 63}

Before delving into a further analysis of this weak signal due to the water combination mode, it is important to discuss several factors that are often neglected when analyzing intense VSF signals but are important to consider when investigating weak resonant responses such as the one studied here. Namely, the nonresonant contribution to the VSF spectrum and any IR beam dispersion from Fresnel factors must be considered.

Analysis of VSF spectra is often complicated by the background nonresonant response, and understanding this response is important for evaluating accurate resonant mode features. The magnitude of the nonresonant response can be dependent on several factors including experimental laser setup, surface charge and surface medium.^{38, 64-66} The picosecond experimental system used in this study is able to detect a small but measurable nonresonant response at the oil/water interface. The nonresonant response shown in Figure 3.1 as the straight fit line through the CCl₄/D₂O spectrum (circles trace) is incorporated into all subsequent fits of VSF spectra at the oil/water interface. This weak nonresonant response was determined by experimentally measuring the VSF signal produced by the purely D₂O aqueous phase in the high-energy region of the H₂O spectrum where no resonant VSF signal is produced from D₂O. Thus, the constant VSF signal detected in this region is from the flat nonresonant background. Some previous VSF publications investigating the oil/water interface have deemed the nonresonant VSF signal negligible when compared to the intensity of the free OH or water stretching modes, which is consistent with what is shown here.^{26, 33-34, 38} However, when much weaker resonant modes are present, the small nonresonant signal can interfere with vibrational responses, affecting the spectral analysis if not included in the fitting procedure (full fit parameters can be found in Appendix A).

The nonresonant background detected with the picosecond laser system in these studies at the oil/water interface is significantly less intense than what has been shown to be present at the more commonly studied air/water interface.^{43, 49, 67} Because the resonant modes of interest in these studies are very broad and weak, the small nonresonant background of the oil/water surfaces makes it an ideal interfacial system for investigating these water modes, as there is minimal interference between the weak resonant and

nonresonant signals. While the water modes investigated in this study are likely present at the air/water interface as well, the more intense nonresonant background interfering with the weak resonant signal would make it more difficult to experimentally detect. It is possible that utilizing a heterodyne detection VSF experimental design would allow the investigation of these weak resonant modes at other hydrophobic/water interfaces by eliminating interferences; however, appropriate sensitivity for these studies must first be experimentally achieved.

Taking into account any changes to the VSF spectrum from IR beam dispersion as calculated by the Fresnel factors must also be considered for the present study, as the spectral shape of these very weak resonant modes can be significantly affected by IR dispersion. As the tunable IR beam changes frequency, the refractive indexes of the interfacial media may allow increased IR beam dispersion into the bulk phases at particular wavelengths, affecting the maximum amount of VSF signal intensity that can be detected at each incoming IR wavelength. This phenomenon is dependent upon several factors, including the incoming angles of the visible and IR beams, as well as the refractive index of the bulk phases comprising the interface. Although our experimental design allows for total internal reflection of both the visible and IR beams, any wavelength-dependent IR dispersion can still affect the resulting features in the overall spectrum detected. To account for these wavelength-dependent effects, the Fresnel factors are used to calculate any dispersion at each IR wavelength for a particular interface.⁶⁸⁻⁶⁹ The experimentally obtained spectrum can then be normalized to account for any dispersion effects. The most significant effects of normalizing to the Fresnel factors occur when there is enough variation in the IR beam dispersion that the experimentally detected VSF peaks show spectral shapes that are artifacts of the refractive index IR wavelength-dependence and are not actual resonant modes of interfacial molecules. Thus, it is important to analyze VSF spectra of weak signal intensity to verify the observed spectral shapes are in fact due to resonant modes.

The Fresnel factors were calculated for this experimental system by accounting for both the real and imaginary parts of the refractive index of water.⁶⁹ The red trace in Figure 3.2 shows the original spectrum as normalized by our routine normalization process (see Chapter II), and the blue trace is normalized further by accounting for the

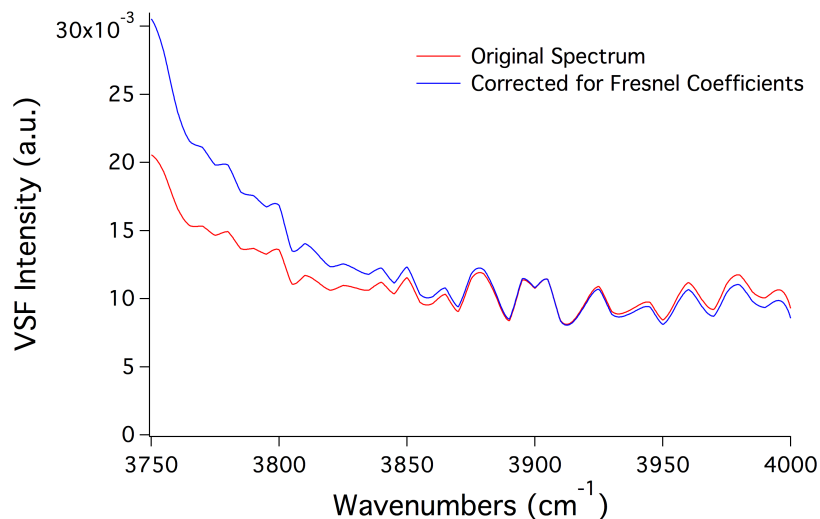


Figure 3.2: The VSF spectrum of the neat H₂O/CCl₄ surface as detected experimentally with (blue trace) and without (red trace) normalization of the calculated Fresnel factors, including both the real and imaginary part of the refractive index of water. Lines connect experimental data points for visual clarity.

system's calculated Fresnel factors. It can be seen that while there are slight variations in intensity, the overall spectral shape of the water spectrum's high energy region remains largely unchanged. This indicates that the IR dispersion for the system in this region causes largely negligible effects on the overall analysis of the spectrum's resonant features. Thus, all subsequent spectra shown in this chapter were not normalized to Fresnel factors. This analysis provides further confidence in the weak signal detected in this region originating from resonant modes at the oil/water surface.

With this confidence in the resonant nature of the weak signal of interest, Figure 3.3 shows an isotopic dilution study at the neat oil/water interface to further understand the high energy region of the neat water spectrum. The isotopic dilutions consist of varying ratios of H₂O:D₂O, which are summarized in Table 3.1 along with the respective mole fraction ratios of H₂O, D₂O, and HOD populations. HOD is produced from hydrogen-deuterium exchange, and the mole ratios at each H₂O:D₂O ratio were calculated as in previous publications.⁴⁹

As different ratios of H₂O and D₂O are mixed, the aqueous phase consists of varying amounts of H₂O, D₂O, and HOD molecules. Because the water stretch + libration combination band arises from the combination of stretch and libration vibrations from intramolecularly coupled H₂O molecules, VSF signal from this band is expected to only appear when there is a significant amount of H₂O in the aqueous phase. Isotopic dilutions

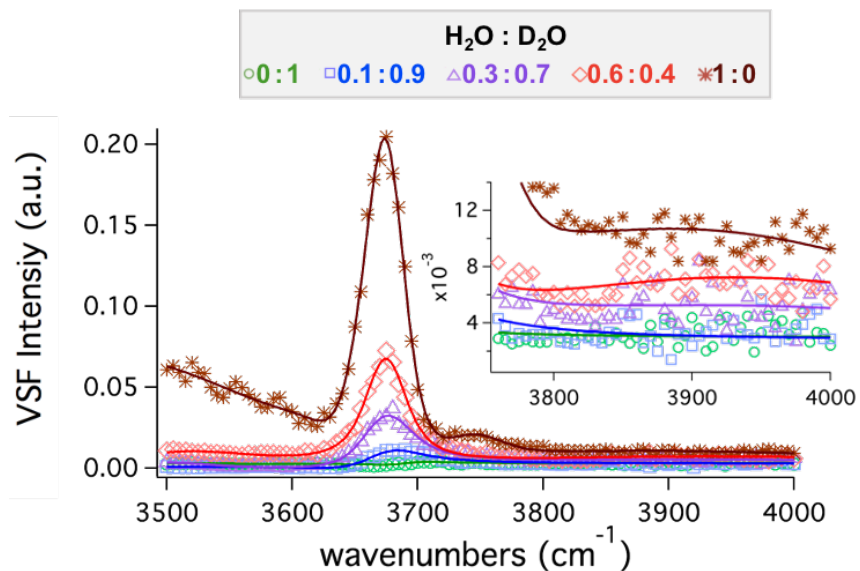


Figure 3.3: Isotopic dilution VSF spectra at the $\text{CCl}_4/\text{water}$ interface of the neat surface. $\text{H}_2\text{O}:\text{D}_2\text{O}$ ratios of 0:1, 0.1:0.9, 0.3:0.7, 0.6:0.4, and 1:0 are shown as the circle, square, triangle, diamond, and star traces, respectively. The peak at 3665 cm^{-1} is the free OH. The spectral inset displays the region of the stretch + libration combination band for clarity. Lines are fits to spectra. Full fit parameters can be found in Appendix

$\text{H}_2\text{O}:\text{D}_2\text{O}$	$X_{\text{H}_2\text{O}}$	$X_{\text{D}_2\text{O}}$	X_{HOD}
0:10	0	1	0
1:9	0.01	0.81	0.18
3:7	0.09	0.49	0.42
6:4	0.36	0.16	0.48
10:0	1	0	0

Table 3.1: Mole fractions (X) for H_2O , D_2O , and HOD at the various $\text{H}_2\text{O}:\text{D}_2\text{O}$ isotopic dilution ratios used in Figure 3.3.

of $\text{H}_2\text{O}:\text{D}_2\text{O}$ can help elucidate what signal is produced by this water combination band, as the VSF response will disappear as uncoupled HOD molecules and fully deuterated D_2O molecules populate the aqueous phase. As the fraction of H_2O molecules in the isotopic dilution shown in Figure 3.3 increases, the VSF signal in this vibrational region also increases until the aqueous phase consists purely of H_2O (brown stars trace). Note that the highest HOD concentration produced in this series occurs at a $\text{H}_2\text{O}:\text{D}_2\text{O}$ ratio of 0.6:0.4 (diamonds trace), at 0.48 mf. Additionally, the $\text{H}_2\text{O}:\text{D}_2\text{O}$ ratio of 0.1:0.9 (squares trace) produces the highest ratio of HOD: H_2O (0.18mf : 0.01mf) in this series. For this isotopic mixture, resonant VSF contributions of O-H vibrations can be attributed primarily to the uncoupled O-H bonds of HOD.

The free OH feature in the neat $\text{CCl}_4/\text{H}_2\text{O}$ interface grows in intensity as the concentration of O-H oscillators replace the deuterated O-D oscillators present in the aqueous phase. The lineshape of the free OH mode also narrows as the ratio of $\text{H}_2\text{O}:\text{D}_2\text{O}$ increases to 1:0, as the O-H stretches contributing to the free OH at this ratio arise solely from H_2O molecules at the interface instead of a mixture of H_2O coupled O-H stretches and HOD uncoupled O-H stretches.

As the high energy broad peak is comprised of the energetic combination of an H_2O stretch with an H_2O libration, no signal is observed at 3830 cm^{-1} when the majority of water molecules are fully deuterated (0% in the circles trace and 1% in the squares trace). When the population of H_2O species in the aqueous phase increases to 9% (triangles trace), signal from this broad band is weakly observed and included in the spectral fits (see Appendix A). As the population of H_2O molecules continues to increase to 36% and 100%, the intensity of the combination band peaks continues to increase.

The breadth of this peak is consistent with what is expected for this mode. Because the VSF signal from the interfacial water stretch + libration combination band is dependent on the behavior of water stretches, it is expected to manifest the same lineshapes as the water stretching bands and librational bands.^{43, 49, 62} Water O-H stretching modes are known to have broad spectral peaks due to their extended hydrogen bonding environments, thus the water combination band would be expected to mirror these broad lineshapes.^{67, 70-72} Because of its broad lineshape, the water combination band can influence spectral features across a large frequency range beyond where its peak is centered, which Figure 3.3 shows to be true.

Through these isotopic dilution studies, it is concluded that the broad VSF resonant signal at energies higher than the free OH originate from a resonant H_2O response, specifically the water libration + stretch combination mode. Previous studies have confirmed the O-H water stretching region is very sensitive to surface charge. To further confirm the presence of the stretch + libration combination band in the surface water spectrum and to understand how it responds to a charged interface, the behavior of the water combination band region in the presence of cationic and anionic surface charge is discussed next.

B) Isotopic dilution studies of the water spectrum at the oil/water interface in the presence of surface charge

It is well established that the vibrational region of O-H stretch modes ($2800\text{-}3700\text{ cm}^{-1}$) from interfacial water is sensitive to surface charge.³⁵⁻³⁶ When a charged surfactant is present at an oil/water surface, water molecules orient their dipole in response to the electrostatic field. Due to the field induced by the charged surfactant, the VSF spectrum in SSP polarizations probes water molecules that have a net orientation perpendicular to the interface in an extended interfacial region, beyond the first few Angstroms probed in a bare surface spectrum.^{35, 37, 73-77} These field-oriented water molecules in the extended region experience more hydrogen bonds to surrounding water molecules. Thus, the surface spectrum of a charged surface shows O-H stretching features of more strongly coordinated water molecules in the $2800 - 3600\text{ cm}^{-1}$ region.³⁵

The sensitivity of water modes in the high energy region of the water spectrum to surface charge has been noted in previous studies³⁵⁻³⁶, however, it has not been examined in any detail before. To understand how these high energy water modes are affected by charge at the interface, the water combination band behavior of $\text{H}_2\text{O}:\text{D}_2\text{O}$ isotopic dilutions in the presence of cationic and anionic surface is studied here.

Figure 3.4 shows the water spectrum as probed by VSF spectra at different isotopic dilutions at the oil/water interface with either cationic or anionic surfactant present. Water modes interfere with each other differently when surface charge is introduced to the interface due to their different phases as water dipoles reorient. These charge-induced interferences in the water modes result in different lineshapes observed around the free OH ($3600\text{-}3750\text{ cm}^{-1}$) for the neat water spectrum in Figure 3.1 compared to the anionic and cationic surfaces shown here in Figure 3.4.

Both Figures 3.4a and 3.4b show different VSF intensities for the fully D_2O (circles) trace than what is reported as the nonresonant spectra from a bare interface in Figure 3.1. As a charge is introduced to the surface, the VSF spectrum is affected by nonresonant signal produced from a field-dependent background, referred to in previous work as a type of $\chi^{(3)}$ effect.⁷⁸ The properties of this nonresonant background are dependent on the sign of charge and the strength of the electrostatic field produced at the surface, causing the VSF intensity of the circles traces in Figures 3.1, 3.4a, and 3.4b to

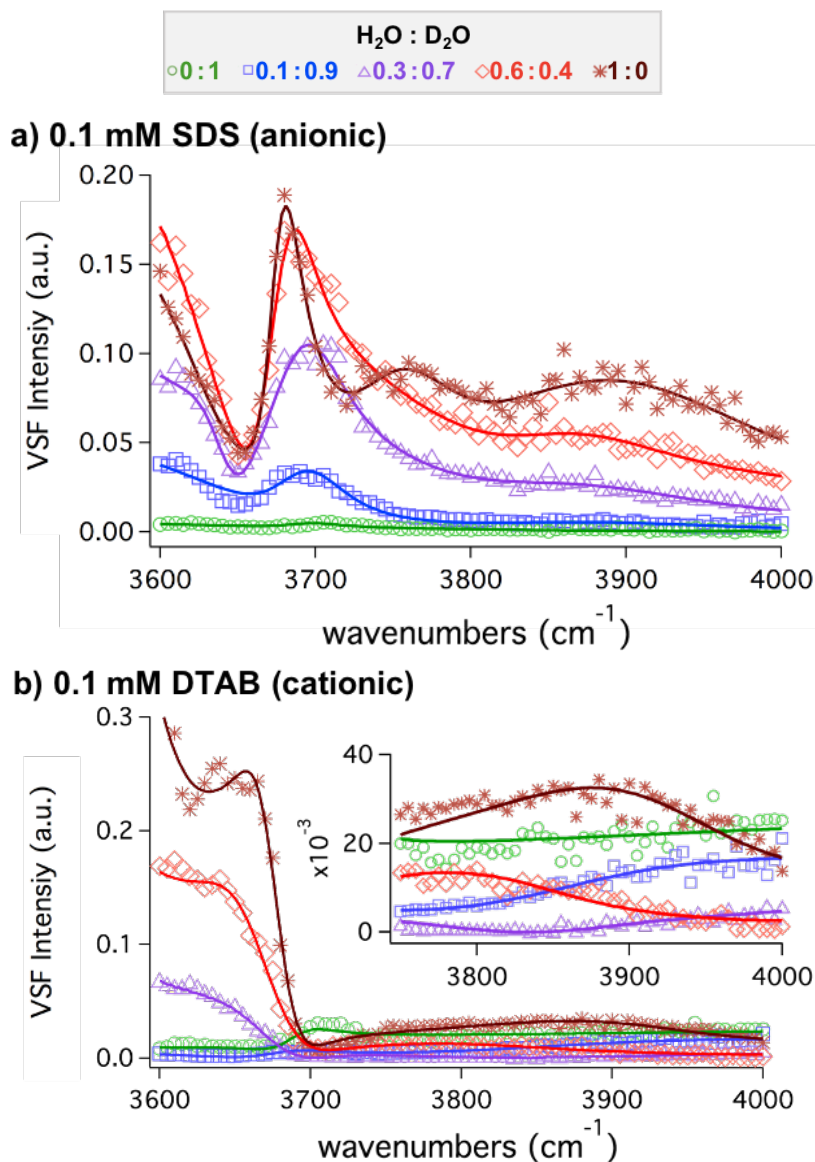


Figure 3.4: Isotopic dilution VSF spectra at the CCl₄/water surface with 0.1 mM anionic SDS (a), and 0.1 mM cationic DTAB (b). H₂O:D₂O ratios of 0:1, 0.1:0.9, 0.3:0.7, 0.6:0.4, and 1:0 are shown as the circle, square, triangle, diamond, and star traces, respectively. The respective mole fractions of H₂O, D₂O and HOD can be found in Table 3.1. The peak at 3665 cm⁻¹ is the free OH. The spectral inset in (b) displays the region of the stretch + libration combination band. Lines are fits to spectra. Full fit parameters can be found in Appendix A, Tables A.3 and A.4.

vary. Where the D₂O/oil spectrum in Figure 3.1 only consists of the nonresonant signal from the bare oil/water interface, the D₂O/oil spectra of the 0.1 mM SDS and 0.1 mM DTAB also contain contributions of the field-dependent nonresonant signal that varies with surface charge. The nonresonant signals containing the field-dependent responses from charged D₂O/oil interfaces are hereafter referred to as the systems' corresponding VSF nonresonant background signals.

It is noted that the D₂O/oil spectra with DTAB in Figure 3.4b shows a slight free OH feature at 3690 cm⁻¹. This is attributed to trace amounts of non-deuterated water contaminants from deuteration impurities. This peak is also present in the spectra of bare and anionic surfaces; however, it is most apparent in the 0.1 mM DTAB spectra due to the elevated VSF nonresonant background of the cationic system.

Comparing Figures 3.4a and 3.4b, it can be seen that the behavior of the water stretch + libration combination band above 3800 cm⁻¹ shows significant differences between negatively and positively charged surfaces. This is expected, as the interfacial water modes interfere differently with variations in the surface charge. A discussion of the high-energy region of the water spectrum under both an anionic and cationic surface charge follows.

Figure 3.4a shows the isotopic dilution spectra of water in the presence of 0.1 mM anionic SDS. The VSF signal from the water combination band at this anionic surface (fit to 3848 cm⁻¹, see Appendix A) is more intense than that of the neat oil/water spectra in Figure 3.1 due to more water molecules being probed by VSF at an extended surface region in the presence of a surface charge. This is most evident at isotopic dilutions with significant amounts of H₂O. When the H₂O population is very low at 0% and 1% (circles and squares trace of Figure 3.4a, respectively), the signal from the H₂O combination band at the negatively charged surface has a correspondingly weak signal intensity, even with the charge causing an extended interfacial region probed by VSF. However, as the amount of H₂O in the aqueous phase increases through the isotopic dilution to 9%, 36%, and 100% (triangle, diamond, and star traces, respectively), the VSF signal from the H₂O combination band continuously increases, reaching peak intensities higher than the same H₂O compositions at a bare surface.

Figure 3.4b shows the effects of an oppositely charged surface (0.1 mM cationic DTAB) on the isotopically diluted H₂O combination band surface behavior. Although the overall intensity of the region encompassing the combination mode in these spectra appear much lower than in the anionic SDS system, the signal intensity solely from the water combination band at this cationic surface is continually increasing as the amount of H₂O increases from 0% to 100%, as would be expected (see Appendix A). As this signal from the combination mode negatively interferes with the nonresonant signal at this

surface, the overall VSF intensity in this region first appears to decrease (going from 0% to 1% and 9% H₂O) before increasing (to 36% and 100% H₂O) through the isotopic dilution series. The interference between the flat nonresonant signal of the cationic surface with the broad resonant signal from the combination mode causes this dip and rise in the overall intensity through the isotopic dilution series, even though the signal intensity from the combination mode continually increases as the population of H₂O molecules in the aqueous phase increase.

If the broad signal detected in this region at these charged surfaces are indeed due to a resonant water mode, the same isotopic dilution series performed at anionic and cationic surfaces should display VSF responses from water modes with opposite phases. The comparison of spectral features in the 2800 – 3000 cm⁻¹ region in Figures 3.4a and 3.4b shows this to be true, further confirming that interfacial water modes are the origin for the weak VSF signal the high energy region of the water spectrum.

The addition of salt to a charged interface electrostatically screens the surface charge, causing the probed interfacial depth to decrease and become more similar to that of a bare surface, even when charged surfactants are present.^{43, 79} As fewer water molecules are probed, the signal intensity from the water modes decreases. Figures 3.5a and 3.5b display the H₂O and D₂O water spectra, respectively, of 0.01 mM d-SDS in the presence of a high salt concentration (1 M NaCl). The VSF intensity in the water combination band region in these figures decreases as salt is added to the system, true when the aqueous phase is either H₂O or D₂O.

It is noted that in Figure 3.5b, some VSF signal intensity is still observed in the high-energy region of the D₂O spectrum. Several factors are likely contributing to this signal: (1) the D₂O combination mode is still present, although weaker, (2) the nonresonant signal of the d-SDS + NaCl system is more intense than the d-SDS system alone (see Appendix A), and (3) the charge screening upon addition of salt allows a much higher adsorption of d-SDS molecules to the surface, causing trace amounts of C-H stretching signal from deuteration impurities to become detectable in the salt system (C-H stretches are found in the 2750-3100 cm⁻¹ region). Factors 2 and 3 listed above cause the VSF signal in the salt system to increase, however, the spectrum in Figure 3.5b still shows an overall lower VSF intensity in the water combination band region. The only

plausible factor that would cause a decrease in the signal detected in this region upon the addition of salt is a decrease in the D₂O stretch + libration combination mode contribution to the VSF signal due to charge screening. Thus, the lower intensity observed for both the H₂O and D₂O spectra in Figure 3.5 upon surface charge screening with the addition of salt provides further evidence of the water stretch + libration combination mode's responsibility for the signal detected blue of the free OH(D).

The detection of signal in this high energy region of 3800-4000 cm⁻¹ at all three interfacial systems of neat, cationic, and anionic, as well as the VSF signal dependence on the addition of salt provides strong evidence of the presence and surface charge dependence of the water stretch + libration combination band in VSF spectra at the

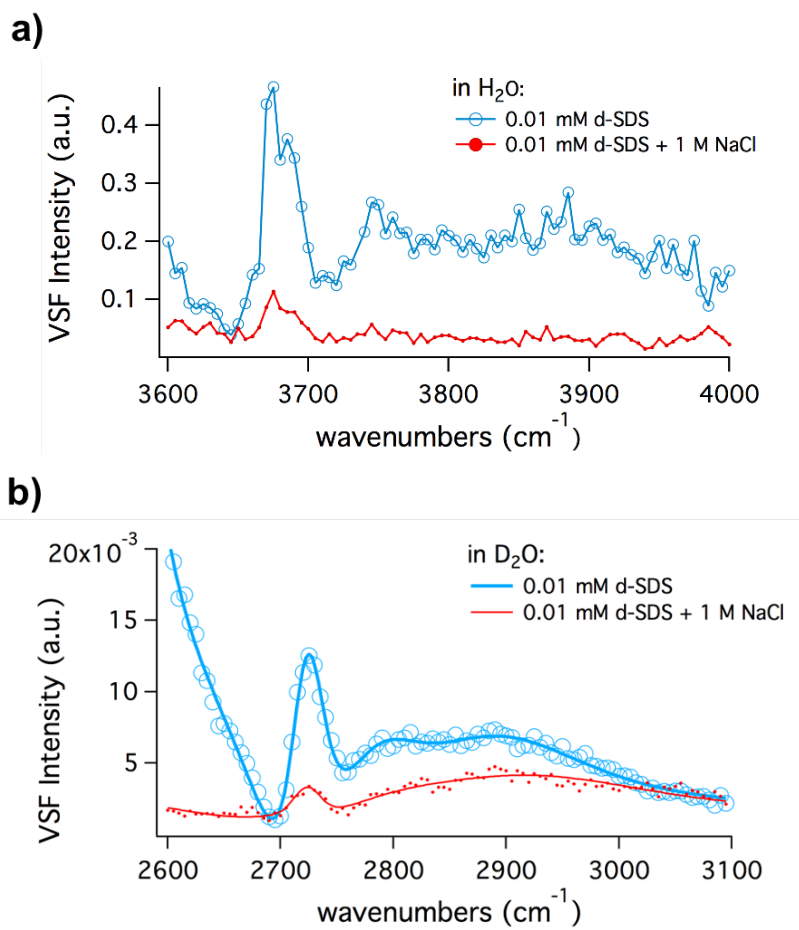


Figure 3.5: VSF spectra at the oil/water interface with aqueous solvents of H₂O (a) and D₂O (b). Both spectra show the water combination mode region blue of the free OH(D) in the presence of 0.01 mM d-SDS (blue trace) and 0.01 mM d-SDS + 1 M NaCl (red trace). The free OH is the sharp peak located at ~3665 cm⁻¹ in 5a, and the free OD is that located at ~2720 cm⁻¹ in 5b. In 5a lines are guides to the eye and in 5b lines are fits to spectra. Full fit parameters for Figure 3.5a can be found in Appendix A, Table A.4.

oil/water interface. The following section further discusses the dependence of this high energy signal on the water libration mode behavior.

C) Combination band frequency shift upon surface charge

Further exploration of the surface charge effect on the combination band shows that in addition to intensity and phase changes, there is also a frequency shift between the neat and charged surfaces. The presence of anionic or cationic surfactants at the surface causes the water stretch + libration combination band to blueshift in frequency to higher wavenumbers compared to a bare surface. At a bare H₂O/CCl₄ surface, spectral fitting reports the combination band centered at a frequency of $3805 \pm 8 \text{ cm}^{-1}$. However, the frequency position of the combination mode blueshifts to fit frequencies of $3848 \pm 3 \text{ cm}^{-1}$ with 0.1 mM anionic surfactant and $3857 \pm 13 \text{ cm}^{-1}$ with 0.1 mM cationic surfactant (full fit parameters can be found in Appendix A).

This blueshift is evidence of this water mode's dependence on the libration motion. Water's libration motion becomes increasingly frustrated upon additional hydrogen bonding, causing the energy of the movement to increase (blueshift).^{61-62, 70, 73, 80-82} As either cationic or anionic surfactant is added to the oil/water interface and surface water molecules reorient their dipoles in response, their hydrogen bonding networks are altered and the coordination between water molecules at the surface increases. This causes the libration motion of interfacial water molecules probed by VSF to be higher in energy than when at a bare uncharged surface, evidenced by a blueshift in the stretch + libration combination band of water molecules at the surface.

To further elucidate the details of the blueshift in the water combination band and altered hydrogen bonding environment upon addition of surfactant, Figure 3.6 shows the VSF spectra of the D₂O vibrational stretching region at various concentrations of anionic surfactant at the D₂O/oil interface. The VSF spectra in the wavenumber region of D₂O vibrations ($2600 - 3100 \text{ cm}^{-1}$) displays a higher signal-to-noise ratio than compared to the H₂O region due to more stable tunable IR energy production, allowing for more clarity when analyzing a surfactant concentration series. Figure 3.6 shows the VSF spectra of a bare D₂O/oil interface, as well as the D₂O/oil interface with 0.01 mM and 0.1 mM deuterated SDS (d-SDS). The peak at $\sim 2720 \text{ cm}^{-1}$ is from the free OD oscillators at the

interface. The rise in intensity at wavenumbers lower than the free OD is due to the enhancement of the O-D stretches upon surface charge, and the broad signal at higher wavenumbers ($2800 - 31000 \text{ cm}^{-1}$) arises from the D_2O stretch + libration combination band. The SDS surfactant used in these systems was deuterated to shift its C-H stretching modes out of the D_2O combination band region ($2800-3100 \text{ cm}^{-1}$), removing any interference between the surfactant C-H stretches and signal from the D_2O combination band. Anionic SDS was used instead of a cationic surfactant because the combination band's behavior is more visually apparent with anionic surfactant due to the phase interaction between the water resonant modes and the VSF nonresonant background signal, as discussed previously. It is noted that the features of the D_2O /oil interface vary slightly from that of the H_2O /oil surface, as a vibration's deuterated analogue is known to have slightly different spectral features.^{3, 48, 66, 83} Additionally, there may be trace amounts of impurities in the D_2O solvent, as the H_2O used in this study was purified to $18.2 \text{ M}\Omega \cdot \text{cm}$, while the D_2O solvent was not. It is also noted that an isotopic dilution study in the D_2O region is not beneficial for the sake of this study, as the addition of O-H oscillators would introduce signal in this region from O-H stretches ($2850-4000 \text{ cm}^{-1}$), which are further amplified by the presence of a surface charge.

Because the broad nature of the combination mode causes its frequency position to be difficult to visually approximate, mathematical fitting of the spectra is necessary to quantitatively analyze its peak position. The spectra in these studies were extensively fit both individually and globally, and the results report a blueshift in the frequency position of the interfacial water stretch + libration combination band from $2815 \pm 30 \text{ cm}^{-1}$ at a bare surface to $2851 \pm 10 \text{ cm}^{-1}$ with 0.01 mM d-SDS. This is expected, as our surfactant studies at the H_2O /oil interface above discusses this same blueshift. However, when the concentration of d-SDS is further increased to 0.1 mM at the D_2O /oil interface, the frequency position does not show any further blueshift, fitting to a peak position of $2856 \pm 10 \text{ cm}^{-1}$ (see Appendix A for full fit parameters). This lack of further blueshift upon increased surfactant concentration indicates that the libration movement of the probed surface water molecules is not further frustrated by changes in the hydrogen bonding network with increased surface charge.

Although the peak for the stretch + libration combination band of interfacial water in Figure 3.6 does not blueshift further upon the addition of more SDS (from 0.01 mM to 0.1 mM), the intensity of the combination band continues to increase, indicating a limit to how much the water libration is hindered by surface charge. The increase in intensity of the combination band with the increase in surfactant suggests more water molecules at further interfacial depths are contributing to the VSF signal; however, the additional surface charge does not further hinder the interfacial water libration. The observation of a blueshift in the broad water combination mode peak in the presence of both cationic and anionic surfaces in H₂O, as well as with an aqueous solvent of either H₂O or D₂O provides evidence of the mode's dependence on the water libration behavior, supporting the assignment of this high-energy mode as a response from the water stretch + libration combination band.

D) Implications for studying the C-H stretching region with VSF

In many studies using VSF to investigate the structure of surface adsorbates, the intensity ratio of the C-H symmetric methylene and methyl stretches near 2850 cm⁻¹ and 2870 cm⁻¹, respectively, are commonly used to determine the relative chain conformational order of an adsorbed alkyl surfactant.^{18, 34, 66} Larger methylene mode intensity relative to the methyl mode intensity indicates higher chain disorder. These

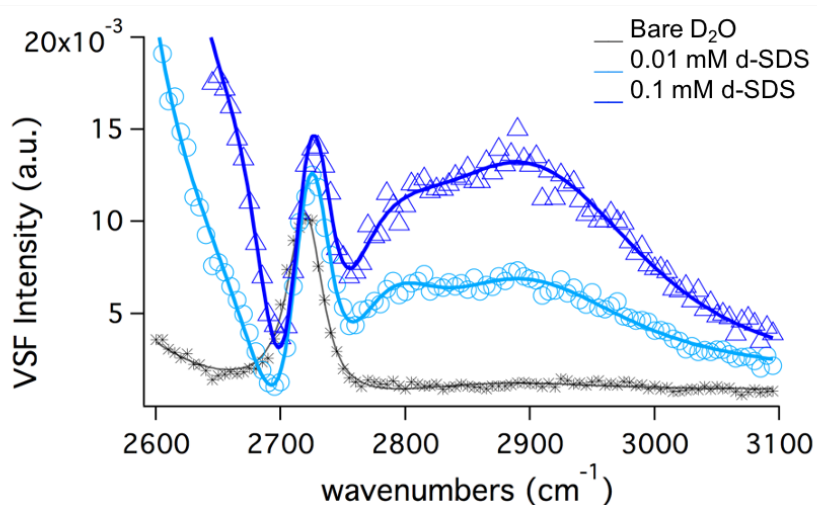


Figure 3.6: VSF spectra of the CCl₄/D₂O interface with no surfactant (grey stars), 0.01 mM d-SDS (light blue circles), and 0.1 mM d-SDS (dark blue triangles). The broad signal in the region blue of the free OH from 2850-3100 cm⁻¹ is amplified upon the presence of surface charge. Lines are fits to spectra. Full fit parameter can be found in Appendix A, Table A.6.

experiments are often performed in an aqueous solvent of D₂O to avoid interference between the C-H stretch modes with the O-H stretches of H₂O.^{65-66, 84-87} As shown by Figure 3.6, the D₂O stretch + libration combination band produces signal at wavenumbers encompassing the range where C-H stretch vibrations are detected (2750-3100 cm⁻¹). Thus, neglecting to incorporate the presence of this combination mode into the mathematical fits of the spectra can introduce inaccuracies in the resulting fit parameters. It is imperative to take into account the presence of the water combination band when analyzing C-H stretches in an aqueous solvent of D₂O— a consideration this section will discuss in detail using model co-surfactant systems.

Figure 3.7 shows the VSF spectra of two different co-surfactant mixtures of a nonionic surfactant with either an anionic or cationic surfactant, demonstrating the interference of the interfacial D₂O combination band with C-H stretches at the D₂O/oil surface. The C-H peaks observed in Figure 3.7 are due to nonionic Span-80 surfactant at the surface. In addition to nonionic Span-80, the spectra in Figure 3.7 include either anionic d-SDS (purple circles), or cationic d-DTAB (blue triangles). The charged surfactants are deuterated to shift their C-H stretches out of the spectral region shown, allowing the C-H modes in these spectra to be produced solely from the nonionic Span-80 surfactant.

As discussed previously, the broad underlying signal from the interfacial water combination band at an anionic surface (circles) is visually higher and has an opposite phase than the combination band at a cationic surface (triangles). This causes the C-H stretches of Span-80 to interfere oppositely with the combination band signal between these the cationic and anionic surfaces. Most visually apparent, the sharp peak centered at 2933 cm⁻¹ from Span-80 displays a lineshape with a dip in intensity as it interferes with the broad water mode signal when in the d-SDS system. This same C-H mode manifests a more distinct Gaussian-like lineshape when in the cationic d-DTAB system, due to the differing phase of the underlying combination band signal between these two charged systems.

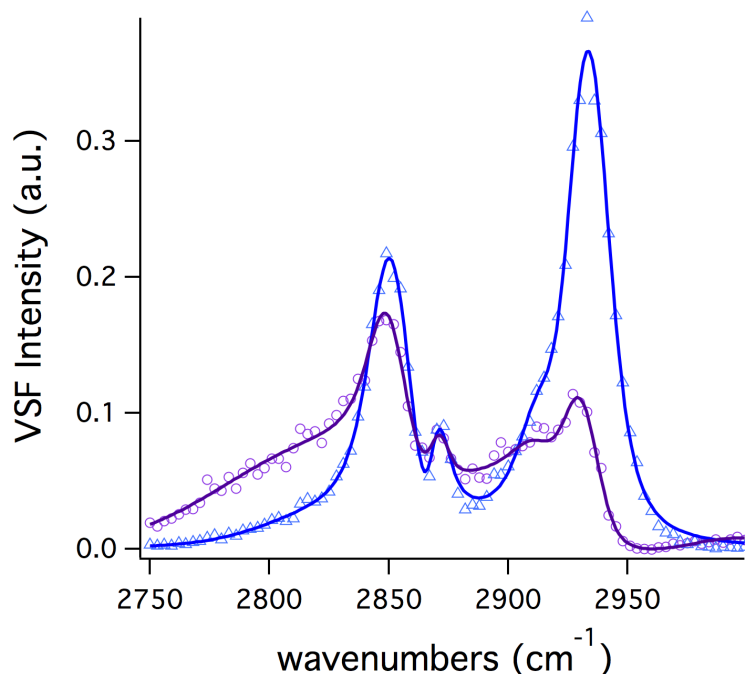


Figure 3.7: VSF spectra in the C-H region of 0.02 mM Span-80 with 0.015 mM d-SDS (circles) and 0.02 mM Span-80 with 0.015 mM d-DTAB (triangles). The C-H stretches of Span-80 are affected by the underlying response from the D₂O stretch + libration combination mode when in the presence of surface charge. Lines are fits to spectra. Full fit parameters can be found in Appendix A, Table A.7.

Additionally, the combination band at these oppositely charged surfaces affects the spectra in the region of the methylene symmetric stretch peak (d⁺) from Span-80, located at $\sim 2850\text{ cm}^{-1}$. Although the underlying combination band signal in the Span-80 + anionic d-SDS system causes this peak to visually appear similar in intensity to the system with cationic DTAB, the mathematical fits report a much higher intensity for this mode when cationic surfactant is present in the co-surfactant mixture versus anionic surfactant, as the water combination band is taken into account (see fit values in Appendix A). Failing to account for the presence of VSF signal produced from the water stretch + libration combination band signal can cause inaccurate results regarding the relative VSF intensities produced by other vibrational modes of interest in the same region.

Although the presence of this VSF signal due to water modes is apparent in the study discussed here, there may be experimental systems where choosing to not account for the combination mode is still appropriate, such as analyzing a spectrum of C-H modes in D₂O at a surface with a net charge close to zero. It is important to understand the experimental factors impacting the surface behavior and spectral features of the

combination mode and analyze systems of interest appropriately. Chapter IV investigates various mixed chemical systems at the oil/water interface where accounting for the water stretch + libration combination mode is imperative for the accurately understanding the system.

This section has investigated the presence of the water stretch + libration combination band at the oil/water surface and its implications for studying the C-H stretching region with vibrational spectroscopies. The following section demonstrates the presence of another broad and weak combination mode from H₂O at the oil/water surface, which is found to be important for studies investigating deuterated hydrocarbon stretches by VSF spectroscopy.

The Water Bend + Libration Combination Band:

The purpose of this section is to report and analyze the presence of H₂O's bend + libration combination band, also known as the "association band", located in the C-D stretching region, arising from interfacial water molecules. This section will show that this water mode is charge dependent, as is expected for interfacial water responses, and that understanding its behavior at the oil/water interface is important when considering what aqueous solvent to use in VSF analysis of deuterated surfactant studies.

Literature has confirmed the presence of a very weak and broad vibrational response from bulk H₂O molecules in the 2000 – 2400 cm⁻¹ range that arises when water bend and water libration motions are excited simultaneously.^{80, 88-92} Because of the weak and broad nature of this mode, its vibrational response spans a large wavenumber region, causing the determination of its peak position maxima to be problematic. These studies have investigated the properties of this combination band in bulk water, however, it is well understood that the behavior of interfacial water molecules varies from that of bulk solution. Thus, this study investigates the water bend + libration combination mode behavior at the oil/water surface by VSF spectroscopy.

Understanding the behavior of this mode at the surface of water is important for any VSF studies investigating C-D stretches (deuterated C-H stretches) in an aqueous H₂O solvent, as the broad response from this combination mode can interfere with the sharp peaks arising from C-D stretches. One previous VSF study by Tyrode et. al.

observed a charge-sensitive background in the C-D stretching region at the air/H₂O interface when investigating the C-D stretching modes from deuterated SDS (d-SDS).⁶⁶ Tyrode et. al. suggested three possible sources for the detected background: 1) the CD₂ methylene Fermi resonance, 2) the symmetric stretch of the CD₂ group next to the sulfate headgroup of SDS, or 3) the combination band of the bending and libration modes of H₂O. Tyrode et. al. provide reason for why either source 1 or 2 from C-D modes listed above are not very plausible sources of signal for the given system, and thus hypothesize the most likely contributing factor to the broad background signal is due to the water bend + libration combination mode. However, their analysis of this background terminates at suggesting the water bend + libration combination mode as the most likely source, and no further investigation on the presence or charge dependence of the mode at the air/water surface is pursued.

The studies in this section investigate the presence and charge sensitivity of the VSF response from this water combination mode in detail at the oil/water surface. By first investigating the region with non-deuterated charged surfactants, we eliminate any potential C-D contributions and can assume all signal observed in the probed region is due to a water response in the presence of a charged surface. Unlike the study performed by Tyrode et. al., the use of non-deuterated surfactants in investigating the behavior of this broad signal excludes any possible contribution of CD₂ methylene Fermi resonance or CD₂ symmetric stretch modes.

We then investigate the features observed when the surfactants are instead deuterated and their C-D stretching modes are detected in the region along with the water response, at both anionic and cationic surfaces. Using our understanding of the water bend + libration combination mode and its effects on C-D spectra at charged surfaces, we will discuss what factors should be considered when determining an aqueous solvent for studying deuterated surfactants with VSF spectroscopy.

A) Experimental considerations for detecting VSF signal in the C-D stretching region at the oil/water interface

Before investigating the VSF signal from the water bend + libration combination mode, we must consider the experimental limitations in the chosen interfacial system. The picosecond VSF laser system used in this study utilizes a bottom-up geometry for observing the CCl_4 /water interface, as discussed in Chapter II. Due to this experimental design, the tunable IR beam passes through ~ 4 cm of CCl_4 oil phase before reaching the water surface. Thus, any absorption of the IR beam at wavelengths within the C-D stretching region by the CCl_4 oil phase must be considered. Figure 3.8 shows the IR transmittance spectrum of liquid CCl_4 with a thickness of ~ 3 mm. It can be seen that CCl_4 molecules begin to absorb IR light at wavenumbers on either side of the C-D stretching region, at ~ 2020 cm^{-1} and ~ 2250 cm^{-1} . Similarly, the IR transmittance spectrum of CO_2 contains a strong IR absorbance beginning at ~ 2200 cm^{-1} . Due to the absorbance of IR light by the CCl_4 oil phase and ambient CO_2 , there is a window of \sim

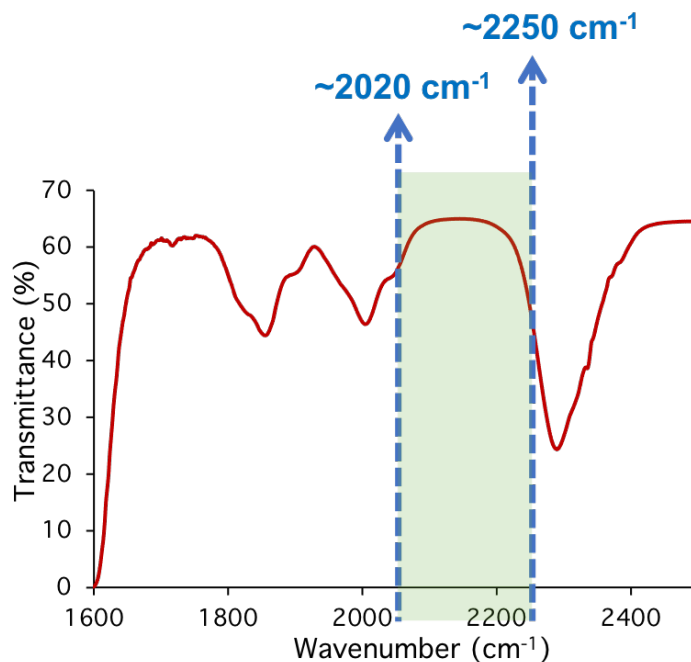


Figure 3.8: IR transmittance spectrum through a CCl_4 layer of ~ 3 mm thickness. The onset of CCl_4 IR absorption in the C-D stretching region is marked by the blue arrows and the region shaded in green corresponds to the window for detecting C-D stretching modes.

2020 – 2200 cm^{-1} for detecting the C-D stretching modes in this experimental system. While C-D stretches are found in the 1950 – 2300 cm^{-1} region and the broad H₂O bend + libration combination mode has been detected in the region of 1900 – 2350 cm^{-1} , the spectral window of 2020 – 2200 cm^{-1} probed in these studies provides a sufficient window for observing both the C-D stretches, as well as the most intense region of the H₂O bend + libration combination mode response.

B) Charge-dependence of the water bend + libration combination mode

Figure 3.9 shows the charge dependence of the H₂O bend + libration combination mode in the presence of both anionic and cationic surfaces. Figure 3.9a shows the VSF spectra from H₂O water molecules as h-SDS (nondeuterated) surfactant is added to the surface. The VSF signal increases in intensity with increased anionic surface charge. This is expected, as the interfacial depth probed by VSF increases as water molecules orient their dipoles in response to the surface charge, as discussed in the previous section. Because the surfactant used in this system is not deuterated, it can be assumed all VSF response detected originates from surface water molecules.

To confirm this charge-dependent water response, Figure 3.9b shows the H₂O bend + libration combination mode signal in the presence of cationic h-DTAB. Similar results of an increase in VSF signal upon increased charged surfactant adsorption is observed. The VSF spectra shown in Figure 3.9 are largely featureless, as expected for the response of the broad H₂O bend+ libration combination mode.⁸⁰ Nevertheless, the increase in intensity upon the addition of either anionic or cationic charge supports the assignment of this broad mode to a VSF resonant response from water.

It is noted that an isotopic dilution study would not be beneficial for this spectral region. As O-D oscillators are introduced into the aqueous phase through deuterated water, the O-D stretch modes would begin to appear in the region of 2000 – 2700 cm^{-1} , which would interfere with the analysis of the O-H stretching modes.

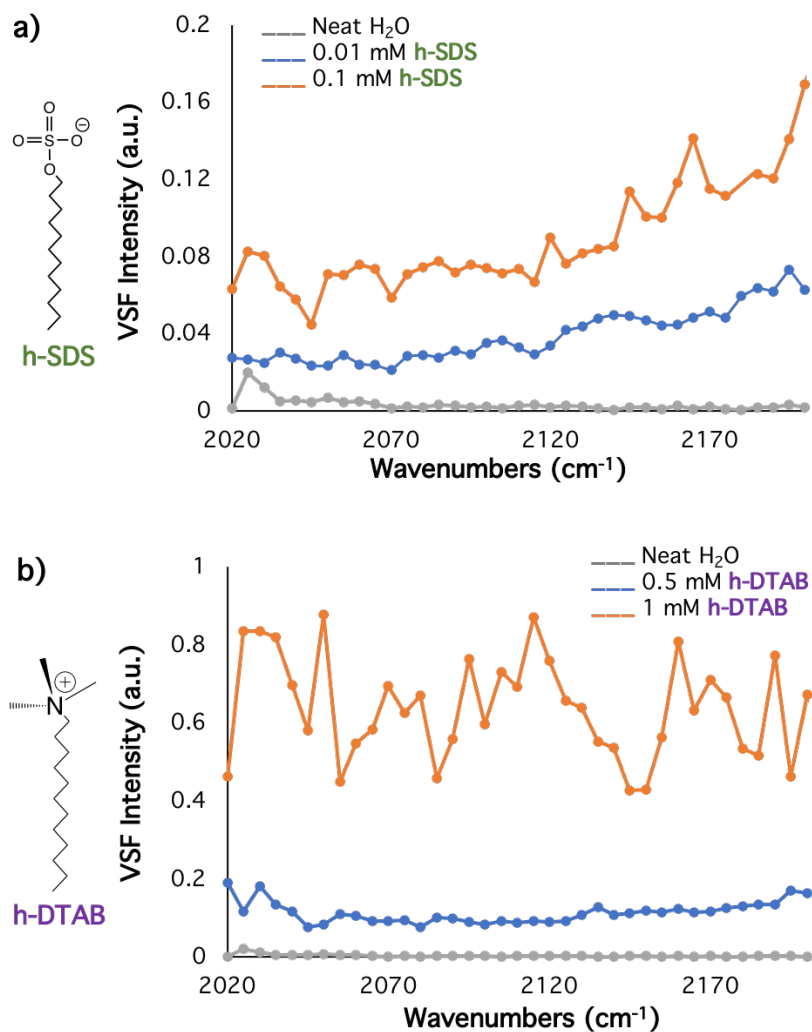


Figure 3.9: VSF spectra of the H₂O bend + libration combination mode in the presence of a concentration series of anionic h-SDS (a) and cationic h-DTAB (b) surfactants. The broad signal in this region attributed to the water bend + libration combination band is amplified upon the presence of surface charge. Lines are guides to the eye.

C) C-D stretching VSF response in the water bend + libration region

With an understanding of the surface charge dependence of the water bend + libration combination mode from Figure 3.9, deuterated surfactant systems containing C-D stretching modes are investigated for both anionic and cationic surfactants. Figure 3.10a shows the VSF spectrum of d-SDS in H₂O in SSP polarizations. The methyl CD₃ symmetric stretch (r+) is observed as a peak at ~2070 cm⁻¹. The broad signal detected from 2100 – 2200 cm⁻¹ contains contributions from the CD₂ methylene symmetric (d+) and asymmetric (d-) stretches, and the CD₃ Fermi resonance mode, located at ~ 2100 cm⁻¹

¹, 2185 cm⁻¹, and 2135 cm⁻¹, respectively.⁶⁶ The intensity of these modes are elevated and their spectral features obscured by the underlying broad H₂O bend + libration combination mode response.

To confirm the contribution of the H₂O bend + libration combination mode response in this region, Figure 3.10b shows the VSF spectra in this region when cationic surfactant is present, allowing a comparison between the two oppositely charged surfaces in Figure 3.10. Due to the 180-degree flip in phase of water molecules between the anionic and cationic surfaces in Figure 3.10, the water modes interfere oppositely in the two spectra with the C-D stretching modes of the deuterated surfactants. This results in the overall lower intensity in the 2100-2200 cm⁻¹ region in the presence of cationic surfactant (Figure 3.10b), and the oppositely increased intensity in this same region in the presence of anionic surfactant (Figure 3.10a) as the C-D stretches and H₂O combination mode interfere.

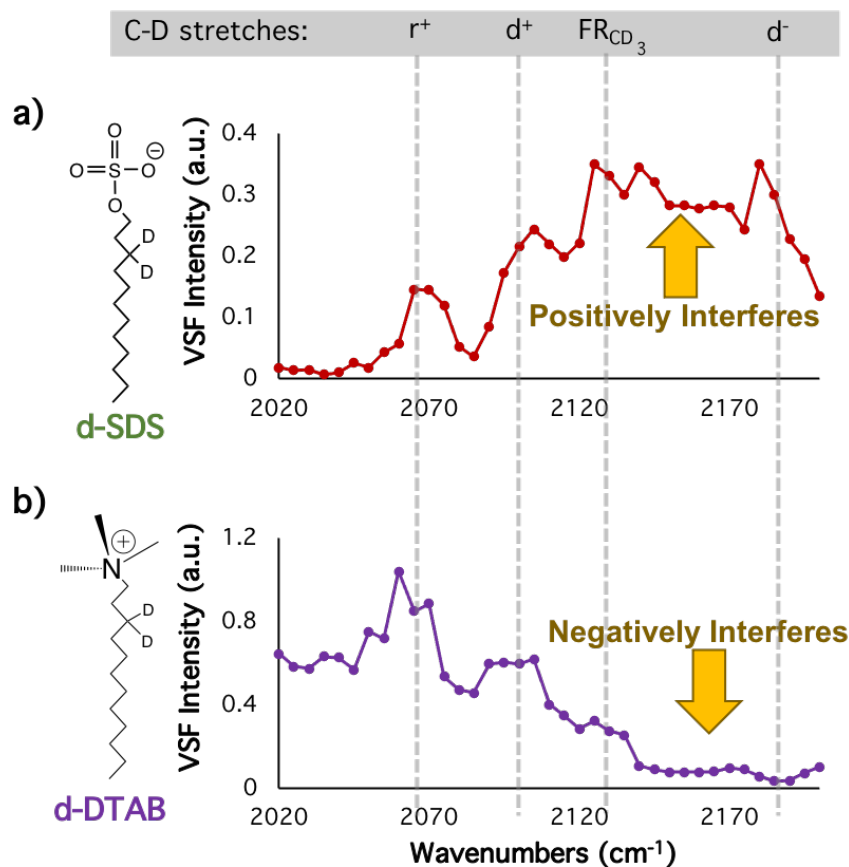


Figure 3.10: VSF spectra of 1.5 mM d-SDS in H₂O (a) and 5 mM d-DTAB in H₂O (b) at the oil/water interface. Due to the oppositely charged surfaces, the C-D stretching modes of the deuterated surfactants interfere oppositely with the underlying water bend + libration combination mode. Lines are guides to the eye.

It is important to consider the presence and charge dependence of the water bend + libration combination mode in the C-D stretching region of VSF spectra when designing and analyzing studies investigating deuterated surfactants at charged aqueous surfaces. Figure 3.11 compares the VSF signal of d-DTAB adsorbed to the oil/water interface in an aqueous solvent of H₂O and D₂O. The use of deuterated water (D₂O) avoids detection of the H₂O bend + libration combination mode in this region. However, interfacial D₂O introduces signal from O-D stretching modes that are also amplified in the presence of a charged surfactant.²⁶ It is seen from Figure 3.11 that both aqueous solvents of H₂O and D₂O produce broad underlying resonant responses, resulting in very similar spectral features between the two systems. However, it is noted that the intensity of the overall response from the H₂O combination mode is weaker than that from the O-D stretching modes from coordinated D₂O molecules. This is an important factor to consider when analyzing C-D stretching modes at a charged surface: If the C-D stretching modes of interest are weak in intensity, an aqueous phase of H₂O may allow less interference of the C-D bands with the aqueous background; however, full

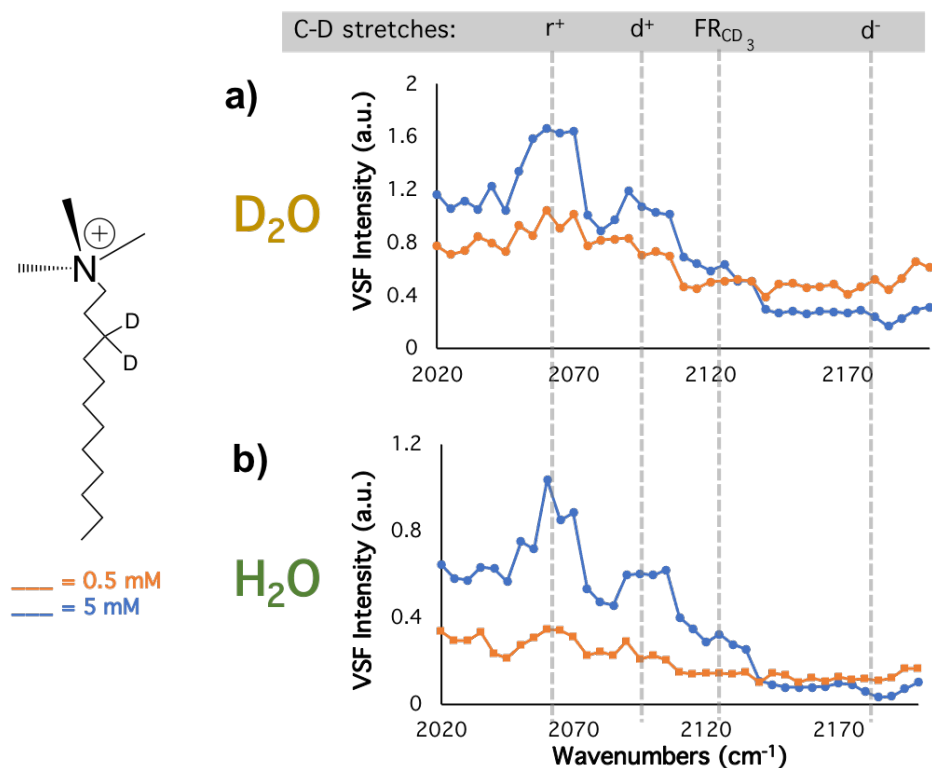


Figure 3.11: VSF spectra of 0.5 mM (orange trace) and 5 mM (blue trace) d-DTAB in D₂O (a) and H₂O (b) aqueous solvents. Either aqueous phase displays background signal in the C-D stretching region, either due to D₂O coordinated O-D stretches, or the H₂O bend + libration combination band. Lines are guides to the eye.

extermination of any underlying resonant response from the aqueous phase is likely not possible.

The work described in this chapter investigates the presence of broad signal in the surface water vibrational spectrum from water combination bands and discusses their implications for analyzing VSF spectra containing other vibrational modes interfering with the water combination mode signal. The following chapter discusses several different mixed systems where both C-H and C-D vibrational modes from surface adsorbates are of interest, incident with the same region encompassed by signal from water combination modes. As such, both the water stretch + libration and bend + libration modes are taken into consideration when investigating the surface structure of mixed systems by VSF spectroscopy at the oil/water interface.

CHAPTER IV:

MIXED SYSTEMS AT THE OIL/WATER INTERFACE

This chapter contains work that will be published with co-authors Evan Christoffersen and Konnor Jones, who performed additional experiments to those reported here investigating the competitive adsorption of nonionic Span-80 and anionic AOT surfactants. I, Rebecca Altman, was the primary contributor to the design and development of the experimental studies and performed the data analysis. Dr. Geraldine Richmond was the principal investigator for this work. This chapter also contains work published in the following citation:

Altman, R. M.; Richmond, G. L., Coming to Order: Adsorption and Structure of Nonionic Polymer at the Oil/Water Interface as Influenced by Cationic and Anionic Surfactants. *Langmuir* **2020**, *36* (8), 1975-1984.

Surface chemistry applications utilize the chemical properties of various surface-active molecules to alter the structure and behavior of interfaces.^{9, 65, 93-105} Surface adsorbates allow the controlled functionalization of interfaces, which is crucial to applications such as targeted drug delivery, environmental remediation techniques, and the formation of functionalized polymer films.^{9, 11, 106-121} However, the surface dynamics of mixed systems can vary significantly depending on the chemicals involved. Because many surface chemistry applications rely on the details of chemical adsorption at buried liquid/liquid interfaces, a molecular-level understanding of the structure of these buried interfaces is needed.

This chapter includes studies that use VSF spectroscopy and surface pressure measurements to investigate several different mixed systems at the oil/water interface, including nonionic polymers/surfactant systems, as well as co-surfactant mixtures. Specifically, the interfacial structure formed by the interactions between nonionic functional groups and charged surfactants are probed to understand how they alter the overall interfacial properties at the buried oil/water interface. Building off of the knowledge of water's fundamental behavior at both neat and charged oil/water interfaces

discussed in Chapter IV, the studies investigated here analyze the VSF response of polymer and surfactant functional groups in aqueous solution.

I) Nonionic Polymer + Surfactant Systems

Polymer-surfactant mixtures have been studied extensively both in bulk solution and at surfaces, due to their prevalent use in industrial, environmental, and pharmaceutical application.^{99, 103, 108, 115, 122-133} The majority of these studies have focused on the behavior of charged polyelectrolytes and surfactants with oppositely charged headgroups. The strong electrostatic interactions between these polyelectrolytes and charged surfactants significantly impact their cooperative attraction, both in bulk solution and at surfaces. However, many applications of polymer-surfactant solutions utilize mixed systems of nonionic polymers with surfactants, where the strong charge-charge interactions between species no longer exist.^{98, 108, 115, 127, 134-138}

This section investigates several different nonionic polymers and their behavior at the buried oil/water interface when alone in solution and in mixed systems with charged surfactants. Nonionic polymers that favorably adsorb to the oil/water interface when alone in solution are found to be minimally affected by the added presence of charged surfactant. However, surface-inactive nonionic polymers are drawn to the interface by synergic interactions with charged surfactants. The molecular functional groups present on the nonionic polymer play a significant role in the polymer's interaction (or lack thereof) with charged surfactants.

A) Nonionic polymers alone at the oil/water surface

Understanding the surface behavior of nonionic polymers alone at the surface allows comparison of their behavior when in the presence of charged surfactants. Here, the surface behaviors of three different nonionic polymers are studied at the CCl₄/H₂O surface: polyvinyl alcohol (PVA), polyethylene glycol (PEG), and polyacrylamide (PAM). Full chemical specifications for each of these polymers can be found in the materials section in Chapter II.

Figure 4.1 shows the VSF spectrum in SSP polarizations of 0.15 mM PVA at the D₂O/CCl₄ interface. The peak at $\sim 2915 \text{ cm}^{-1}$ is due to the methylene symmetric stretch

(d+) of the C-H bonds on the polymer backbone. The weak shoulder at $\sim 2950\text{ cm}^{-1}$ results from the methylene asymmetric stretch (d-). Although the polymer has an alcohol functional group bonded to the backbone, the D_2O solvent readily causes hydrogen-deuterium exchange to occur on this alcohol group, causing the O-H stretch of the polymer to be found in the region of O-D stretch oscillators ($2400 - 2700\text{ cm}^{-1}$), which is obscured from VSF signal of the D_2O solvent, encompassing the same region.

It can be observed that this polymer is not only present at the surface, but also adopting an orientation that allows the methylene symmetric stretch (d+) to be detected by VSF in SSP polarizations, suggesting the d+ vibrational dipole has a net order perpendicular to the surface. PVA's hydrocarbon backbone is likely interacting with the hydrophobic oil phase while the alcohol functional groups are solvated in the aqueous phase, causing favorable adsorption to the interface. This differs notably from the behavior of polyelectrolytes, whose charged functional groups cause the polymer chains to be more favorably solvated in bulk solution, rather than adsorbing to the surface. In this way, the PVA polymer acts as a surface-active molecule that alone can alter the molecular properties of the interface as it adsorbs.

Where the alcohol group on PVA is branched from the polymer backbone, PEG is instead a nonionic polymer with a continual chain of carbon and oxygen atoms, with no functional groups other than hydrogen atoms bonded to the chain. Figure 4.2 shows the VSF spectrum in SSP polarizations of 0.015 mM PEG at the $\text{CCl}_4/\text{D}_2\text{O}$ surface. The

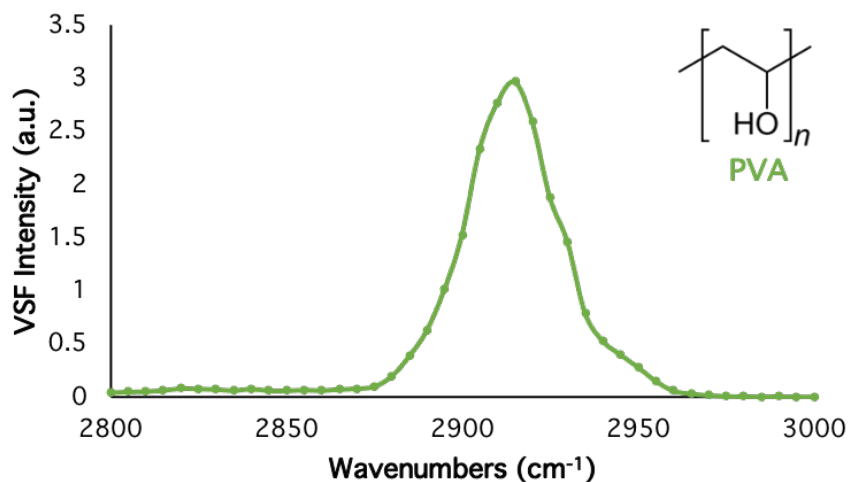


Figure 4.1: The VSF spectrum in SSP polarizations of 0.15 mM PVA at the $\text{CCl}_4/\text{D}_2\text{O}$ interface. The sharp peak at $\sim 2915\text{ cm}^{-1}$ is due to the methylene symmetric stretch of the polymer backbone, showing PVA is surface-active and ordered at the surface. Line is a guide to the eye.

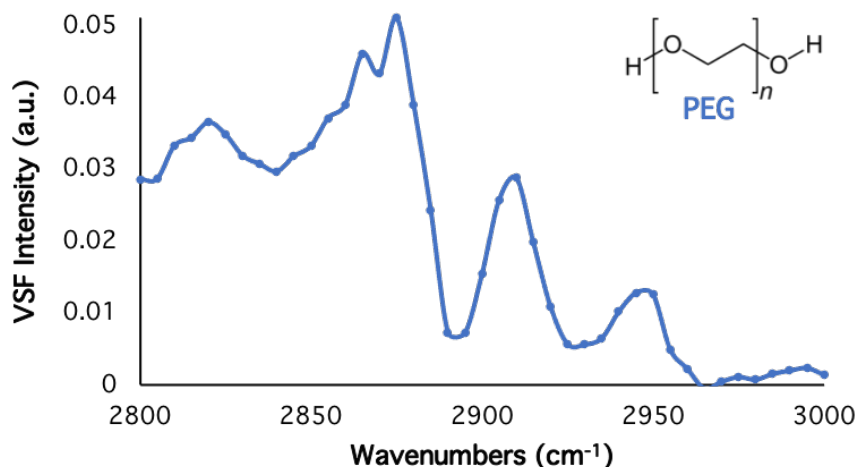


Figure 4.2: The VSF spectrum in SSP polarizations of 0.015 mM PEG at the $\text{CCl}_4/\text{D}_2\text{O}$ interface. The sharp C-H stretches due to the polymer backbone show PEG is present and ordered at the surface. Line is a guide to the eye.

methylene symmetric (d+), methylene asymmetric (d-), and methylene Fermi resonance (FR_{CH_2}) peaks are observed at ~ 2865 , 2910 , and 2940 cm^{-1} , respectively.¹³⁹ Where the methylene asymmetric stretch (d-) was not as prevalent in the SSP spectrum perpendicular to the interface with PVA, it is much more present in the spectra of PEG. Interestingly, PEG also adsorbs readily with a net structure to the interface even though it does not have a continual hydrocarbon backbone as PVA does, hydrophobically interacting with the oil phase.

The long, broad tail to the red region of the spectrum is attributed to the presence of VSF signal from the water stretch + libration combination mode discussed in Chapter III. The interaction of the oxygen groups of PEG with the water molecules at the surface likely induces a net order in the water molecules that allows detection of the weak water stretch + libration combination mode. If the broad signal in the $2800 - 2850 \text{ cm}^{-1}$ region of the PEG spectrum in Figure 4.2 is in fact due to the presence of the water stretch + libration combination mode, the same feature should be observed in the $3750 - 4000 \text{ cm}^{-1}$ VSF spectral region in an aqueous phase of H_2O , as discussed extensively in Chapter III. Figure 4.3 shows the VSF spectrum in SSP polarizations of 0.15 mM PEG in H_2O . The signal detected blue of the free OH ($\sim 3770 \text{ cm}^{-1}$) supports the claim that the VSF signal from the water stretch + libration combination mode is enhanced at the oil/water interface in the presence of PEG.

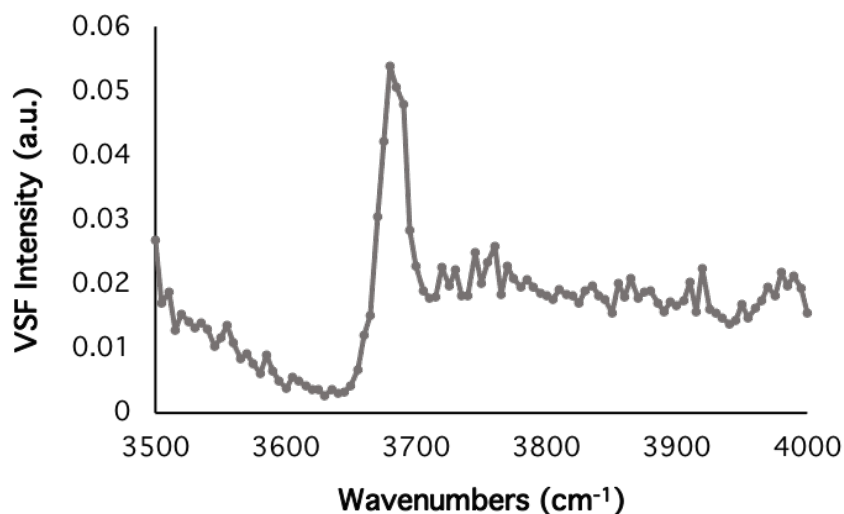


Figure 4.3: The VSF spectrum in SSP polarizations of 0.15 mM PEG at the $\text{CCl}_4/\text{H}_2\text{O}$ interface in the H_2O vibrational region. Signal in the $3800\text{-}4000\text{ cm}^{-1}$ region is observed, indicating the water stretch + libration combination band signal is amplified upon the surface presence of PEG. Line is a guide to the eye.

Surface pressure measurements show that PEG is even more surface active than PVA, with a surface pressure value of $21 \pm 1\text{ mN/m}$ for 0.15 mM PEG and $10 \pm 1\text{ mN/m}$ for 0.15 mM PVA. Although the oxygen atoms are imbedded in the PEG's chain, the large conformational space of this flexible polymer allows it to favorably adsorb to the oil surface in a manner allowing a net orientation of the methylene stretch dipoles to have a component perpendicular to the surface, as detected by VSF in SSP polarizations.

The conformational structures and functional groups of these first two nonionic polymers, PVA and PEG, cause the chains to be surface active. However, this behavior is not the case for all nonionic polymers. Figure 4.4 shows the VSF spectrum of nonionic PAM in SSP polarizations at the $\text{CCl}_4/\text{D}_2\text{O}$ surface. Figure 4.4 shows weak signal from interfacial PAM in the C-H stretching region. Due to PAM's extremely low surface activity, a higher concentration is necessary to observe any signal in the C-H stretching region, compared to PVA and PEG. The peak at $\sim 2930\text{ cm}^{-1}$ corresponds to the methylene symmetric stretch (d^+) of the PAM backbone.¹⁴⁰ While this weak peak is detectable for a solution of 1.4 mM PAM at the oil/water interface, corresponding surface pressure measurements of this system are unable to detect any molecular adsorption to the surface, resulting in a value of $0 \pm 1\text{ mN/m}$ for 1.4 mM PAM. This indicates that the PAM polymer does not readily adsorb to the surface in a manner that causes the chemical

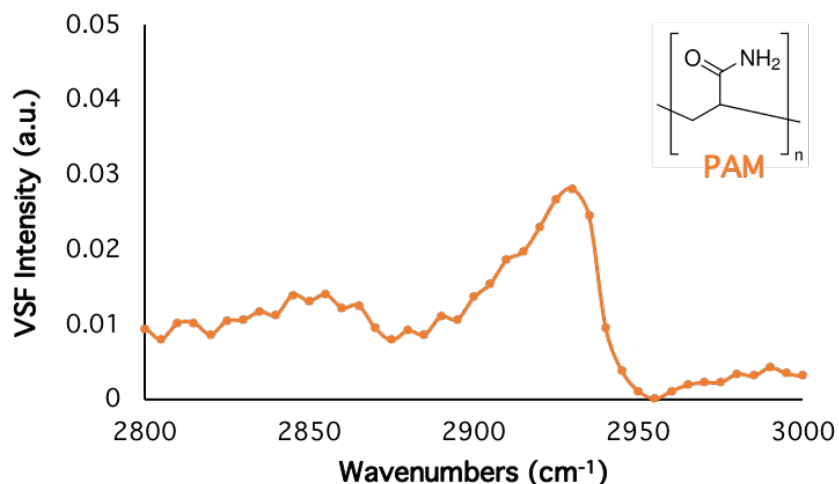


Figure 4.4: The VSF spectrum in SSP polarizations of 1.4 mM PAM at the $\text{CCl}_4/\text{D}_2\text{O}$ interface. Slight C-H stretching signal from the polymer backbone is observed at $\sim 2930 \text{ cm}^{-1}$. Line is a guide to the eye.

bonding environment between surface molecules in this system to differ than that of a bare water/oil surface. Because VSF is a more sensitive surface technique than pendant drop tensiometry, slight signal from PAM is observed in Figure 4.2 despite the surface pressure measurements indicating no adsorption. This weak signal from PAM could in part be due to the polymer's random dispersion throughout the bulk aqueous phase, rather than favorable interactions causing the polymer to preferentially adsorb to the surface. Due to the weak VSF signal and inability of surface tensiometry to detect any presence of PAM at the oil/water surface, PAM is referred to in this study as a surface in-active polymer when alone in solution, while PEG and PVA display high levels of surface activity.

The next section will investigate and discuss the effects on these polymers' surface activities when they are components of a mixed system with charged surfactant molecules.

B) Surface-active nonionic polymers with charged surfactants

To investigate the role of electrostatic interactions on the structure of nonionic polymer-surfactant mixed systems at the oil/water interface, PVA and PEG were analyzed by VSF spectroscopy in the presence of both cationic and anionic surfactants. Because PVA and PEG are both surface-active polymers, any changes to their interfacial structure in the mixed system is attributed to their interaction with the charged surfactants

at the surface. Figure 4.5 shows the chemical structures of the two surfactants used in this section.

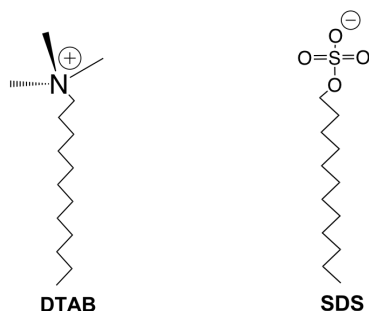


Figure 4.5: The chemical structures for the two charged surfactants investigated in this section: dodecyltrimethylammonium bromide (DTAB) and sodium dodecyl sulfate (SDS).

Figure 4.6 compares the VSF spectra of the polymer PVA by itself at the surface and in the presence of cationic or anionic charged surfactants. All surfactants used in these mixed systems were fully deuterated, so the only C-H stretch modes detected are due to the polymer's presence at the surface. Figure 4.6 shows both the SSP and SPS spectra for these systems, probing the components of the polymer's C-H vibrational dipole moments that are perpendicular and parallel to the interfacial surface, respectively. It is noted that where the methylene asymmetric stretch (d-) is simply a weak shoulder in the SSP spectrum of PVA alone (blue trace), it is much more prevalent in the SPS spectrum, indicating the d- mode has a higher component of its vibrational dipole oriented parallel to the surface.

Upon the addition of deuterated charged surfactant to the PVA aqueous system, the SSP spectrum in Figure 4.6 shows slight changes in intensity of the PVA d+ mode. The intensity appears to increase slightly from the PVA only system (blue trace) with the addition of both cationic and anionic charged surfactant (green and orange traces, respectively). However, the SPS spectrum shows no evidence of a corresponding intensity change in the d- mode upon the addition of charged surfactants. Surface pressure measurements report a surface pressure for the bare surface as 10 ± 1 mN/m, and values of 11 ± 1 mN/m and 12 ± 1 mN/m for 0.15 mM PVA with 0.015 mM d-DTAB and 0.015 mM d-SDS, respectively. The small change in the VSF spectra of PVA alone compared to its presence in the mixed systems, along with the negligible changes in

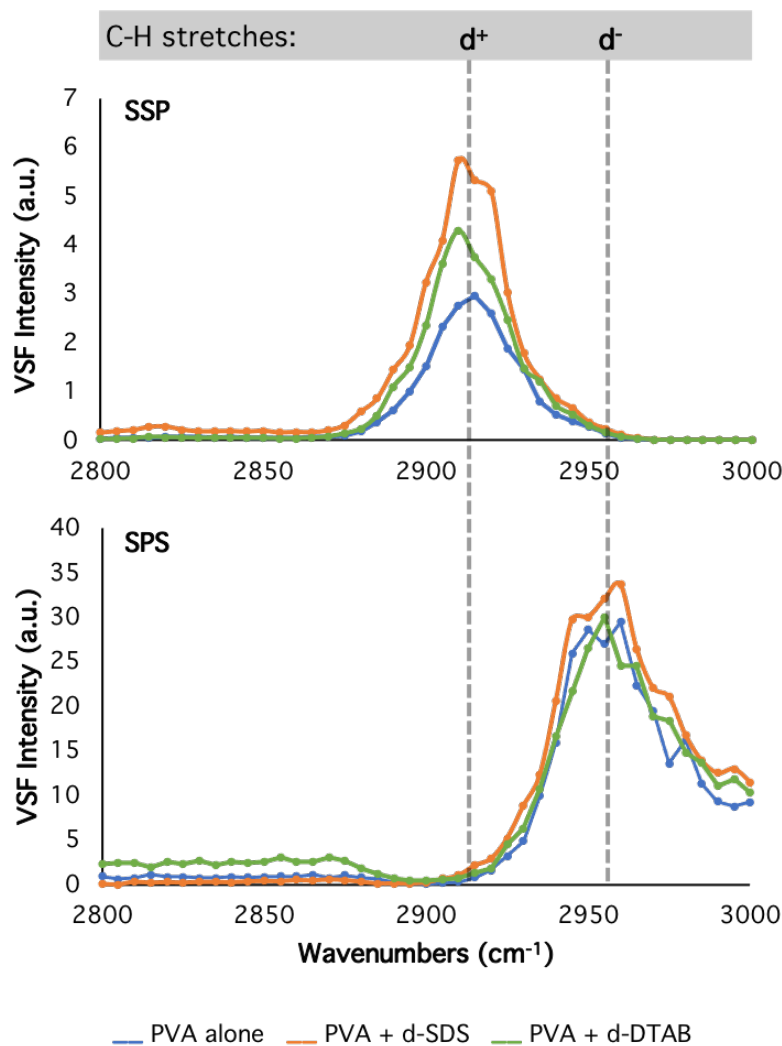


Figure 4.6: The VSF spectra in SSP and SPS polarizations of 0.15 mM PVA at the $\text{CCl}_4/\text{D}_2\text{O}$ interface with no surfactant (blue trace), 0.015 mM anionic d-SDS (orange trace), and 0.015 mM cationic d-DTAB (green trace). Signal intensity from the C-H stretching modes of the polymer are analyzed with the presence of cationic and anionic surfactant. Lines are guides to the eye.

surface pressure measurements for the three systems indicates that PVA's interfacial population and dipole orientations do not change significantly upon the addition of charged surfactant. This could indicate that PVA's attractive interactions with the oil and water molecules at the $\text{CCl}_4/\text{D}_2\text{O}$ interface are more favorable than any intermolecular interactions between PVA and DTAB or SDS molecules. It is noted that evidence of the water stretch + libration combination mode is not apparent in any of the spectra in Figure 4.6, even upon the addition of anionic surfactant, which has been shown to increase the visual appearance of the combination mode in this region (Chapter III). While the water combination mode is still present at this interface, it is likely the C-H stretch modes

detected in this spectrum display such strong signal that the combination mode has negligible effects on the spectra of these PVA systems.

The VSF spectra of chemical systems with the surface-active nonionic polymer, PEG, is shown in Figure 4.7 in SSP and SPS polarizations. The spectra of 0.015 mM PEG alone at the CCl₄/D₂O surface and with 0.015 mM d-DTAB and 0.015 mM d-SDS are shown as the blue, green, and orange traces, respectively. Once again, the surfactants in the mixed system are fully deuterated so the only observable VSF signal in this region comes from the PEG polymer. As discussed in Figure 4.2, PEG shows three peaks in the SSP spectrum, corresponding to the methylene symmetric (d⁺), asymmetric (d⁻) and Fermi resonance (FR_{CH₂}) modes. Figure 4.7 also shows C-H signal in the SPS spectrum,

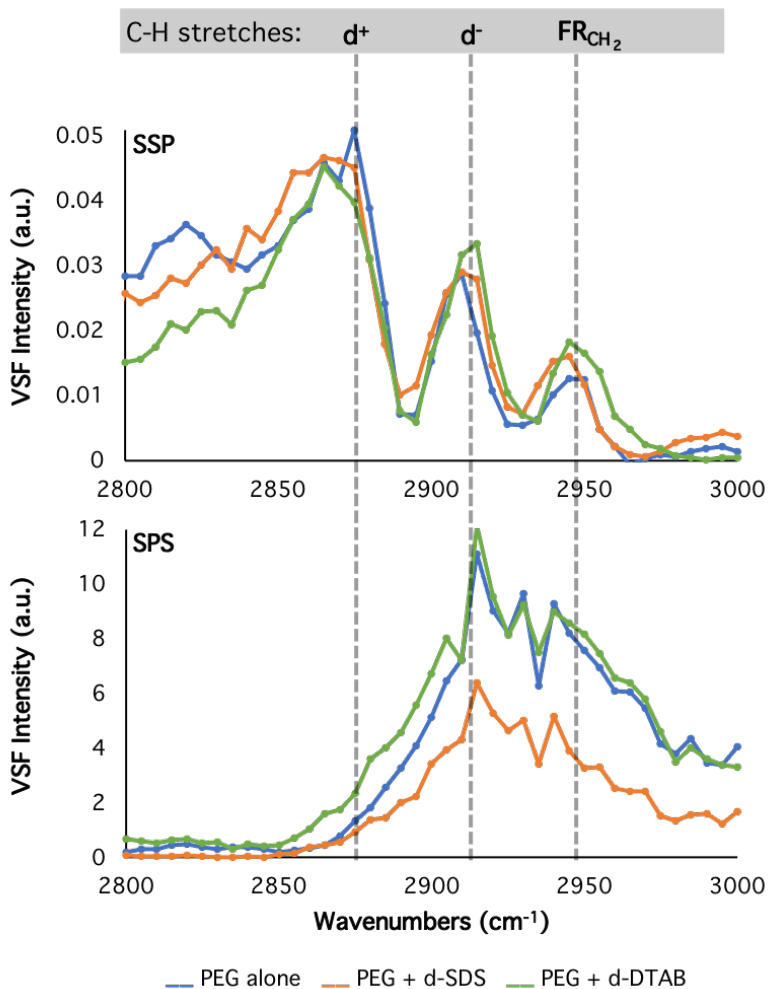


Figure 4.7: The VSF spectra in SSP and SPS polarizations of 0.015 mM PEG at the CCl₄/D₂O interface with no surfactant (blue trace), 0.015 mM anionic d-SDS (orange trace), and 0.015 mM cationic d-DTAB (green trace). Signal intensity from the C-H stretching modes of the polymer are analyzed with the presence of cationic and anionic surfactant. Lines are guides to the eye.

which indicates the methylene asymmetric and Fermi resonance dipoles have contributions parallel to the interfacial surface. As discussed above from Figure 4.3, PEG alone causes VSF detection of the water combination mode at the $\text{CCl}_4/\text{water}$ surface, evidenced here by the broad signal in the $2800 - 2850 \text{ cm}^{-1}$ region.

Comparison between the VSF spectra in Figure 4.7 of PEG alone (blue trace), and PEG with cationic and anionic surfactants (green and orange traces, respectively) in both SSP and SPS polarizations indicate very little, if any, changes to the polymer's surface behavior with the addition of either cationic or anionic charged surfactant. Similar to what was observed in Figure 4.6 with PVA, the interfacial structure of this surface-active polymer appears to be minimally influenced by the presence of charged surfactants. To further investigate the apparent lack of change in the surface behavior of PEG when in a mixed system, Figure 4.8 compares the VSF spectra of the chemical systems containing PEG in a PPP polarization combination, which probes VSF-active modes that are either perpendicular or parallel to the surface.

Figure 4.8a shows the PPP spectra for PEG alone compared to PEG with anionic d-SDS surfactant. Once again, the spectra for these two systems display very little differences in the polymer's interfacial behavior with and without anionic surfactant. Figure 4.8b, however, shows the PPP spectra for PEG alone at the surface compared to in a mixed system with cationic d-DTAB surfactant. These spectra in Figure 4.8b, while still largely similar, do display some differences in PEG's C-H stretching region when d-DTAB is also present. However, analysis of the slight changes to the spectral features upon addition of d-DTAB reveals this difference is likely not due to changes in the polymer's C-H stretch behavior at the surface, but rather differences in how the D_2O stretch + libration combination mode manifests in the spectrum when cationic DTAB is present at the surface.

From the understanding of the water stretch + libration combination mode behavior in the presence of cationic surfactant discussed in Chapter III, cationic surfactants at the surface cause the phases of the water combination mode to destructively interfere with the nonresonant response, resulting in a very low overall VSF signal detected for the overall region of the water combination mode at the surface. In Figure 4.8b, this phase relationship of the water mode and the cationic nonresonant causes the C-

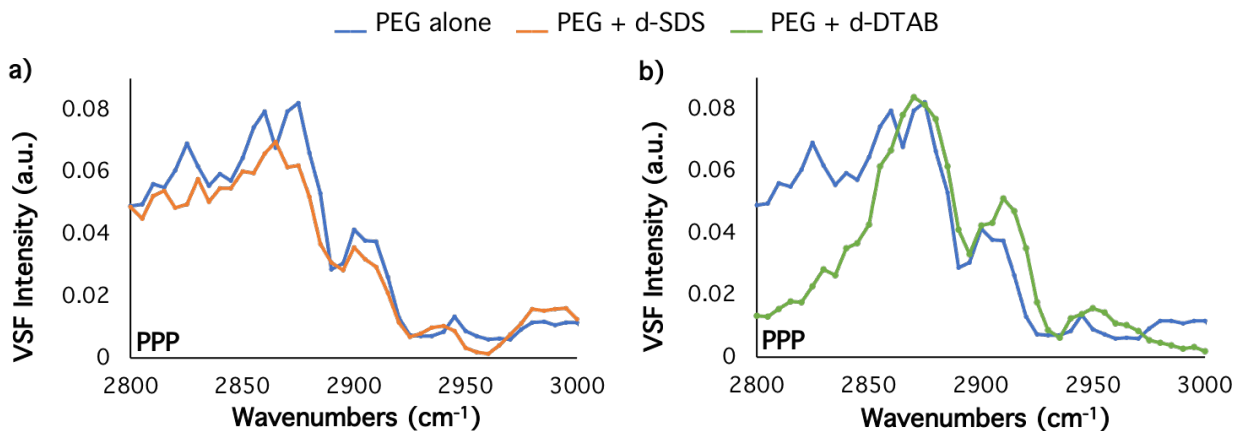


Figure 4.8: The VSF spectrum in PPP polarizations of 0.015 mM PEG at the $\text{CCl}_4/\text{D}_2\text{O}$ interface with no surfactant (blue trace), and with 0.015 mM anionic d-SDS (orange trace, 7a), and 0.015 cationic d-DTAB (green trace, 7b). Signal intensity from the C-H stretching modes of the polymer are analyzed with the presence of cationic and anionic surfactant. Lines are guides to the eye.

H stretch modes of PEG to interfere differently with the signal from the water combination mode than what is observed for PEG alone at the surface, where the water stretch + libration combination mode is detected by VSF (see Figure 4.3). This difference in interference results in an overall lower VSF intensity detected in the $2800 - 2850 \text{ cm}^{-1}$ region, as well as slightly different spectral shapes for the C-H stretch modes of PEG. Thus, while the few differences between the spectra shown in Figure 4.8b may initially appear to indicate that PEG's interfacial behavior is affected by the presence of cationic surfactant, it's surface behavior is likely unchanging, and rather producing different spectral features due to a different interference with the combination mode.

It is noted that a similar observation is not seen when PEG is in the presence of anionic SDS in Figure 4.8a. Compared to PEG, anionic surfactant causes very similar spectral features of the water combination mode at the surface as detected by VSF spectroscopy (see Figure 3.4a in Chapter III). Thus, the combination mode in Figure 4.8a does not display a difference between the PEG systems when the polymer is alone at the surface and when it is in a mixed system with anionic surfactant.

The PPP spectra shown in Figure 4.8 confirm the lack of change in PEG's surface activity upon the addition of other charged surface-active molecules, similar to what was observed for PVA. As charged surfactant does not alter PEG's surface behavior, the following discussion investigates two additional experimental factors that may affect the surface behavior of PEG in a mixed system: polymer concentration and hydrophobicity.

Figure 4.9 shows the VSF spectra of the same PEG chemical systems discussed above in Figure 4.7, however, with the polymer concentration increased by an order of magnitude. The spectra in Figure 4.9 show more apparent changes in the C-H stretches of the PEG polymer when charged surfactant is present. In the SSP spectra in Figure 4.9, the C-H peaks of PEG appear to increase significantly upon the addition of anionic d-SDS. However, the elevated background VSF signal intensity in the 2800 – 2850 cm^{-1} region also increases significantly, indicating a possible increase in the signal contribution from the water stretch + libration combination mode.

To help better understand the source of the increased signal in Figure 4.9 upon addition of anionic surfactant, surface pressure measurements were taken. The surface

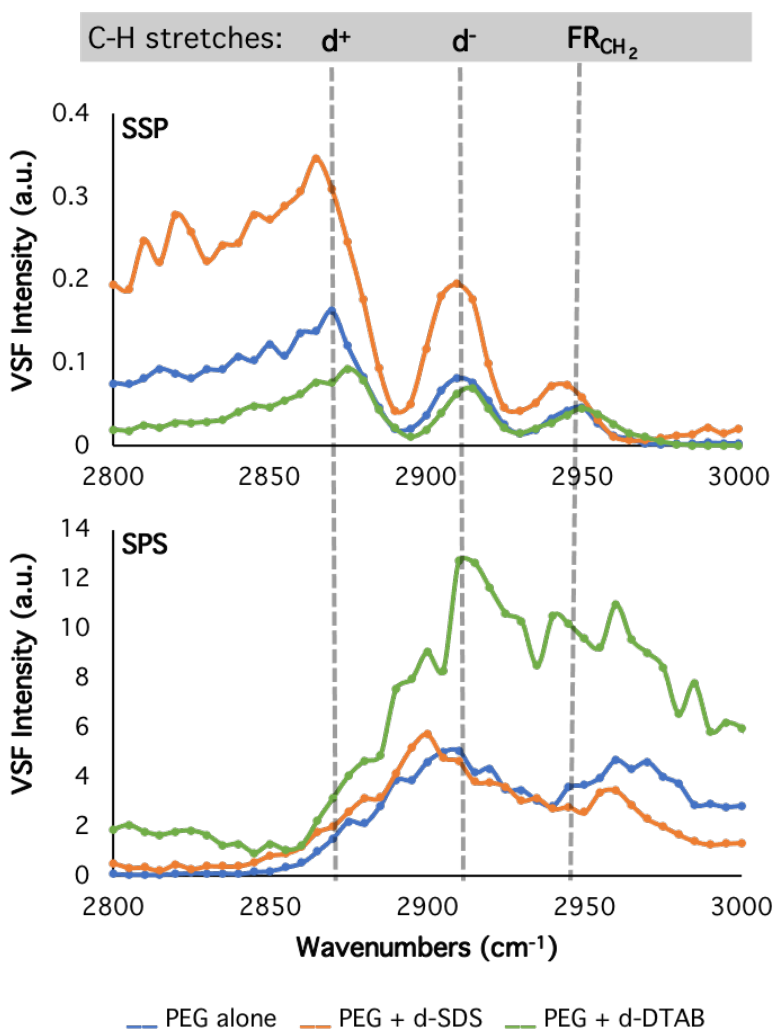


Figure 4.9: The VSF spectrum in SSP and SPS polarizations of 0.15 mM PEG at the $\text{CCl}_4/\text{D}_2\text{O}$ interface with no surfactant (blue trace), 0.015 mM anionic d-SDS (orange trace), and 0.015 mM cationic d-DTAB (green trace). Signal intensity from the C-H stretching modes of this higher concentration of polymer are analyzed with the presence of cationic and anionic surfactant. Lines are guides to the eye.

pressure of 0.15 mM PEG alone at the surface is measured to be 21 ± 1 mN/m. When combined with 0.015 mM d-SDS, the surface pressure does not significantly change, equilibrating to a value of 22 ± 1 mN/m. This indicates that the presence of anionic surfactant does not induce additional adsorption of PEG to the surface. Before the studies performed in Chapter III, these surface pressure measurements would seem to indicate a reorientation of the polymer's conformation at the surface, causing the increase in VSF signal intensity of the C-H stretches. However, now that we understand the water stretch + libration combination mode is present in this region and affected by surface adsorbates, there are actually two factors that could be contributing to the increase in PEG's C-H stretch intensity upon the addition of d-SDS in the SSP spectrum of Figure 4.9: 1) the increase in the water combination band intensity causes PEG's C-H stretching modes to interfere with the underlying signal, displaying an overall higher intensity, or 2) the C-H dipoles of the PEG backbone reorient in response to the anionic charge at the surface, causing larger components of the C-H stretch vibrational dipoles perpendicular to the surface. Additional studies would need to be performed to distinguish the true source for this increase in signal. It is noted that the spectra of 0.15 mM PEG alone and 0.15 mM PEG with cationic d-DTAB in the SSP spectra in Figure 4.9 do not show significant variation.

Interestingly, the SPS spectra in Figure 4.9 show a different trend in PEG's C-H stretches. When probing the methylene asymmetric stretch (d-) and methylene symmetric stretch (d+) vibrational dipoles parallel to the oil/water surface, PEG alone at the surface does not show much variation in the SPS spectrum compared to the addition of anionic d-SDS. However, there is an overall increase in intensity of these C-H stretches when cationic d-DTAB is introduced into the polymer mixed system. Comparing the surface pressure values of 0.15 mM PEG by itself to that of 0.15 mM PEG with 0.015 mM d-DTAB suggest no significant effect on the interfacial adsorption between the two systems, with measured surface pressure values of 21 ± 1 mN/m and 20 ± 1 mN/m for PEG alone and PEG with d-DTAB, respectively. Thus, the increase in the C-H stretches of PEG in the SPS spectrum could be due to a reorientation of the C-H modes in the presence of cationic surfactant so that its signal detected by VSF parallel to the interface increases. However, future studies would need to be performed to confirm this behavior.

This analysis of mixed systems with a higher concentration of PEG unveils the complicated structures that flexible polymers with large conformational spaces such as PEG can form at the surface. While the spectra shown in Figure 4.9 suggest that charged surfactants may have some effect on the interfacial behavior of PEG, determining its specific behavior and interaction with surfactants is experimentally challenging due to the large conformational space of the polymer. However, the effects of one last variable on the interactions between polymers and surfactants are tested: the hydrophobicity of the polymer chain.

To investigate the impact of the polymer's hydrophobicity on intermolecular interactions with charged surfactants a mixed system, a polymer similar to PEG but with additional hydrophobic properties was studied. Pluronic F127 (hereafter referred to as F127) is a block co-polymer that has polyethylene glycol (PEG) monomers on either end of the polymer strand and polypropylene glycol (PPO) monomers in the middle, as shown in Figure 4.10. The PPO monomers contain an additional methyl group bonded to the polymer backbone, thus increasing F127's overall hydrophobic nature when compared to the PEG polymer studied above.

Figure 4.10 shows the VSF spectrum in SSP polarizations for the polymer F127 alone at the surface (blue trace), and in the presence of 3 mM and 8 mM d-SDS (light and

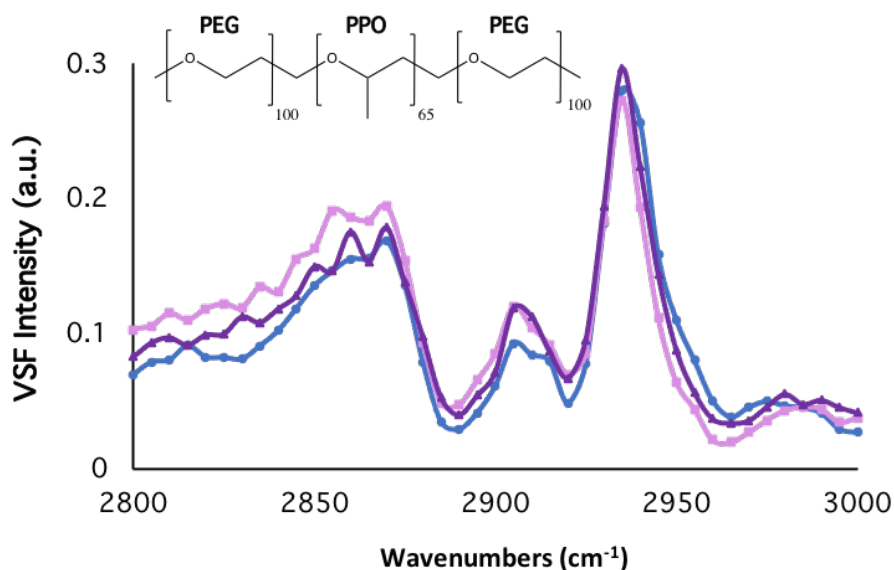


Figure 4.10: The VSF spectrum in SSP polarizations of 132 ppm F127 at the $\text{CCl}_4/\text{D}_2\text{O}$ interface with no surfactant (blue trace), 0.27 mM d-SDS (light purple trace), and 0.8 mM d-SDS (dark purple trace). Signal intensity from the C-H stretching modes of this more hydrophobic polymer are analyzed with the presence of anionic surfactant. Lines are guides to the eye.

dark purple traces, respectively). The SDS surfactant used in these mixed systems was fully deuterated so the only observable C-H modes in this region are from the polymer's VSF response at the surface. The concentration of F127 is reported in parts per million (ppm), as there are two different monomer units in each polymer strand. For reference, the 132 ppm of F127 contained in all systems shown in Figure 4.10 corresponds to monomer concentrations of 2 mM ethylene glycol (from PEG ends) and 0.7 mM propylene glycol (from PPO center).

The SSP spectra of all three systems probing the C-H stretches of F127 in Figure 4.10 show three peaks corresponding to the same methylene symmetric (d+), methylene asymmetric (d-), and Fermi resonance modes that were probed for the PEG polymer (see Figures 4.7 and 4.9). However, there are additional modes contributing to the signal of large peak at $\sim 2935\text{ cm}^{-1}$ from the methyl (CH_3) group of PVA, including its strong Fermi resonance response.^{34, 66} Additionally, the SSP spectra of all three F127 systems in Figure 4.9 contain a weak peak around $\sim 2965\text{ cm}^{-1}$, corresponding to the methyl asymmetric stretch (r-), again arising from the presence of the methyl CH_3 functional groups in the PPO monomers in the F127 polymer.

The three spectra in Figure 4.10 of F127 alone at the surface and with increasing amounts of d-SDS are strikingly similar. The lack of variance in the VSF spectra of the three systems indicates that any hydrophobic interactions between the PEG polymer and the charged surfactants does not alter the polymer's surface behavior.

All chemical systems discussed in this section investigated surface-active nonionic polymers in mixed systems with charged surfactants at the oil/water interface. While it could be argued that some spectra displayed in this section imply charged surfactants can have some effect on the interfacial behavior of nonionic polymers, the majority of the data suggests negligible intermolecular interactions between the surface-active nonionic polymers and charged surfactants. Additional studies would need to be performed to verify any possible effects of charged surfactants on the surface activity of the nonionic polymers studied here.

C) Nonionic polymer PAM + charged surfactants

This section investigates the interfacial behavior of a surface-inactive nonionic polymer as induced by its intermolecular interactions with charged surfactants at the oil/water interface. In section A of this chapter, polyacrylamide (PAM) was shown to be surface-inactive when alone in solution. Here, we will investigate how its surface behavior is drastically affected by the hydrophobic and electrostatic properties of charged surfactants. Figure 4.11 shows the chemical structures of the surfactants used in these studies.

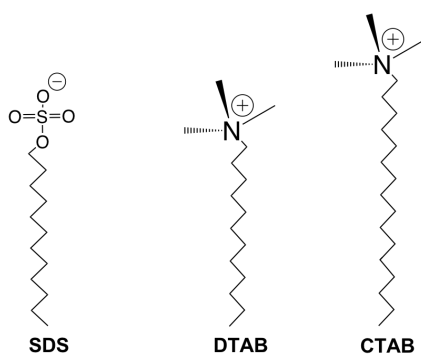


Figure 4.11: The chemical structures for the three charged surfactants used in this section: sodium dodecyl sulfate (SDS), dodecyltrimethylammonium bromide (DTAB) and cetyltrimethylammonium bromide (CTAB).

Figure 4.12 shows surface pressure measurements for polyacrylamide (PAM) systems at the CCl_4 /water interface. PAM is not surface active by itself at the oil/water interface at any concentration, as indicated by the yellow line in Figure 4.12. The orange, green, and blue traces in Figure 4.12 correspond to mixed systems of PAM at different concentrations with cationic CTAB, DTAB, and anionic SDS surfactants, respectively. The concentrations of the surfactants were chosen such that their surface pressure values when alone in solution are similar, indicating comparative levels of surface activity: 1.8 ± 0.1 mN/m, 1.53 ± 0.06 mN/m, 1.6 ± 0.1 mN/m, and 0.001 mM CTAB, for 0.015 mM DTAB, 0.015 mM SDS and, respectively.

Figure 4.12 shows increased surface adsorption for all mixed systems with increased PAM concentration. Both cationic surfactant systems (orange and green traces) show increased surface adsorption beginning at lower concentrations of PAM in solution than the anionic SDS system (blue trace). The mixed system of PAM with CTAB displays the highest surface pressure values. CTAB has the most hydrophobic

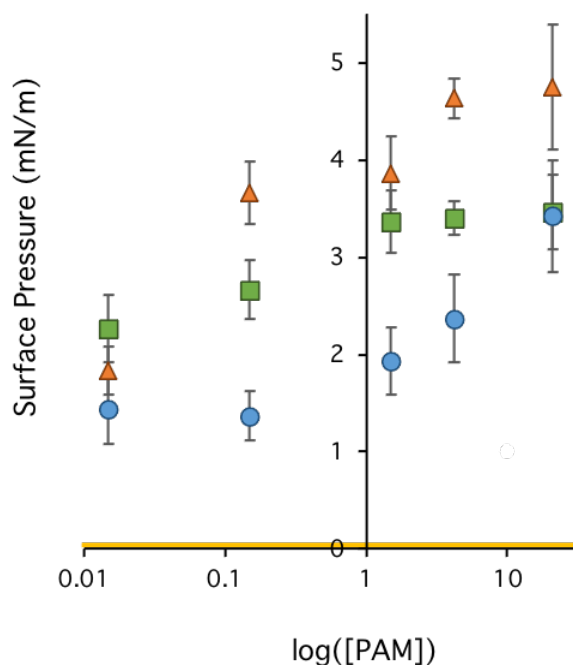


Figure 4.12: Surface pressure of PAM mixtures with surfactants CTAB (orange triangles), DTAB (green squares), and SDS (blue circles). Surface pressure of PAM alone is depicted by the yellow line. Concentrations of PAM used are 0.015, 0.15, 1.5, 4.2, and 21 mM. The log of the PAM concentration is plotted as the x-axis for visual clarity.

characteristics of the three surfactants studied here, as its hydrocarbon tail is the longest. The fact that PAM displays the highest surface pressure values with the most hydrophobic surfactant is consistent with literature that has found certain nonionic polymers interact more strongly with surfactants in bulk solution with increased hydrophobicity of the molecules.¹⁴¹⁻¹⁴⁵ However, this is notably in contrast to what was observed in the previous section with PEG and F127 polymers, where the presence of additional hydrophobic methyl groups on the polymer were not found to affect the surface behavior of those polymers. Where PEG and F127 are surface active on their own, the PAM polymer discussed here is not. The following discussion uses VSF spectroscopy to investigate what specific molecular properties of PAM may play a role in its attraction to the surface upon the addition of charged surfactants, as indicated by the surface pressure trends in Figure 4.12.

Figure 4.13 shows the VSF spectra in SSP polarizations of PAM at three different concentrations with 0.015 mM d-SDS. The SDS surfactant has been fully deuterated in these systems so any modes observed in the C-H stretching region ($2800-3000\text{ cm}^{-1}$) are

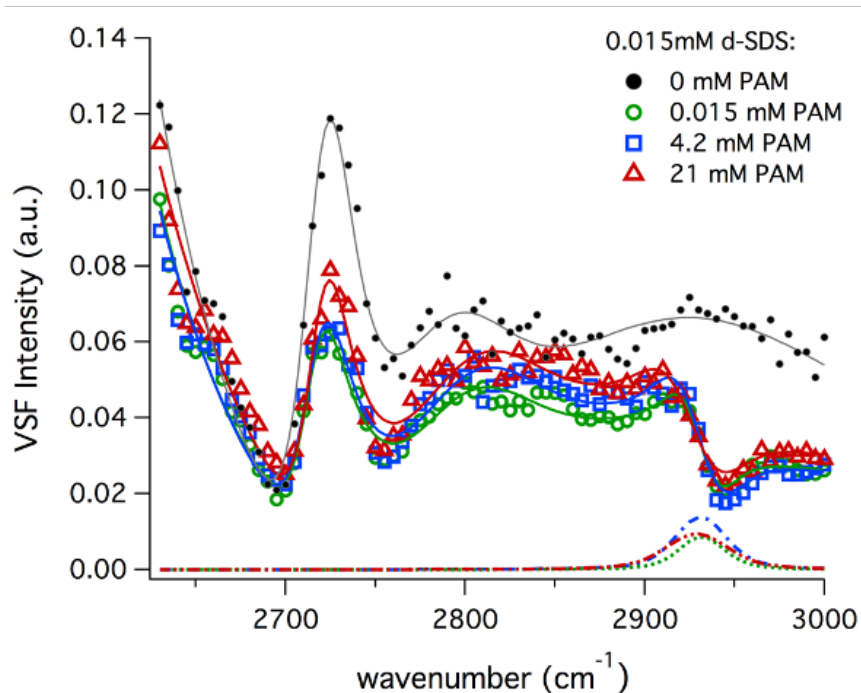


Figure 4.13: The VSF spectrum in SSP polarizations of 0.015 mM d-SDS at the $\text{CCl}_4/\text{D}_2\text{O}$ interface with no polymer (grey trace), and with 0.015 mM, 4.2 mM, and 21 mM PAM (green, blue, and red traces, respectively). Lines are fits to spectra, full parameters can be found in Appendix B, Table B.1. The dotted line traces correspond to the fit peaks of the PAM d^+ mode for each PAM concentration: 0.015 mM, 4.2 mM, and 21 mM shown by the green dot trace, the blue dot-line trace, and the red dot-dot-line trace, respectively.

attributed to the presence of the PAM polymer at the surface. It is noted that C-D peaks from d-SDS at this low concentration are not observable by VSF, as signal from the O-D stretches from coordinated D_2O molecules encompass the same region and obscures the C-D stretch modes. No SPS spectra are shown for these systems because no signal was observed for any of the systems of PAM with d-SDS in SPS polarizations.

The grey trace shows the SSP spectrum of 0.015 mM d-SDS alone at the surface, in the absence of any PAM in solution. This spectrum has been analyzed in detail in Chapter III, but a brief summary here follows. The sharp peak located at $\sim 2720 \text{ cm}^{-1}$ is due to free OD oscillators at the oil/water surface. The increase in VSF intensity at wavenumbers lower than the free OD is due to hydrogen-bonded O-D oscillators from the D_2O solvent. The broad signal in the $2800 - 3000 \text{ cm}^{-1}$ region is due to the D_2O stretch + libration combination mode, which has an amplified VSF response in the presence of the anionic charged surface.

Upon the addition of PAM to the d-SDS system in Figure 4.12, the free OD mode at $\sim 2720\text{ cm}^{-1}$ decreases in intensity. As PAM adsorbs to the surface, there is less surface area for D_2O molecules to protrude into the oil surface, causing this decrease in signal intensity from the free OD mode. The slight decrease in VSF signal at higher wavenumbers in the water stretch + libration combination mode region upon addition of PAM also indicates increased molecular adsorption. There is a sharp dip in the broad VSF intensity, located at $\sim 2930\text{ cm}^{-1}$. This feature is due to the presence of methylene symmetric stretch (d^+) from C-H oscillators on the PAM backbone, as the polymer has adsorbed to the surface. This polymer C-H stretch mode is out of phase with the underlying broad signal from the D_2O stretch + libration combination mode, causing the interference feature to be observed. Figure 4.12 also shows the corresponding fit peak components of the methylene symmetric stretch at $\sim 2930\text{ cm}^{-1}$ from surface PAM in each system, color coordinated to their specific mixed systems. It can be seen that the methylene symmetric stretch of the PAM backbone is present at all PAM concentrations when anionic d-SDS is present, however the intensity of these peaks does not significantly vary (see full fit parameters in Appendix B).

Although the VSF intensity of this mode does not increase with additional PAM concentration, the surface pressure values for the system of d-SDS with PAM in Figure 4.12 indicate an increase in total interfacial adsorption with the increase in PAM concentration. This increase in surface pressure could be due to higher amounts of PAM or SDS adsorbed to the surface, or a combination of both. If the amount of SDS present at the surface increases with higher PAM concentrations, the coordinated O-H stretching region in the VSF spectra in Figure 4.13 would increase as well, as the additional surface charge causes more water molecules to orient their dipoles relative to the surface in response to the stronger electrostatic field. However, Figure 4.13 does not show any changes in the coordinated O-H stretching region upon the increase of PAM concentration. Thus, the increase in surface pressure values in Figure 4.12 for the PAM with SDS system is most likely due to higher amounts of PAM polymer adsorbing to the oil/water surface. The fact that the intensity of the methylene symmetric stretch does not display a corresponding increase indicates all additional PAM polymer adsorbing to the

surface adopts a disordered structure, so an overall C-H stretch dipole is not detected by VSF.

An overall disordered interfacial structure of PAM in the presence of anionic SDS is further supported by the VSF spectra in the carbonyl (C=O) stretching region of these systems. Figure 4.14 shows the VSF spectrum in SSP polarizations of the varying concentrations of PAM in the presence of 0.015 mM d-SDS. Data points that drop below VSF intensity values of 0 a.u. in these traces are due to normalization artifacts and correspond to no detectable VSF signal at those wavenumbers. While the spectra in this region display an overall lower signal to noise ratio due to IR adsorption, it is observed that none of the spectra display evidence of the carbonyl stretch from PAM at the oil/water surface. The absence of a carbonyl stretch in the SSP VSF spectrum from the interfacial PAM confirms the limited overall order in the polymer chain as it adsorbs to the anionic charged surface. While carbonyl stretches from the polymer are certainly present at the surface, they do not adopt an overall dipole orientation that allows their detection by VSF.

Despite its limited overall structural order, the PAM polymer is favorably attracted to the oil/water interface in the presence of anionic charged surfactant, where it otherwise stays solvated in the bulk aqueous phase when alone in solution. To determine if electrostatic interactions between the polymer and SDS surfactant molecules play a role

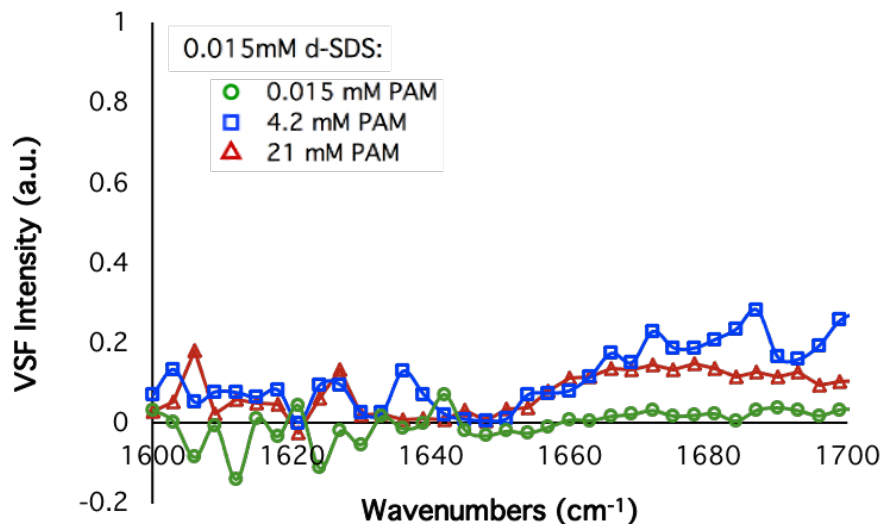


Figure 4.14: The VSF spectrum in SSP polarizations of 0.015 mM d-SDS at the CCl₄/D₂O interface in the carbonyl stretching region with 0.015 mM, 4.2 mM, and 21 mM PAM (green, blue, and red traces, respectively). No signal in the C=O stretching region is observed, indicating the polymer is largely disordered at the surface. Lines are guides to the eye.

in this favorable adsorption of PAM to the surface, a high salt concentration was added to the mixed polymer-surfactant system to screen the electrostatic field induced at the surface when anionic SDS adsorbs. Figure 4.15 shows the VSF spectrum in SSP polarizations of 0.015 mM d-SDS and 1 M NaCl in solution with and without PAM. The two spectra are strikingly similar. Where there was evidence of a weak response from the PAM methylene symmetric stretch when d-SDS was in solution with 4.2 mM PAM in the absence of salt (Figure 4.12), the addition of 1 M NaCl causes any evidence of interfacial PAM in the VSF spectrum to disappear. Additionally, surface pressure measurements indicate no significant difference between the two chemical systems investigated in Figure 4.15: A value of 18.4 ± 0.3 mN/m measured for 0.015 mM SDS + 1 M NaCl, and that of 18 ± 1 mN/m for 0.015 mM SDS + 1 M NaCl with 4.2 mM PAM. This indicates no PAM adsorbs to the surface when salt is present to screen the anionic charge of the SDS headgroups. Thus, the electrostatic interactions between PAM and SDS are likely the primary force causing favorable adsorption of the polymer to the surface in this mixed system. To further investigate these charge-dipole interactions between PAM and surfactants in mixed systems at the surface, PAM was studied by VSF spectroscopy in the presence of oppositely charged cationic surfactants.

Figure 4.16 shows the VSF spectra in the C-H stretching region for mixed systems of PAM with cationic d-DTAB. The DTAB used in these studies were fully

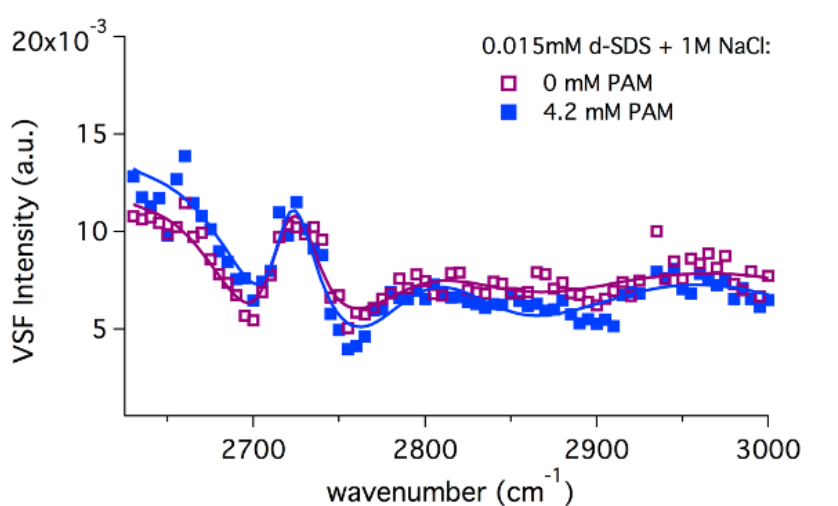


Figure 4.15: The VSF spectrum in SSP polarizations of 0.015 mM d-SDS with 1 M NaCl at the $\text{CCl}_4/\text{D}_2\text{O}$ interface with no polymer (purple trace) and with 4.2 mM PAM (blue trace). The spectra are largely similar, indicating the polymer is not attracted to the surface when salt is present to screen the surfactant charge. Lines are fits to spectra, full parameters can be found in Appendix B, Table B.2.

deuterated so the signal observed in the C-H stretching region is only due to interfacial polymer. In Figure 4.16a, the grey trace corresponds to the spectrum in the C-H stretching region from 0.015 mM d-DTAB alone at the D₂O/CCl₄ interface in SSP polarizations. The free OD mode is detected as the sharp peak around 2720 cm⁻¹. The rise in signal at wavenumbers lower than the free OD correspond to coordinated O-D stretch oscillators, whose VSF signal is enhanced in the presence of the charged surface. As discussed in Chapter III, the water stretch + libration mode in the 2800 – 3000 cm⁻¹ region of the D₂O/CCl₄ interface at the cationic surface of d-DTAB is not as visually apparent as when an anionic charge is present, due to interferences between the resonant combination mode and the nonresonant background. A very weak peak is observed in this spectrum of d-DTAB only around 2950 cm⁻¹ (grey trace, Figure 4.16a), which is attributed to trace amounts of C-H oscillators on the d-DTAB surfactant, as 100% deuteration is not possible. Similar to the discussion in the d-SDS systems above, the C-D peaks from d-DTAB at these low concentrations are not observable by VSF, as strong signal from the coordinated O-D stretches encompasses the same region.

As PAM is added to solution, sharp peaks are detected in the C-H stretching region in both SSP and SPS polarizations (Figures 4.16a and 4.16b), due to PAM

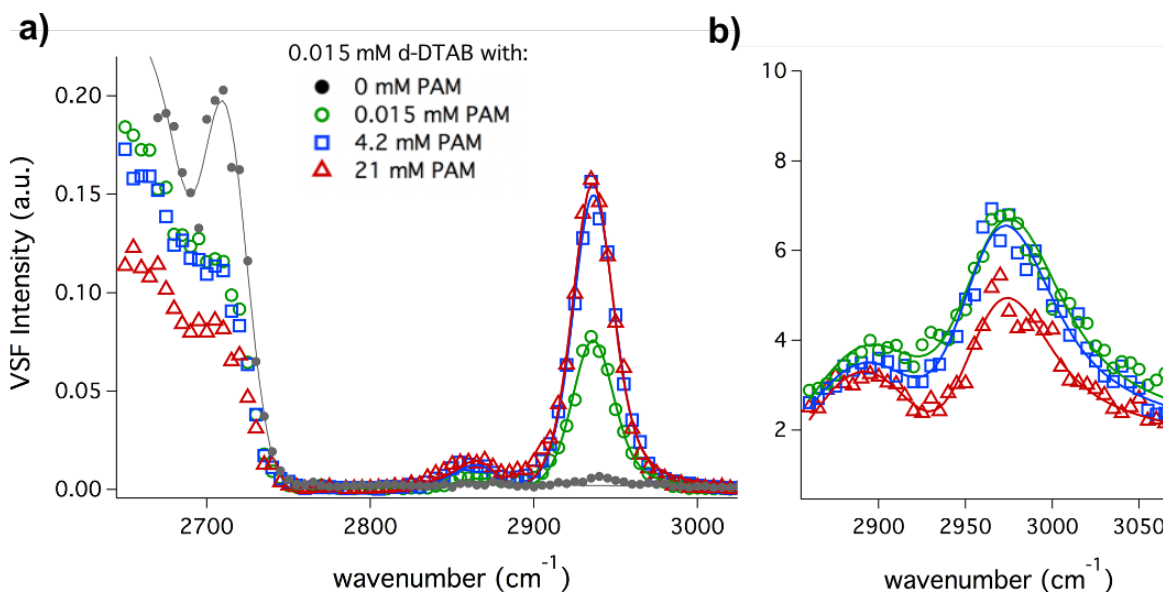


Figure 4.16: The VSF spectrum in SSP (a) and SPS (b) polarizations of 0.015 mM d-DTAB at the CCl₄/D₂O interface with no polymer (grey trace) and with 0.015 mM, 4.2 mM PAM, and 21 mM PAM (green, blue, and red traces, respectively). The sharp peaks due to the polymer backbone indicate PAM is present and ordered at the surface. Lines are fits to spectra, full parameters can be found in Appendix B, Tables B.3, B.4, and B.5.

adsorbing to the interface in an ordered manner. The small peaks fit to $2875 \pm 3 \text{ cm}^{-1}$ in the SSP spectrum in Figure 4.16a and $2873 \pm 3 \text{ cm}^{-1}$ in the SPS spectrum of Figure 4.16b are attributed to the methine C-H stretch of the backbone, indicating that the methine mode has both parallel and perpendicular components of its net dipole relative to the interface. The peak fit to $2935.5 \pm 0.3 \text{ cm}^{-1}$ in the SSP polarized spectra of Figure 4.16a is due to the methylene symmetric stretch (d+) of the polymer backbone. In the SPS polarized spectra of Figure 4.16b, the methylene asymmetric stretch (d-) is fit to a frequency of $2958 \pm 1 \text{ cm}^{-1}$ and is not present in the SSP polarized spectra. (Full fit parameters can be found in Appendix B.)

The strong C-H stretch peaks observed in both SSP and SPS polarizations of PAM in the presence of cationic d-DTAB contrast what was observed for mixed systems of PAM with anionic d-SDS above. Where interfacial PAM is very limited in its overall structural order with anionic surfactant, the VSF spectra in Figure 4.16 suggest the polymer adopts a much more ordered structure at the surface when in a mixed system with cationic surfactant. Additionally, the surface pressure measurements for the system of PAM with DTAB shown in Figure 4.12 imply a continual increase in the amount of surface adsorbates with the increase in PAM concentration, until it plateaus at PAM concentration of $\sim 1.5 \text{ mM}$. The SSP spectra of the PAM + DTAB mixed system in Figure 4.16a show a corresponding increase in intensity of the C-H stretches from 0.015 mM to 4.2 mM PAM concentration and no additional change from 4.2 mM to 21 mM PAM concentration, consistent with the surface pressure trend in Figure 4.12. This suggests the rise in intensity of PAM's C-H peaks in Figure 4.16a is most likely due to the additional adsorption of ordered PAM to the surface upon increased bulk concentration.

To further investigate the order of the polymer at the surface with cationic DTAB, the carbonyl stretching region of these mixed systems was probed by VSF in SSP polarizations. While the signal to noise ratio is lower in this region, Figure 4.17 clearly shows a carbonyl response from ordered PAM at the surface in this mixed system at all three concentrations of PAM, indicating that PAM adsorbs to the surface and adopts an orientation where the carbonyl stretches of the acrylamide monomers have a net vibrational dipole component perpendicular to the interface when a cationic surfactant is present.

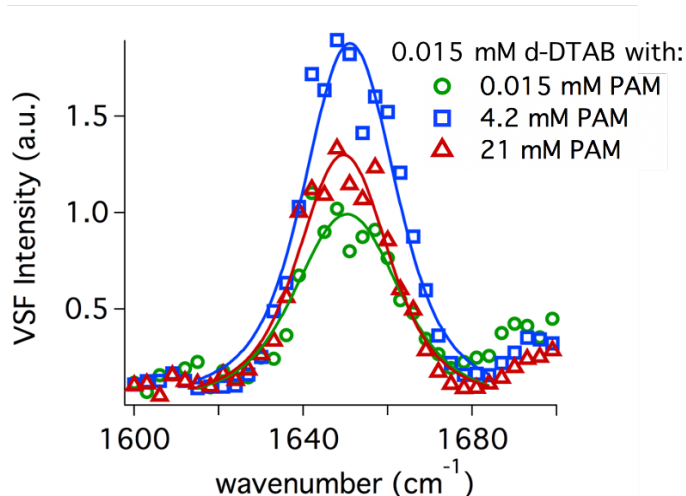


Figure 4.17: The VSF spectrum in SSP polarizations of 0.015 mM d-DTAB at the CCl₄/D₂O interface with 0.015 mM, 4.2 mM PAM, and 21 mM PAM (green, blue, and red traces, respectively) in the carbonyl stretching region. Lines are fits to spectra, full parameters can be found in Appendix B, Table B.6.

Combining the information obtained from the VSF spectra in the C-H and C=O stretching regions of PAM's interfacial structure, Figure 4.18 depicts the likely average orientation of PAM at the surface in this mixed system. The partial negative charge on PAM's carbonyl groups is shown to be attracted to the cationic surfactant headgroups through charge-dipole interactions. This causes the C=O stretch to have a net orientation perpendicular to the interface, which allows its detection by VSF in SSP polarizations (Figure 4.17). This orientation of the acrylamide carbonyl groups causes the backbone of the polymer to order itself as shown in Figure 4.18, where the methylene symmetric

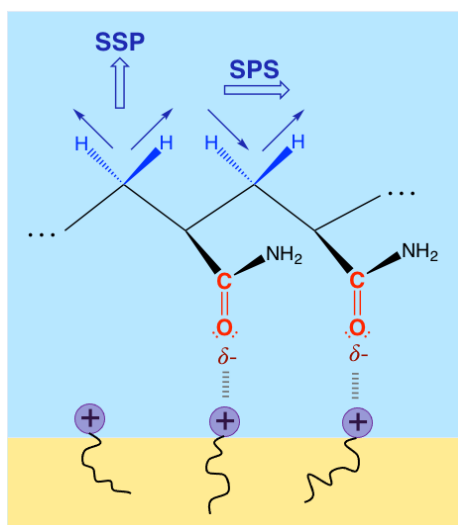


Figure 4.18: A depiction of the structure of interfacial PAM when in a mixed system with cationic surfactant.

stretch (d⁺) has a net vibrational dipole perpendicular to the surface and the asymmetric stretch (d⁻) parallel. The d⁺ mode detected in the SSP spectra and the d⁻ mode detected in the SPS spectra of Figure 4.16 support this conclusion.

The significant difference in PAM's interfacial structure in the presence of anionic surfactant and cationic surfactant is analyzed in Table 4.1 by comparing the surface pressure values and methylene symmetric stretch intensity fit values of the two systems. Where the surface pressure

PAM (mM)	+ 0.015 mM DTAB		+0.015 mM SDS	
	PAM d+ Intensity (a.u.)	SP (mN/M)	PAM d+ Intensity (a.u.)	SP (mN/m)
0.015	0.319 ± 0.003	2.3 ± 0.4	0.08 ± 0.01	1.4 ± 0.4
4.2	0.450 ± 0.003	3.4 ± 0.2	0.09 ± 0.01	2.4 ± 0.5
21	0.459 ± 0.004	3.5 ± 0.4	0.08 ± 0.01	3.4 ± 0.6

Table 4.1: A comparison of the surface pressure (S.P.) values and fit intensities of PAM's methylene symmetric stretch (d+) at different polymer concentrations for mixed systems of nonionic PAM with anionic (SDS) and cationic (DTAB) surfactants.

measurements for each concentration of PAM are closely comparable between the cationic or anionic surfactant mixed systems, the fit intensities of the polymer's methylene symmetric stretch (d+) are significantly higher for the PAM + DTAB mixed system. This suggests that while similar amounts of PAM have adsorbed to the surface in both mixed systems, the polymer's overall structural order at the surface is limited when anionic SDS is present, but much more uniform with a net order when cationic DTAB is present.

This is further understood by analyzing the electrostatic potential map of the acrylamide monomers, shown in Figure 4.19. The partial negative charge of the acrylamide monomer primarily surrounds the carbonyl group, allowing a distinct anchor point for interacting with the cationic surfactant headgroups through charge-dipole interactions. The polymer's partial positive charge, on the other hand, is distributed throughout the NH₂ group and carbon backbone. This allows more polymer

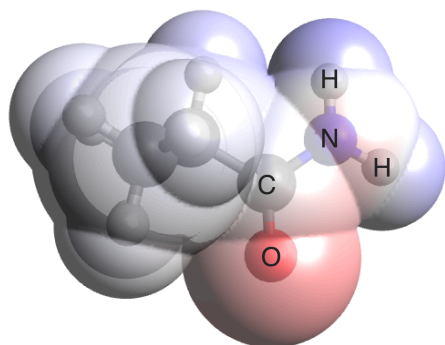


Figure 4.19: The electrostatic potential map of an acrylamide monomer. The partial negative regions are shaded in red, localized around the oxygen atom. The partial positive regions are shaded in blue.

conformations to have weakly attractive charge-dipole interactions between the partial positive regions and anionic surfactant headgroups, causing a more disordered structure of PAM at the surface with anionic SDS. Thus, the partial charge distribution around PAM's functional groups affects the structure it adopts when adsorbing to the surface with charged surfactants.

To investigate whether there is any limit on the ability of the cationic surfactant to induce a net

interfacial structure of PAM, the time-dependent nature of PAM's surface activity with cationic surfactant is analyzed in Figure 4.20, which shows the surface pressure plot for 4.2 mM PAM with 0.015 mM DTAB and the corresponding VSF spectra in SSP polarizations with deuterated DTAB. The surface pressure plot indicates an equilibration time of ~ 11 hours (hrs) for the PAM + DTAB mixed system to reach full adsorption at the oil/water interface. The VSF spectra shown were taken at two different time points: when the mixed system was initially introduced to the oil surface, and after allowing 11 hrs for the chemical system to equilibrate. It can be seen that the intensity of the polymer C-H modes does not change between the initial time and after equilibration, indicating all ordered polymer contributing to the VSF signal adsorbs immediately to the surface. All additional adsorption of the polymer over time must manifest an overall disordered structure, so as not to cause a further increase in the VSF intensity detected for the system. Similar field-limited ordering of interfacial polymer has been shown to exist for charged polyelectrolyte adsorbing to an oil/water interface and is responsible for the multistep adsorption process of disordered polymer chains aggregating on top of an ordered polymer layer.¹⁴⁶

The PAM studies discussed up to this point have investigated the effects of the electrostatic interactions between the polymer and charged surfactant headgroups at the oil/water interface. To understand the effects of any possible hydrophobic interactions between the PAM polymer and the surfactants at the surface, Figure 4.21 shows the VSF

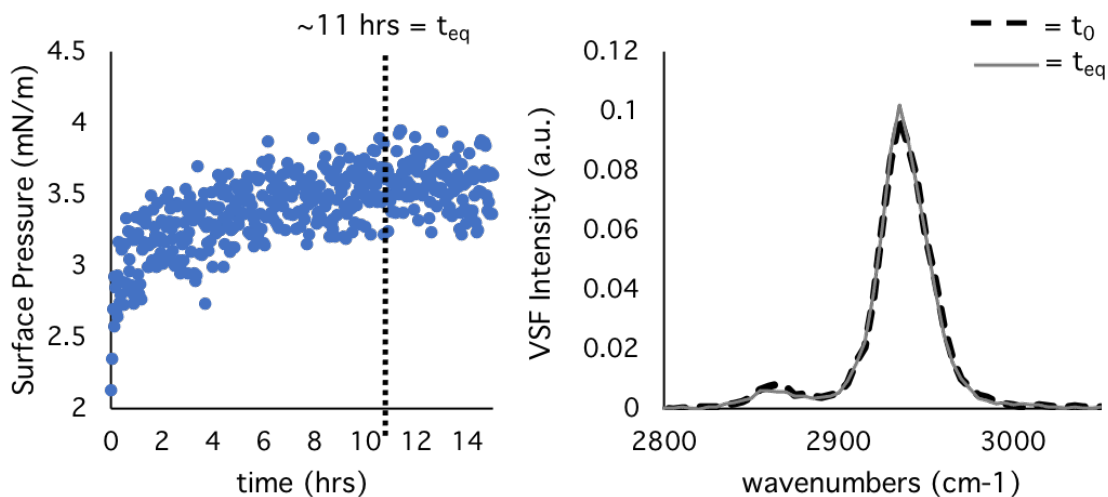


Figure 4.20: The time-dependent surface pressure and VSF spectra (in SSP polarizations) of 4.2 mM PAM with 0.015 mM DTAB at the oil/water interface. Fully deuterated DTAB and an aqueous phase of D₂O were used for the chemical systems probed by VSF. Lines in the VSF spectra are guides to the eye.

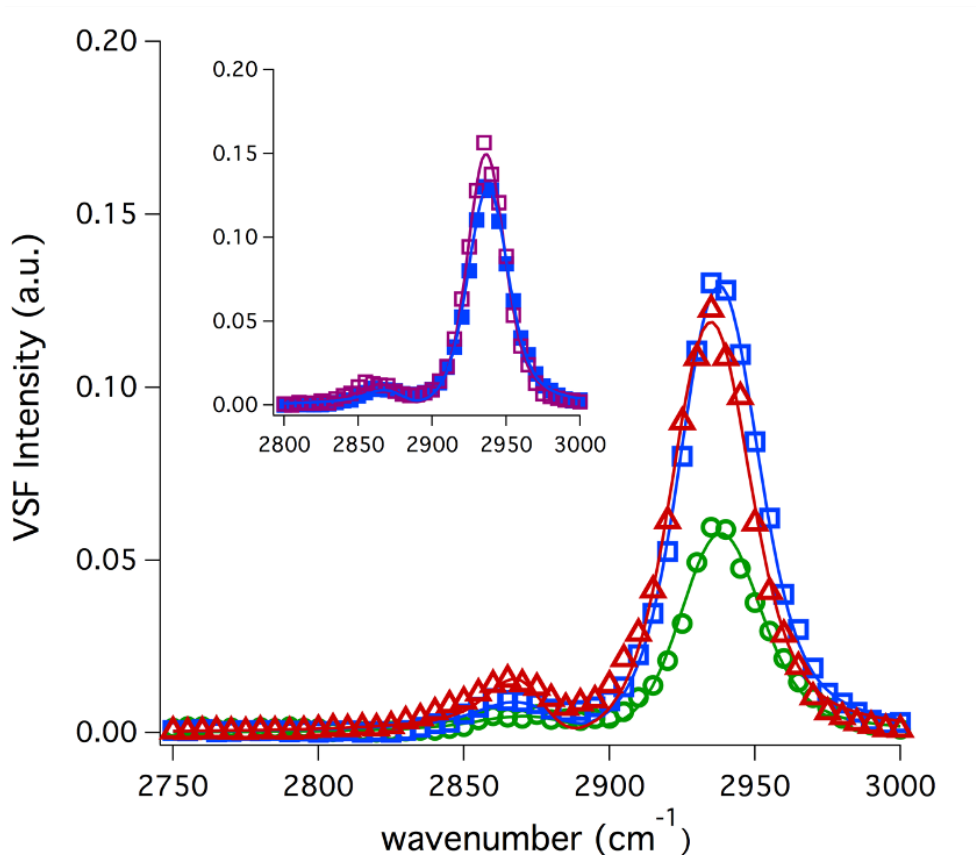


Figure 4.21: VSF spectra at the $\text{CCl}_4/\text{D}_2\text{O}$ surface in SSP polarizations of 0.001 mM d-CTAB with 0.015 mM, 4.2 mM, and 21 mM PAM (green, blue, and red traces, respectively). The spectral inset shows the VSF spectra in SSP polarizations of 0.001 mM d-CTAB + 4.2 mM PAM (blue solid squares) compared to 0.015 mM d-DTAB + 4.2 mM (purple open squares). Although CTAB is more hydrophobic than DTAB, the polymer structure at the surface is unchanging. Lines are fits to spectra and full fit parameters can be found in Appendix B, Tables B.3 and B.7.

spectra in SSP polarizations of PAM at various concentrations with 0.001 mM d-CTAB surfactant. CTAB has the same cationic headgroup as the previously discussed DTAB surfactant, however, the carbon tail is longer, causing it to be more hydrophobic. The CTAB surfactant has been deuterated so that the only C-H modes investigated in these spectra are due to PAM at the surface.

The spectra shown in the PAM + d-CTAB mixed system in Figure 4.21 are strikingly similar to what was observed in Figure 4.16 for the PAM with d-DTAB system. The C-H stretch of the methine group is detected at $\sim 2875 \text{ cm}^{-1}$, and the methyl symmetric stretch is observed at $\sim 2935 \text{ cm}^{-1}$ (see Appendix B for full fit parameters). The intensity of PAM's C-H stretches increase when the PAM concentration increases from 0.015 mM to 4.2 mM and does not change further with a PAM concentration of 21 mM. This is consistent with the trend in the surface pressure measurements for the PAM +

CTAB mixed system shown in Figure 4.12, indicating the rise in intensity of the C-H modes is due to more PAM adsorbing to the surface.

The spectral inset in Figure 4.21 compares the SSP spectra of 4.2 mM PAM with 0.015 mM d-DTAB (purple open squares) and with 0.001 mM d-CTAB (blue solid squares), showing very little difference between the VSF spectra of the two systems. However, the surface pressure measurements report a significantly higher surface pressure for the PAM + CTAB system than the PAM + DTAB system (Figure 4.12), indicating higher amounts of PAM surface adsorbates from the mixed system are present at the surface when the cationic surfactant has higher hydrophobicity. However, all additionally adsorbed PAM in the CTAB system must be disordered with no net vibrational dipole moments, so as to not contribute to higher VSF signal. The adsorption of this disordered polymer layer is likely due to the limited penetration depth of the interfacial field induced by the cationic surfactant headgroups.¹⁴⁶

The investigation of nonionic PAM at the oil/water interface with various charged surfactants have provided a picture of how this surface-inactive polymer is affected by both electrostatic and hydrophobic properties of surfactants. While the surfactant hydrophobicity affects the amount of polymer attracted to the interface, the surfactant's headgroup properties are responsible for the overall structure adopted by PAM at the surface. Figure 4.22 depicts a summary of PAM's interfacial behavior with both cationic and anionic surfactant. When alone in solution, PAM does not favorably adsorb to the oil/water interface. However, when in a mixed system with either anionic or cationic

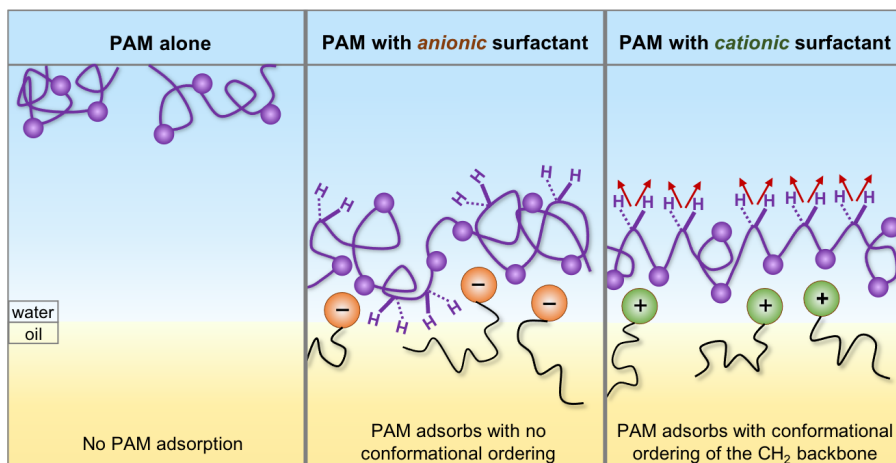


Figure 4.22: A depiction of the surface activity at the oil/water interface of PAM when alone in solution and when in mixed systems with anionic and cationic surfactants.

surfactant, the polymer readily adsorbs to the surface. With cationic surfactants, PAM adopts an overall ordered structure where the carbonyl groups are attracted to the cationic surfactant headgroup through charge-dipole interactions, causing a net structure in the interfacial polymer's carbon backbone. However, when anionic surfactants are present, PAM favorably adsorbs to the surface in a largely disordered structure, due to the larger special distribution of the partial positive charge on the acrylamide monomers.

The polymer-surfactant studies investigated in this chapter provide valuable insight to the behavior of various nonionic polymers at the oil/water interface. However, some applications utilizing mixed systems of nonionic polymers and surfactants may require further investigation into the dynamics and surface properties of these systems. Specifically, studies aiming to understand why certain surface-active polymers, such as PVA and PEG, tend to be minimally affected by the presence of charged surfactants could be beneficial to the environmental and pharmaceutical applications in which they are used.^{9, 98, 117, 138, 147} Additionally, studies providing further investigation into how the partial charge distribution around branched monomer structures of other nonionic polymers affect their ability to adsorb to charged surfaces could be valuable to applications dependent on the functionalization of various polymer films.¹¹⁰⁻¹¹²

II) Nonionic Surfactant + Charged Surfactant Mixed Systems

The previous section has investigated the interfacial behavior of mixed systems involving nonionic polymers and charged surfactants at the oil/water surface. Many applications utilizing mixed systems at the oil/water interface also involve co-surfactant mixtures. One such application is the use of dispersants as an oil spill remediation technique, as the mixture of various surfactants and solvents aid the dissipation of surface oil into droplets accessible to degradation by microorganisms. However, the 2010 Deepwater Horizon oil spill in the Gulf of Mexico was a major environmental disaster whose effects called into question the use of chemical dispersants as a remediation technique. While the dispersants succeeded in dissipating the surface oil, the chemical mixture used to remediate the Horizon spill themselves introduced toxic effects on marine and shore life, further amplifying the disaster.^{4, 136, 148} To engineer safe dispersant

mixtures, a fundamental understanding of the interplay between surfactants in these mixtures is necessary.

This section investigates the behavior of a nonionic surfactant, Span-80, as a component in co-surfactant mixtures with anionic surfactants. Span-80 is a current ingredient used in oil spill dispersant mixtures, as it is known to be biodegradable and nontoxic.^{7-8, 134, 149-151} Anionic surfactants have also been shown to be an effective ingredient of oil spill dispersants, as they are known to have high surface activities.^{6-7, 152} Thus, understanding how nonionic Span-80 interacts with anionic surfactants at the oil/water interface and how the surface behaviors of these molecules are affected by each other is important for understanding the effectiveness of Span-80's use in dispersant applications, and what interfacial properties of co-surfactant mixtures may be desirable for the engineering of safe dispersant solutions.

The chemical structures of the surfactants investigated in this section are shown in Figure 4.23. It is noted that some studies included in this section investigate very weak signal from the chiral C-H stretches of the Span-80 headgroup. Thus, the beam energies and pulse stability of our experimental laser system (described in Chapter II) required careful optimization, and figures shown of PSP polarizations probing chiral signals are an average of at least ten different spectra, to produce appropriate signal-to-noise ratios for analysis.

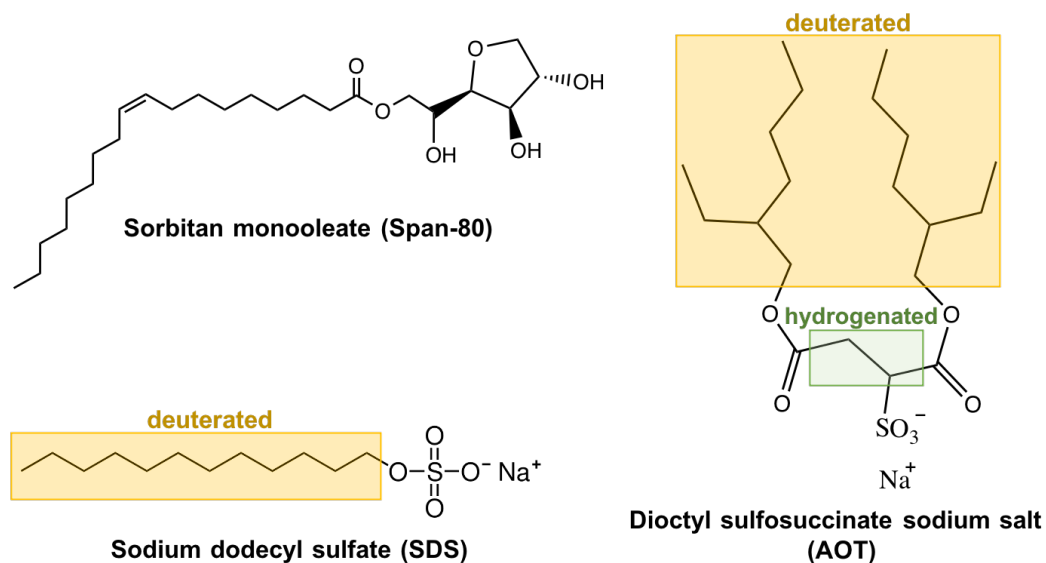


Figure 4.23: The chemical structures of surfactants used in these studies. Sodium dodecyl sulfate (SDS) was fully deuterated. Dioctyl sulfosuccinate sodium salt (AOT) was deuterated in the alkyl tails. Sorbitan monooleate (Span-80) was not deuterated.

A) Nonionic Span-80 surfactant with anionic SDS

This section uses VSF to investigate the interfacial behavior of a co-surfactant mixed system of nonionic Span-80 with SDS, a widely used anionic surfactant.¹⁵³⁻¹⁵⁷ However, before studying the surface dynamics of Span-80 in a co-surfactant mixture, it is important to understand its behavior alone at the oil/water surface.

Figure 4.24 shows the VSF spectra in SSP polarizations of 0.025 mM Span-80 alone at the D₂O/CCl₄ interface. D₂O was used as the aqueous solvent to avoid interference from O-H stretch oscillators in the region of 2750 – 3000 cm⁻¹. Figure 4.24 shows the VSF response from 0.025 mM Span-80 in the C-D stretching region (2020 – 2200 cm⁻¹), and the C-H stretching region (2750 – 3000 cm⁻¹) at 1 hour after the 0.025 mM solution of Span-80 was allowed to adsorb to the surface, and 24 hours after (blue and orange traces, respectively).

Figure 4.24 also shows the VSF signal detected in the region of the O-D stretch oscillators from the D₂O solvent modes, which can be observed in the 2450 – 2750 cm⁻¹ region. VSF signal from D₂O modes are known to be enhanced upon the presence of a surface charge, as the water molecules orient their dipole in response to the interfacial field. When this occurs, VSF signal from the O-D stretch oscillators can encompass an extended region including 2000 – 2750 cm⁻¹, due to the highly coordinated hydrogen-bonding environment of the O-D stretches.²⁶ However, Figure 4.24 does not show any VSF intensity detected in the 2020 – 2200 cm⁻¹ due to O-D stretch oscillators, as the

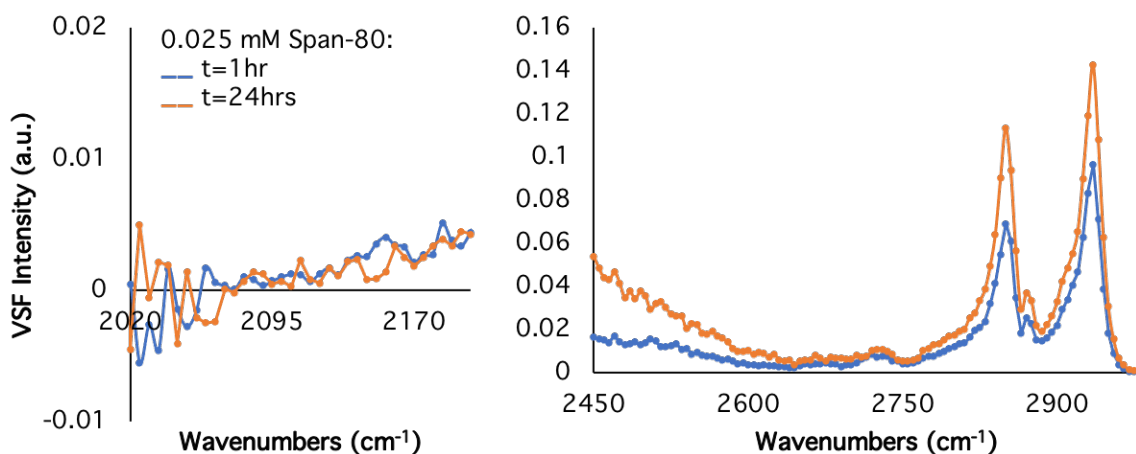


Figure 4.24: VSF spectra in SSP polarizations of 0.025 mM Span-80 at the CCl₄/D₂O interface, taken 1 hour and 24 hours after formation of the interface (indicated by the blue and orange traces, respectively). The C-H stretches due to Span-80 increase in intensity over time. Lines are guides to the eye.

uncharged Span-80 headgroup does not produce a significant field at the surface to enhance the hydrogen-bonding coordination of water molecules. Additionally, no VSF response from C-D stretch modes are detected in this region, as all Span-80 surfactant molecules in this system are non-deuterated and do not contain any C-D bonds. It is noted that the data points in the 2020 – 2200 cm^{-1} region in Figure 4.24 that dip below a VSF intensity of 0 a.u. are due to normalization artifacts and indicate no VSF signal is detected at those wavenumbers.

Analyzing the 2450 – 3000 cm^{-1} spectral region, the weak mode detected at ~ 2720 cm^{-1} in both spectra correspond to free OD oscillators from D_2O molecules protruding into the oil phase. The sharp and narrow peaks at ~2850 cm^{-1} and 2870 cm^{-1} are due to the VSF response from the methylene symmetric (d+) and methyl symmetric (r+) stretches, respectively. The peak at ~2930 cm^{-1} contains signal from several VSF-active C-H stretching modes, including the methylene Fermi resonance and methyl Fermi resonance modes, and is hereafter referred to as the Fermi resonance (F.R.) response.^{34, 66} Additionally, the methylene asymmetric stretch (d-) appears as a slight shoulder to the red (lower wavenumbers) of the Fermi resonance mode, at a peak position of ~2920 cm^{-1} .

As the amount of time Span-80 has to adsorb to the surface increases from 1 to 24 hours, the VSF signal produced by all C-H stretches from Span-80 increases. Understanding from Equation 9 in Chapter II, this could either be due to continual adsorption of more Span-80 molecules to the surface, or a reorientation of the C-H vibrational dipoles already present at the surface, causing a larger component of their vibrational dipoles to be detected perpendicularly to the surface. Surface pressure measurements report an equilibration time of ~1 hour for the 0.025 mM Span-80 solution (at an equilibration surface pressure of 0.4 ± 0.2 mN/m), indicating this concentration of Span-80 allows maximum adsorption to the oil/water interface after 1 hour. Thus, the increase in intensity of the C-H stretches in the SSP spectra between the 1 hour and 24 hour traces are likely due to the reorientation of the Span-80 hydrocarbon tails after they have adsorbed to the interface. This re-structuring of the Span-80 tail groups once they have adsorbed to the surface could be driven by the favorable interactions between the surfactant's hydrophobic C-H bonds and the oil solvent molecules.¹⁵⁸⁻¹⁵⁹

The D₂O O-D stretch oscillators detected in the region of 2450 – 2750 cm⁻¹ also contribute additional signal to the VSF spectra over time, indicating more interfacial water molecules are engaged in coordinated hydrogen bonding over time. This could be due to the reorientation of the hydrophilic Span-80 headgroup at the surface after it adsorbs, maximizing favorable interactions with solvent water molecules. As the hydrocarbon tail of Span-80 reorients to maximize favorable interactions with the oil phase, the hydrophilic headgroup could also be reorienting, optimizing favorable hydrogen bonding interactions between the Span-80 headgroup and water molecules. However, additional studies would need to be performed to confirm this behavior.

Nevertheless, despite the very low surface pressure value of 0.4 ± 0.2 mN/m for the 0.025 mM Span-80 system at the oil/water interface, it can be seen from the VSF spectra in Figure 4.24 that Span-80 molecules are present with a net orientation of vibrational dipoles at the surface in this system, producing significant signal in the C-H stretching region of the SSP polarized spectra.

When SDS is added to create a co-surfactant system with Span-80, the SDS molecules are fully deuterated to allow differentiation between the VSF response of both surfactants. SDS was chosen to be deuterated, as the process of fully deuterating Span-80 molecules is much more experimentally difficult, causing deuterated Span-80 to be more expensive and rare to find. The features of the VSF spectra of d-SDS alone at the D₂O/CCl₄ interface is discussed in detail in Chapter III.

Figure 4.25 shows the VSF spectra in SSP polarizations of the co-surfactant system containing 0.025 mM Span-80 with 0.25 mM deuterated SDS (d-SDS) at the D₂O/CCl₄ interface at 1 hour and 24 hours after the interface was formed. The C-H stretching region from 2750 – 3000 cm⁻¹ shows the same C-H peaks discussed above from Span-80 surfactant present at the surface. The overall VSF signal in the C-H stretching region again increases over time. The sharp peaks in the C-H stretching region suggests Span-80 is present and ordered at the surface at both 1 hour and 24 hours after formation of the interface.

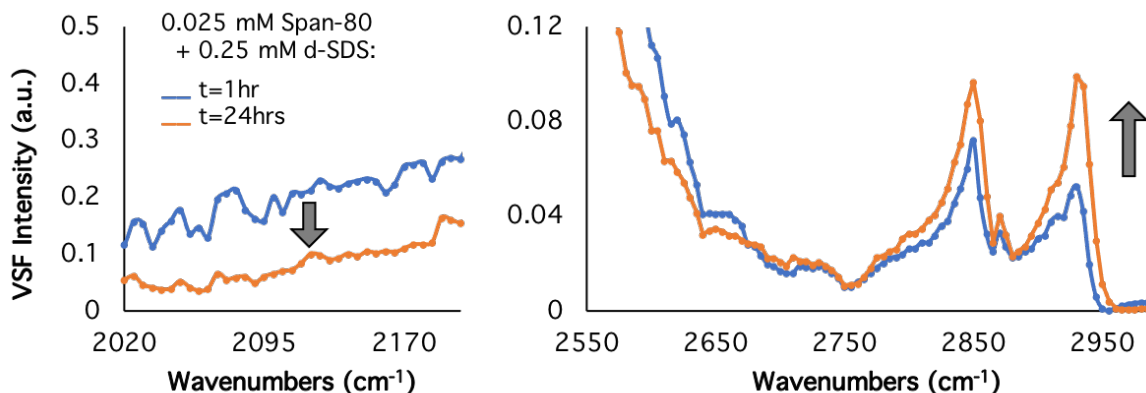


Figure 4.25: VSF spectra in SSP polarizations of 0.025 mM Span-80 with 0.25 mM d-SDS at the $\text{CCl}_4/\text{D}_2\text{O}$ interface at 1 hour and 24 hours after the interface was formed. The C-H stretches from Span-80 increase in intensity over time, while the signal from the coordinated water O-D stretches decreases. Lines are guides to the eye.

Signal in the O-D stretching region of $2550 - 3000 \text{ cm}^{-1}$ is considerably higher in intensity than what was observed for Span-80 alone at the surface in Figure 4.24, due to the presence of charged d-SDS surfactant at the interface in the co-surfactant system. Where Span-80 alone at the surface does not induce the coordination of water molecules at further interfacial depths due to its nonionic headgroup, the anionic charge of the d-SDS surfactant causes water molecules to orient their dipole in response to the surface charge, allowing more VSF signal to be detected in the coordinated water stretching region compared to an uncharged surface.

The VSF spectra in the $2020 - 2200 \text{ cm}^{-1}$ region in Figure 4.25 probes the region of O-D stretch oscillators from coordinated D_2O molecules as well as any C-D stretches from the deuterated SDS surfactant. While distinct C-D stretching peaks are not observed in the $2020 - 2200 \text{ cm}^{-1}$ region in Figure 4.25, this does not necessarily imply that d-SDS has not adsorbed to the surface. In fact, the presence of broad signal in this region due to highly coordinated hydrogen-bonded D_2O molecules implies the charged d-SDS is in fact present at the surface, as Span-80 alone does not induce signal in this region from interfacial water molecules (Figure 4.24). There are two likely reasons why the C-D stretching modes from adsorbed d-SDS molecules, while present, are not detectable by VSF as distinct peaks: either their lack of significant population or net dipole orientation at the surface causes their overall VSF signal to be too weak to allow their detection as distinguished peaks from the broad O-D stretching signal. This is consistent with

literature that shows that the presence of SDS at the oil/water interface affects the signal from water stretch modes at low enough concentrations where the C-H modes from the surfactant are not yet visible as peaks in VSF spectra.³⁶

One possible experimental consideration that may help the C-D modes of d-SDS be observed by VSF in this system is to probe the same system in an aqueous solvent of H₂O, to remove the signal from the O-D stretch oscillators. This consideration is investigated for a similar co-surfactant system in the next section, however, as discussed in Chapter III, the use of H₂O as the aqueous solvent introduces a broad signal in this same region due to the H₂O bend + libration combination mode, which could also obscure the VSF detection of C-D oscillators.

Despite the lack of distinct C-D modes observable in this region, the spectra encompassing 2020 – 2200 cm⁻¹ of the mixed co-surfactant system still contributes interesting information regarding the behavior of Span-80 with d-SDS at the oil/water surface. Over time, the VSF signal intensity due to O-D stretch oscillators from coordinated water molecules in this region decreases, possibly implying a weaker interfacial field from fewer d-SDS surfactants is at the surface over time. If so, the concurrent increase in intensity of Span-80's C-H stretches may suggest competitive adsorption at the surface between nonionic Span-80 and anionic SDS, where Span-80 more favorably adsorbs to the surface over time, causing the increase in VSF C-H stretching signal, and d-SDS is removed from the surface, causing the decrease in the coordinated water O-D stretching signal.

Competitive adsorption between Span-80 and SDS at the oil/water interface is further supported by the surface pressure values and VSF spectra shown in Figure 4.26. Figure 4.26a shows the VSF signal from coordinated water O-D stretch oscillators for Span-80 and SDS alone at the surface (red and blue traces, respectively) and as a mixed co-surfactant system (green trace). The very low VSF intensity of 0.025 mM nonionic Span-80 in this region is expected, as discussed earlier. The intensity due to the coordinated D₂O molecules is weaker for the mixed system than when 0.25 mM d-SDS is alone at the surface, implying a weaker field at the surface from fewer SDS charged headgroups adsorbed to the interface in the co-surfactant mixture. However, the surface pressure plot in Figure 4.26b displays higher surface pressure values for the mixed

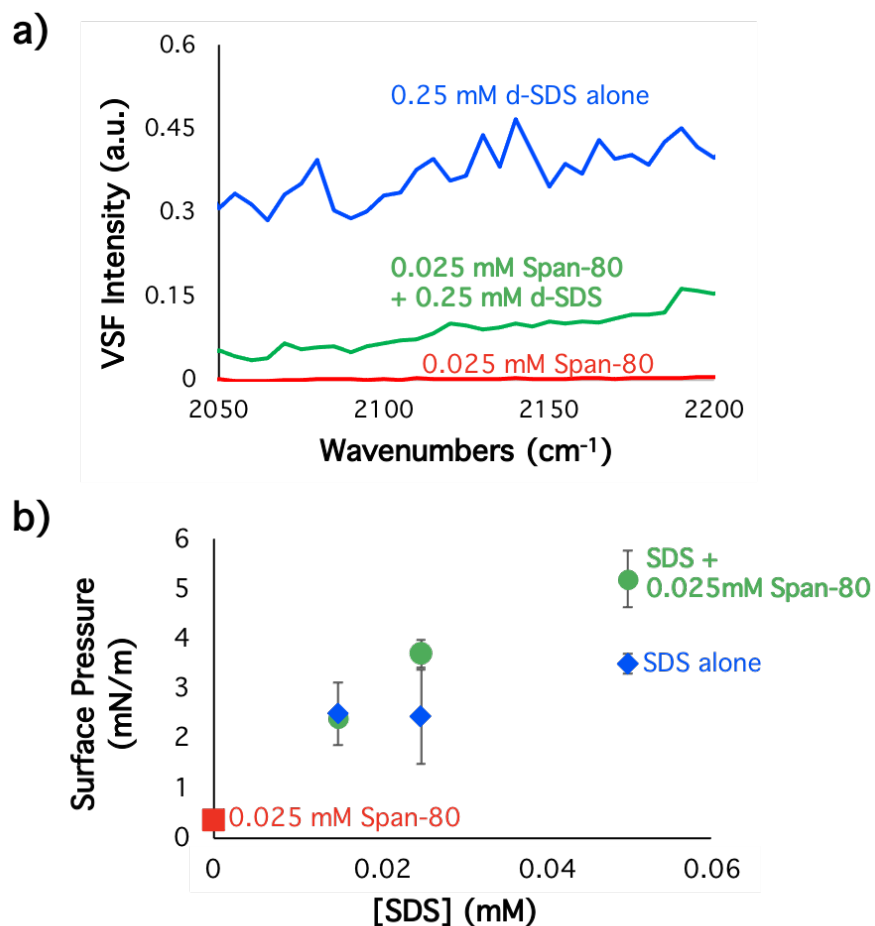


Figure 4.26: VSF spectra in SSP polarizations (a) and surface pressure values (b) for Span-80 alone (red), SDS alone (green), and the mixed system of Span-80 with SDS (blue). The concentration of Span-80 in all systems was 0.025 mM. In the VSF spectra of (a), the concentration of SDS alone and in the mixed system was 0.25 mM. In the surface pressure measurements of (b), the concentrations of SDS alone and in the mixed systems were 0, 0.015, 0.025, and 0.5 mM. Lines in VSF spectra are guides to the eye.

systems than that of either Span-80 or SDS alone, indicating more overall surface adsorbates in the mixed systems. The lower VSF intensity from coordinated D₂O molecules in the mixed system spectra of Figure 4.24a suggest less SDS is at the surface in the co-surfactant mixture; thus, additional adsorption of Span-80 molecules is likely responsible for the higher surface pressure value of this system. These studies suggest some amount of competitive adsorption is present in the co-surfactant mixture of anionic SDS and nonionic Span-80, with favorable adsorption of Span-80 to the oil/water surface. However, without a distinct analysis of the C-D vibrational modes of interfacial d-SDS and further studies, these conclusions are not confirmed.

To gain a better understanding of Span-80's behavior in a mixed system with anionic surfactant, an experimental system that allows VSF to probe the vibrational response of the adsorbed anionic surfactant must be investigated. The next section discusses such a study, investigating Span-80 and anionic AOT at the oil/water surface. However, before introducing the details of the new experimental system, one consideration warranted by the preliminary results of the Span-80 with SDS system described above is that of preparation procedure. Specifically, if Span-80 is truly competitively adsorbing with SDS at the surface over time, is this behavior amplified if Span-80 is allowed to adsorb first to the interface, followed by the addition of SDS? Figure 4.27 shows the VSF spectra of the co-surfactant system 0.025 mM Span-80 with 0.25 mM d-SDS in D₂O at the CCl₄/water interface with three different preparation procedures: (a) the equilibration of Span-80 first, with the subsequent addition of d-SDS, (b) the equilibration of d-SDS first, with the subsequent addition of Span-80, and (c) Span-80 and d-SDS are mixed together in solution, and then added to the CCl₄ surface. For reference, the spectra shown above in Figure 4.25 utilized preparation procedure (c), where both Span-80 and d-SDS were first mixed together in solution.

The trends in the VSF spectra over time for each of the three preparation procedures in Figure 4.27 are strikingly similar. This suggests that the order in which surfactants are introduced into the system does not have a significant effect on the resulting VSF spectra. All three procedures produce VSF spectra with a decrease in the signal from the coordinated O-D stretch oscillators in the 2020 – 2200 cm⁻¹ region over time, and a corresponding increase in the intensity of the Span-80 C-H stretch modes found in the 2750 – 3000 cm⁻¹ region. This suggests that any possible competitive adsorption between Span-80 and SDS to the oil/water interface is not impacted by the order of sample preparation. In light of these observations of preparation method, the next section investigates the co-surfactant system of Span-80 with anionic AOT, utilizing the same sample preparation procedure as used in these studies to observe the behavior of nonionic Span-80 in the co-surfactant mixed system.

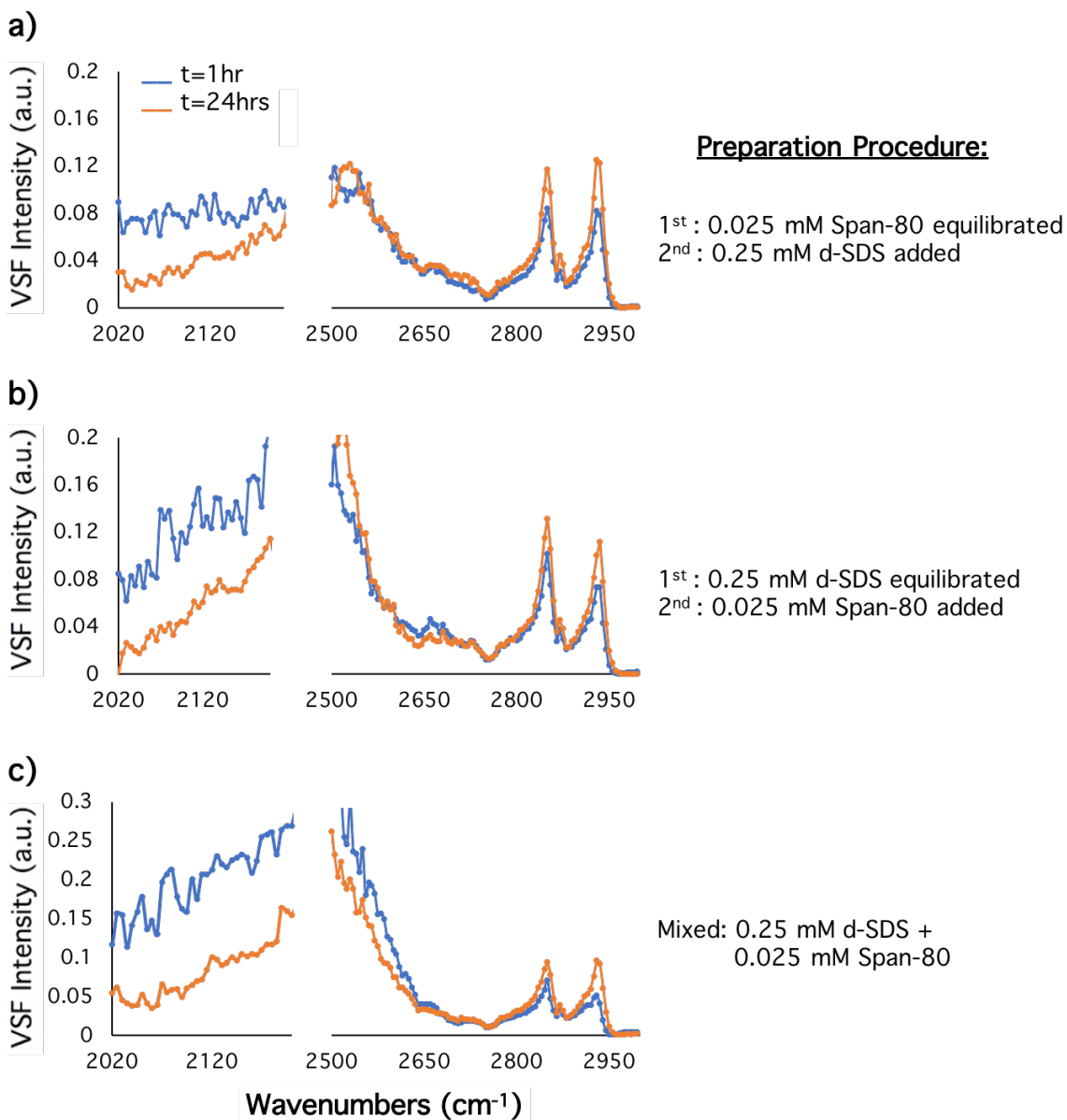


Figure 4.27: VSF spectra at the CCl₄/D₂O in SSP polarizations for three different preparation procedures of the mixed system containing 0.25 mM d-SDS with 0.025 mM Span-80 surface at 1 hour and 24 hours after the interface was formed. The similar spectra of each preparation procedure indicates the preparation procedure does not significantly affect the surface activity of the co-surfactant system.

B) Nonionic Span-80 surfactant with anionic AOT

This section investigates the co-surfactant system of 0.1 mM Span-80 with 0.01 mM deuterated AOT (d-AOT). AOT is a surfactant commonly used as an ingredient in oil spill dispersant mixtures, as it is very surface active.^{6-7, 152} Understanding how Span-80 and AOT behave in a mixed system is important for evaluating Span-80's performance as a nontoxic ingredient in dispersant mixtures. As shown in Figure 4.23, the d-AOT used in this study is only deuterated in the surfactant alkyl tails; the headgroup of d-AOT contains one methylene (CH₂) group and one methine (CH) group. Thus, the majority of VSF signal detected in the C-H stretching region is due to Span-80, however, it is possible that a small contribution to that signal is due to the headgroup of the d-AOT molecules, discussed later in more detail.

AOT was chosen for this mixed co-surfactant system because of its high surface activity and contribution to very intense VSF signal at the oil/water interface, as well as its relevance in dispersant mixture applications. Where the C-D stretching modes from d-SDS at the surface were not observable in the VSF spectra, d-AOT has a higher likelihood of contributing C-D peaks to the spectrum, even at lower bulk concentrations than SDS, due to its high surface activity. Additionally, the experimental laser system used in these studies allow the detection of the carbonyl (C=O) stretch modes of the AOT headgroup, however, the sulfate (S=O) modes of the SDS headgroup are not able to be probed with the given tunable IR range of this experimental system. Thus, for these studies investigating Span-80 with anionic d-AOT, the detection of the C-D stretching and C=O stretching regions by VSF spectroscopy allow two spectral markers that provide information regarding the population and net order of adsorbed AOT molecules at the oil/water surface.

Due to the weak contribution in the C-H stretching region from the C-H modes on the d-AOT headgroups, the VSF polarization combination of PSP was utilized to probe the signal from the chiral C-H modes of Span-80's headgroup. The PSP spectra uniquely probe Span-80 molecules without any interference with d-AOT modes, complementing the SSP spectra of the C-H stretching modes for the co-surfactant system. It is noted that Span-80 also has carbonyl (C=O) modes in its headgroup and will contribute signal in this region when present with a net vibrational dipole at the surface.

Because this mixed system is analyzing VSF signal in both the C-H and C-D stretching regions, the aqueous solvent used in these solutions must be considered. O-H stretching oscillators from coordinated H₂O molecules encompass the same spectral region as the C-H stretches (2800 – 3100 cm⁻¹). Synonymously, the O-D stretching oscillators from coordinated D₂O molecules encompass the same spectral region as the C-D stretch modes (2000 – 2250 cm⁻¹). Chapter III discussed the presence and surface charge dependence of the bend + libration combination mode from H₂O molecules, which also appears in the C-D stretching region. Thus, either aqueous phase of H₂O or D₂O may affect the spectral peaks that arise from C-D stretches.

Figure 4.28 shows the VSF spectra of the C-D stretching region for the co-surfactant system of d-AOT with Span-80 in aqueous phases of H₂O and D₂O. There is an elevated background from resonant water modes detected when the system has either a deuterated or non-deuterated aqueous solvent, although that of the O-D stretching modes from coordinated D₂O molecules is more intense than the H₂O bend + libration combination mode. This difference in intensity is expected due to the combination mode's weaker response discussed in Chapter III. The sharp peak at ~2070 cm⁻¹ in the co-surfactant system with a D₂O aqueous phase (purple trace) is due to a C-D stretch

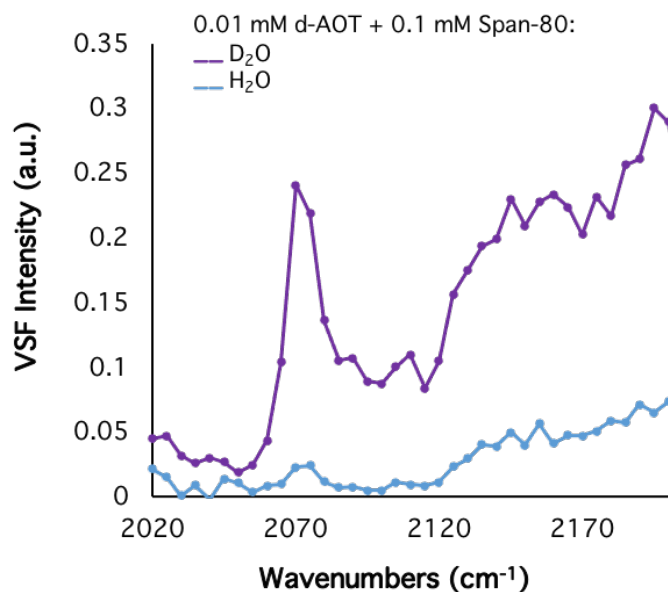


Figure 4.28: VSF spectra in SSP polarizations of 0.01 mM d-AOT with 0.1 mM Span-80 at the CCl₄/D₂O surface with an aqueous solvent of H₂O (blue trace) and D₂O (purple trace). The purple trace is elevated due to signal from the coordinated water O-D stretching modes. Underlying signal from the H₂O bend + libration mode is present in the blue trace. Lines are guides to the eye.

mode from interfacial d-AOT molecules. This peak is also detectable when the aqueous phase is H₂O (blue trace), although much weaker than what is seen in the D₂O system.

Because the only aspect of this chemical system that has changed is the aqueous phase, it can be assumed that the presence and structure of d-AOT at the surface of this system is equivalent in either aqueous phase. Thus, the higher overall VSF intensity detected for the 2070 cm⁻¹ C-D stretch peak in D₂O is a consequence of the presence of the more intense underlying O-D stretch modes elevating the C-D stretching peak in the spectrum. Such elevation from the constructive interference of resonant modes in the D₂O system allows detection of a much more distinct C-D stretch mode. For this reason, all spectra taken for this co-surfactant system investigated here utilize D₂O as the aqueous solvent; however, it must be kept in mind that the overall intensity observed for the C-D stretching peaks contain contributions from the underlying water signal.

It is important to understand the spectral features arising from the d-AOT molecules alone at the interface before analyzing spectra of the mixed co-surfactant system. Figure 4.29 shows VSF spectra of 0.01 mM d-AOT at the D₂O/oil interface at 1 hour and 24 hours after the interface was formed. Anionic AOT induces an enhancement of the D₂O stretch + libration combination mode detected as the broad signal in the 2800 – 3000 cm⁻¹ region of the SSP spectra, similar to what was discussed in Chapter III for

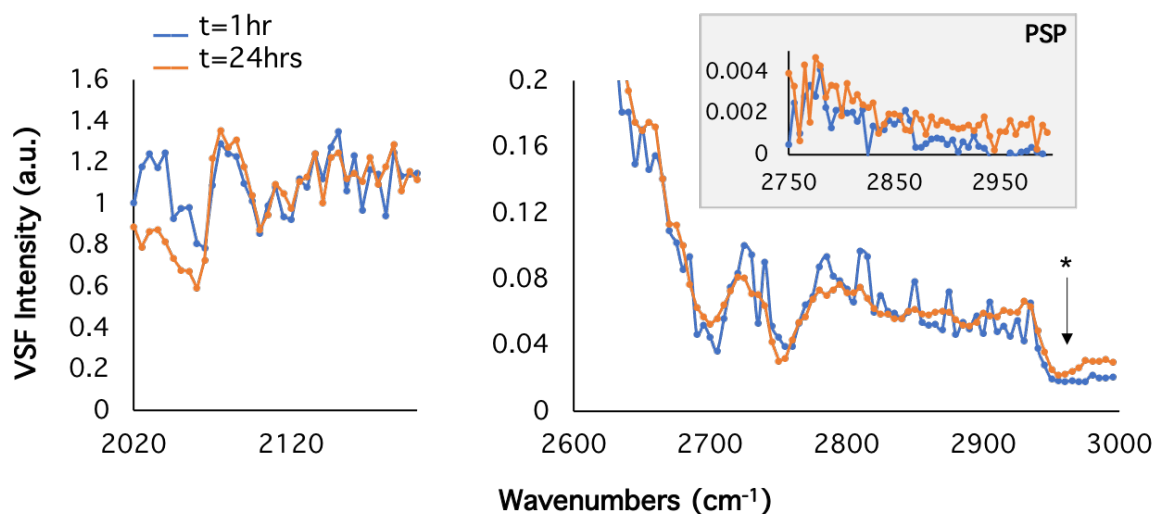


Figure 4.29: VSF spectra in SSP polarizations of 0.01 mM d-AOT at the CCl₄/D₂O surface at 1 hour (blue trace) and 24 hours (orange trace) after the interface was formed. The spectral inset in the grey box was taken with a polarization combination of PSP. The surface behavior of d-AOT does not change significantly over time. Lines are guides to the eye.

the anionic SDS surfactant system. The peak at 2720 cm^{-1} is due to the free OD mode, and the sharp increase in signal at wavenumbers in the region $2600 - 2700\text{ cm}^{-1}$ is due to the O-D stretch oscillators strongly coordinated D_2O molecules, enhanced by the presence of the anionic charge at the surface. There is a noticeable dip in intensity at $\sim 2950\text{ cm}^{-1}$ (labeled with the asterisk), that is not present in the similar VSF spectra of d-SDS at the D_2O /oil surface in Figure 3.6. This dip in intensity is due to the interference between the broad combination mode signal and the signal from the C-H stretches of the d-AOT headgroups (see Figure 4.23). While weak, the C-H modes of the d-AOT headgroups do indeed contribute some signal to the SSP spectra in the C-H stretching region. The spectra in the grey inset encompassing the same wavenumber region shows the VSF signal detected for the d-AOT system in the PSP polarizations. As expected, no spectral features are detected in this spectral inset, as the d-AOT molecules do not contain any chiral centers that would cause signal in this region to be observed by a polarization combination of PSP.

The SSP spectra in the $2020 - 2200\text{ cm}^{-1}$ region probe the VSF response from C-D stretch modes, as well as O-D stretch oscillators from highly coordinated interfacial D_2O molecules. The broad signal encompassing the entirety of this region is due to the coordinated D_2O molecules, as the anionic charge of the adsorbed d-AOT headgroups enhances the signal from D_2O molecules in this region. However, amidst this broad signal, there is a distinct peak observable at $\sim 2075\text{ cm}^{-1}$, due to the deuterated methyl symmetric stretch ($\text{CD}_3\text{ r}^+$).⁶⁶ Although the broad signal from coordinated water oscillators is present in this region, the high surface activity and net structure of the d-AOT alkyl tails at the oil/water interface allow the CD_3 modes of the d-AOT surfactant to be observed in the VSF spectra.

Signal from the carbonyl stretches in the d-AOT headgroup can also be observed at the surface via VSF spectroscopy. Figure 4.30 shows the SSP spectra in the carbonyl stretching region of 0.01 mM d-AOT in D_2O at 1 hour and 24 hours after the interface was formed. The carbonyl mode creates a dip in the spectrum with a peak position of $\sim 1730\text{ cm}^{-1}$, as it interferes with the broad underlying signal from a low-wavenumber D_2O combination band, which is amplified in response to the anionic surface (see full fit parameters in Appendix C).¹⁶⁰⁻¹⁶¹ Over time, the intensity of this carbonyl peak does not

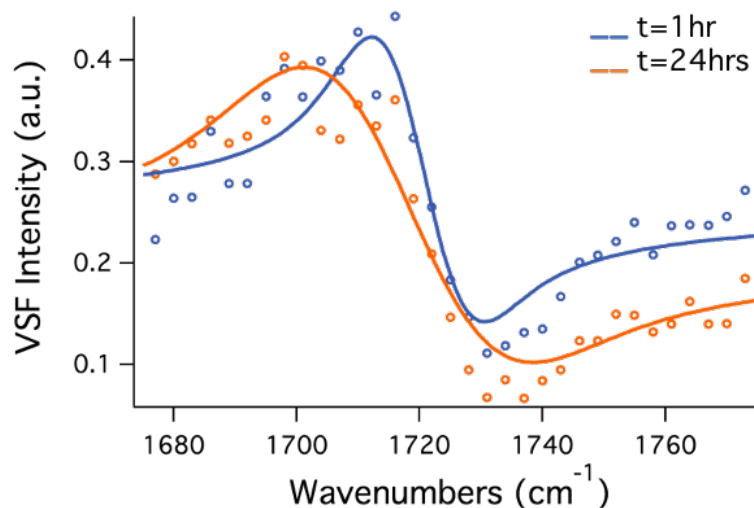


Figure 4.30: VSF spectra in SSP polarizations in the carbonyl stretching region of 0.01 mM d-AOT at the $\text{CCl}_4/\text{D}_2\text{O}$ surface at 1 hour (blue trace) and 24 hours (orange trace) after the interface was formed. Lines are fits to spectra. Full fit parameters can be found in Appendix C, Table C.1.

significantly increase, however, it does broaden slightly. This broadening likely indicates further solvation of interfacial d-AOT headgroups after the molecules have adsorbed to the surface, as the aqueous solvent molecules maximize favorable interactions with the carbonyl modes.

The spectra in Figures 4.29 and 4.30 of d-AOT alone at the surface do not show significant changes in intensity over time from 1 hour to 24 hours after the interface is formed. The VSF detection of the O-D stretching modes from coordinated D_2O molecules and the C-D methyl symmetric stretch suggests d-AOT molecules are present with a net order of the alkyl tails at the surface. As neither the coordinated O-D stretches or C-D stretch modes change in intensity over time, the population and alkyl tail structure of adsorbed d-AOT molecules likely do not change significantly 1 hour to 24 hours after formation of the interface.

The concentration of Span-80 investigated here is higher than that analyzed in the previous section of the SDS co-surfactant mixture (Figure 4.24). Figure 4.31 shows the VSF spectra of 0.1 mM Span-80 alone at the $\text{D}_2\text{O}/\text{CCl}_4$ interface at 1 hour and 24 hours after the formation of the interface. As described previously, the peaks in the C-H stretching region ($2750 - 3000 \text{ cm}^{-1}$) correspond to the methylene symmetric stretch (d+), methyl symmetric stretch (r+), methylene asymmetric stretch (d-), and Fermi resonance modes at $\sim 2850 \text{ cm}^{-1}$, 2870 cm^{-1} , 2920 cm^{-1} , and 2930 cm^{-1} , respectively. The spectral

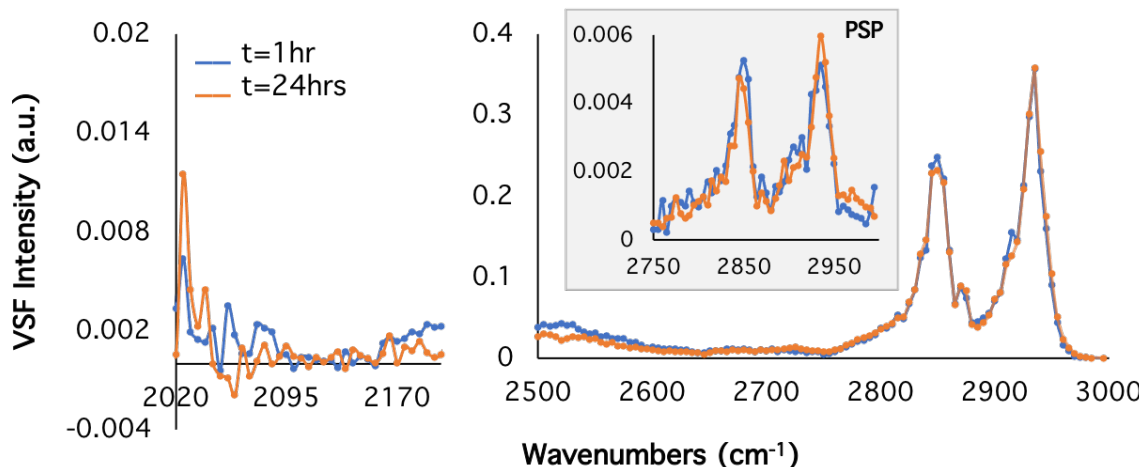


Figure 4.31: VSF spectra in SSP polarizations of 0.1 mM Span-80 at the $\text{CCl}_4/\text{D}_2\text{O}$ surface at 1 hour (blue trace) and 24 hours (orange trace) after the interface was formed. The spectral inset in the grey box was taken with a polarization combination of PSP. The surface behavior of 0.1 mM Span-80 does not change significantly over time. Lines are guides to the eye.

inset in Figure 4.31 shows the VSF spectra of 0.1 mM Span-80 taken with PSP polarizations, probing the C-H stretch responses from Span-80's chiral headgroup (see Figure 4.23). The peaks at $\sim 2850\text{ cm}^{-1}$, 2875 cm^{-1} , and 2935 cm^{-1} in the PSP spectra are attributed to the methylene symmetric stretch (d+), methylene asymmetric stretch (d-), and methylene Fermi resonance (CH_2 FR) modes of the Span-80 chiral headgroup, respectively. The shoulder at $\sim 2900\text{ cm}^{-1}$ in this PSP spectra is due to the methine stretch.¹⁶²

The $2020 - 2200\text{ cm}^{-1}$ spectral region shows the VSF response of any C-D stretching modes or O-D oscillators from highly coordinated D_2O molecules. No signal from the 0.1 mM Span-80 system is detected in this region in either the 1 hour or 24 hours traces, which is expected given Span-80 is not deuterated and has an uncharged headgroup.

Surface pressure measurements report a value of $4 \pm 0.6\text{ mN/m}$ for the solution of 0.1 mM Span-80 at the $\text{CCl}_4/\text{water}$ interface, with an equilibration time of 1 hour. Thus, the amount of Span-80 molecules adsorbed to the surface and contributing to the VSF spectra after 1 hour and 24 hours are expected to be the same. The VSF intensity of the C-H stretching modes from Span-80 do not change in either the SSP or PSP spectra from 1 hour to 24 hours, indicating that the Span-80 molecules adsorbed to the surface at a bulk concentration of 0.1 mM do not undergo any additional reorientation after

adsorption. This differs from what was observed in Figure 4.24 for a lower bulk concentration of 0.025 mM Span-80, where the intensity of Span-80's C-H stretches continued to increase even after the population of adsorbed molecules had equilibrated. The amount of Span-80 molecules adsorbed to the surface in this higher concentration system likely limits the ability of the surfactant alkyl tails to reorient after adsorption. Where at lower concentrations, the Span-80 molecules at the surface have room to restructure the hydrocarbon tails to maximize favorable interactions with the oil phase, the higher concentration of Span-80 molecules causes less room between surfactant nearest neighbors, affecting the net order of the surfactants immediately after adsorption equilibration.

Observing the VSF response of the carbonyl (C=O) mode on Span-80's headgroup further confirms the lack of additional adsorption or reorientation of the molecules after equilibration. Figure 4.32 shows the VSF spectra in SSP polarizations of the C=O stretch for 0.1 mM Span-80 at the D₂O/CCl₄ interface. The carbonyl stretch of the Span-80 headgroup is detected by VSF as a distinct peak in Figure 4.32, contrasting the interference feature observed for the carbonyl stretch mode of d-AOT in Figure 4.29. This is because the nonionic headgroup of Span-80 does not produce a charged surface as d-AOT does, thus the low-wavenumber combination modes from coordinated D₂O

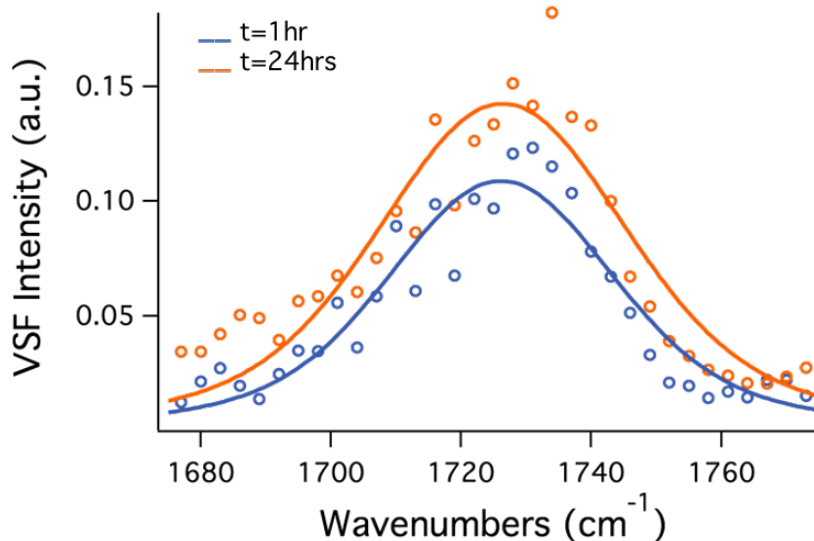


Figure 4.32: VSF spectra in the carbonyl stretching region in SSP polarizations of 0.1 mM Span-80 at the CCl₄/D₂O surface at 1 hour (blue trace) and 24 hours (orange trace) after the interface was formed. Lines are fits to spectra. Full fit parameters can be found in Appendix C, Table C.2.

molecules are not detected by VSF Figure 4.32 and therefore do not interfere with the carbonyl mode.

The overall intensity of the carbonyl mode from interfacial Span-80 does not significantly change between 1 hour and 24 hours, consistent with what was observed in the C-H stretching region (see Appendix C for full fit parameters). The lack of significant change in the VSF intensity due to interfacial Span-80 in Figures 4.30 and 4.31 suggests that the population and surface structure of Span-80 molecules at this concentration does not change after its equilibration time of 1 hour, as supported by surface pressure measurements.

Figure 4.33 shows the VSF spectra of the co-surfactant system containing 0.01 mM d-AOT and 0.1 mM Span-80 at the D₂O/oil interface at 1 hour and 24 hours after formation of the interface. Surface pressure measurements indicate a very long equilibration time of ~ 30 hours for this co-surfactant mixture, with an equilibrated surface pressure value of 14 ± 1 mN/m. This surface pressure value does not vary significantly from that of 0.01 mM AOT alone at the oil/water surface, which equilibrates to a surface pressure of 12 ± 2 mN/m, indicating the surfactants in the mixed system does not interact synergistically to induce additional molecular adsorption to the surface.

The C-H stretching region (2750 – 3000 cm⁻¹) in Figure 4.33 shows the signal from the hydrocarbon tail on interfacial Span-80 molecules increasing over time. This is

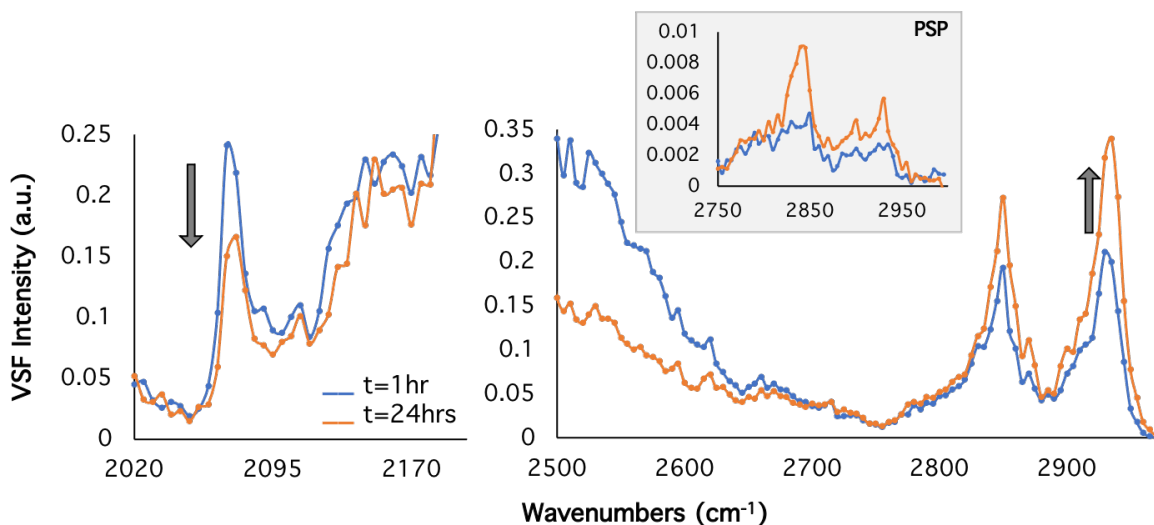


Figure 4.33: VSF spectra in SSP polarizations of 0.1 mM Span-80 with 0.01 mM d-AOT at the CCl₄/D₂O surface at 1 hour (blue trace) and 24 hours (orange trace) after the interface was formed. The spectral inset in the grey box was taken with a polarization combination of PSP. Signal from the C-H stretches of Span-80 increase over time, while signal from the C-D stretches of d-AOT decrease. Lines are guides to the eye.

in contrast to what was observed in Figure 4.31 where the signal from Span-80 did not change over time when alone at the surface. The increase in intensity of Span-80's C-H modes in Figure 4.33 is likely due to additional Span-80 molecules adsorbing to the interface over time, as surface pressure shows a very slow continual adsorption of the co-surfactant system over approximately 30 hours. This trend of increasing C-H mode intensity is present in both the spectra of SSP and PSP polarization schemes, confirming these changes are due to the Span-80 molecules at the surface, and not the few C-H modes from d-AOT.

Interestingly, the signal from O-D stretch oscillators due to coordinated water molecules ($2500 - 2700 \text{ cm}^{-1}$) decreases significantly from 1 hour to 24 hours after the interface is formed. This suggests the amount of charged d-AOT molecules at the surface decreases over time. The spectra in the C-D stretching region of $2020 - 2200 \text{ cm}^{-1}$ supports this observation. The CD_3 methyl symmetric stretch (r^+) from d-AOT, detected as the sharp peak at $\sim 2075 \text{ cm}^{-1}$, decreases in intensity from 1 hour to 24 hours after formation of the interface. It is understood from Equation 9 in Chapter II that such a decrease in the C-D stretching VSF signal is either due to a loss of C-D oscillators at the surface, or a higher amount of disorder in the d-AOT alkyl chains. However, because this decrease in the $\text{CD}_3 r^+$ signal is concurrent with the decrease in the signal from coordinated water O-D stretches, the charged d-AOT molecules are likely leaving the interface over time.

It is noted that the broad signal encompassing the $2020 - 2200 \text{ cm}^{-1}$ region due to the O-D stretch oscillators from highly coordinated D_2O molecules in Figure 4.33 is significantly lower than in Figure 4.29 where 0.01 mM d-AOT was alone at the surface. This decrease in the coordinated water modes causes the $\text{CD}_3 r^+$ peak from d-AOT to be more prominent in the spectra shown in Figure 4.33, as it is less obscured by the water signal. This also indicates less charged AOT surfactant is at the surface when in the co-surfactant mixture with Span-80, compared to when it is alone in solution.

The trends in the VSF spectra shown in Figure 4.33 of the Span-80 with d-AOT co-surfactant system indicates competitive adsorption between the two surfactant molecules, where Span-80 continually adsorbs to the surface over time as d-AOT molecules desorb. This conclusion is supported by previous studies that have found

competitive adsorption of a similar co-surfactant system of AOT with a nonionic surfactant adsorbing to a hydrophobic gold surface.¹⁶³ The VSF spectra of the Span-80 and d-AOT co-surfactant mixture in the carbonyl stretching region further support the competitive adsorption between the two surfactants.

Figure 4.34 shows the VSF spectra in SSP polarizations of 0.01 mM d-AOT with 0.1 mM Span-80 at the oil/water surface in the carbonyl stretching region. Both the d-AOT and Span-80 molecules contain carbonyl modes in their headgroups, allowing both surfactants to contribute to carbonyl stretching peak observed at $\sim 1730\text{ cm}^{-1}$. In Figure 4.29, the spectrum of the carbonyl stretching mode of d-AOT alone at the surface displayed an interference pattern as the carbonyl mode interfered with the elevated signal from the broad underlying D_2O combination band response. However, the spectral shape of the carbonyl stretch peak observed in Figure 4.34 more closely resembles that of Span-80 alone at the surface (Figure 4.32), where the underlying water modes are not amplified due to the uncharged surface, allowing the carbonyl stretch to be detected as a distinct peak. There is a weaker enhancement of the D_2O combination mode in the mixed system compared to the system of d-AOT alone, which is consistent with what was observed for the intensity of the O-D stretch oscillators in the mixed system. This suggests fewer

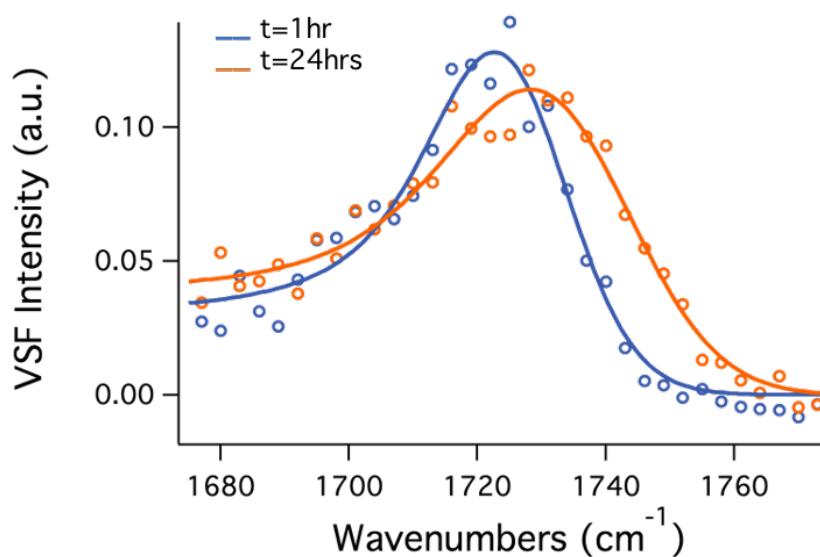


Figure 4.34: VSF spectra in the carbonyl stretching region in SSP polarizations of 0.1 mM Span-80 with 0.01 mM d-AOT at the $\text{CCl}_4/\text{D}_2\text{O}$ surface at 1 hour (blue trace) and 24 hours (orange trace) after the interface was formed. Lines are fits to spectra. Full fit parameters can be found in Appendix C, Table C.3.

charged d-AOT molecules are present at the surface in the mixed system, as the nonionic Span-80 molecules more favorably adsorb to the surface.

Over time from 1 hour to 24 hours after formation of the interface, the carbonyl mode peak in Figure 4.34 does not change in intensity, however, it does broaden (see full fit parameters in Appendix C). It is difficult to distinguish the exact source of the unchanging intensity for this mode, as both AOT and Span-80 molecules contribute to the detected signal. However, it is known from the mathematical fits of the carbonyl modes of AOT and Span-80 alone at the surface (Figures 4.29 and 4.31) that the carbonyl peak of Span-80 is significantly broader than that of AOT. Thus, the broadening of the carbonyl peak for the co-surfactant system in Figure 4.34 likely indicates a higher contribution of signal from Span-80 molecules at the surface over time, consistent with what is observed in the C-H stretching region for this system in Figure 4.33.

All VSF spectra discussed in this section suggest competitive adsorption between Span-80 and AOT surfactant molecules at the oil/water interface. It is possible that the longer hydrocarbon chains of Span-80 cause it to more favorably adsorb to the oil surface over time through stronger hydrophobic interactions. Additionally, the charge-charge repulsion of the d-AOT headgroups likely pose a limiting factor to the adsorption of the charged surfactant, where the Span-80 headgroups do not experience such repulsive forces because they are nonionic. Future studies varying the concentration of Span-80 in solution and investigating the effects of salt added to the mixed system will provide further understanding of the role of Span-80's favorable adsorption to the surface as well as any electrostatic factors limiting the adsorption of AOT to the surface over time.

CHAPTER V:

CONCLUSIONS

The detection and analysis of water vibrational modes at the oil/water surface provide important insight to the intermolecular interactions occurring between molecules at the interface. The water stretch + libration combination band produces a weak, but detectable signal in VSF spectra at wavenumbers slightly higher than that of the free OH. As expected from signal produced by interfacial water molecules, the intensity of the stretch + libration combination mode signal is very sensitive to surface charge, with an anionic surface producing the most visually apparent enhancement of this broad mode. This water combination band's dependence on the libration motion is evidenced by a blueshift in the mode's peak position upon the addition of surface charge, as the enhanced hydrogen bonding network between surface water molecules further frustrates their libration. Due to its dependence on the O-H stretch and H₂O libration motions, the combination mode exhibits a very broad spectral lineshape, affecting spectral features in a wide region beyond its peak location. Specifically, the presence of the D₂O stretch + libration combination mode in VSF spectra at the oil/water interface coincides with the region of interfacial C-H stretching modes detected by VSF spectroscopy (2800 – 3000 cm⁻¹). As the signal from the broad water band and alkyl responses from surface adsorbates mix, constructive and destructive interferences can occur between the modes in the resulting spectrum. Thus, it is imperative to understand the experimental factors affecting the spectral features of the water combination mode, and how its presence may affect the spectral analysis of other vibrational regions of interest.

A second H₂O combination mode arising from the simultaneous excitation of the bend and libration motions, also known as the “association band”, is detected at the oil/water interface in the region of C-D stretches (2000 – 2200 cm⁻¹). Originating from coordinated water molecules, this mode is also very broad in nature and sensitive to surface charge. Its ability to be detected by VSF spectroscopy warrants consideration for an important experimental factor when analyzing deuterated alkyl modes at the surface–

regardless of whether choosing an aqueous phase of H₂O or D₂O, this region of C-D stretches will contain underlying signal from water modes.

It may be beneficial for future studies to investigate the presence of these broad water combination modes through heterodyne-detection VSF spectroscopy, to compliment the findings discussed in this work. These studies would provide further insight to the phase relationship between these weak modes and the underlying nonresonant signal. While signal from these water combination bands are likely present at other interfaces, such as the commonly studied air/water interface, the inherently more intense nonresonant backgrounds of these surfaces may obscure the detection of these weak modes with homodyne VSF spectroscopy. Thus, heterodyne-detection VSF spectroscopy will likely be beneficial for investigating the presence and behavior of these weak resonant water modes at other aqueous/hydrophobic surfaces.

The analysis of these water combination modes is taken into consideration when analyzing mixed systems of nonionic polymers and charged surfactants, as the charged headgroup of the surfactants can cause these water modes to appear in the VSF spectra. The interfacial presence and structure of surface-active nonionic polymers, such as PEO and PVA, are found to be largely unaffected by the addition of charged surfactants. However, polyacrylamide (PAM), a surface-inactive nonionic polymer, is drawn to the oil/water interface in the presence of charged surfactant when it would otherwise remain solvated in the bulk aqueous solution. Cationic surfactants induce a strict ordering of the PAM chain, as the partial negative charge of the carbonyl mode on the acrylamide monomers acts anchor points for attracting the polymer to the adsorbed surfactant headgroups through charge-dipole interactions. Anionic surfactants on the other hand, while attracting the polymer to the surface through charge-dipole interactions, do not induce a strict overall structure to the interfacial polymer due to the spatial distribution of the partial positive charge along the polymer backbone.

Co-surfactant mixtures containing a nonionic species were also investigated; however, similar charge-dipole interactions between the surface adsorbates are not found to be present between the nonionic and anionic surfactants chosen for these studies. Instead, evidence of competitive adsorption between nonionic Span-80 and anionic surfactants SDS and AOT imply the attraction of Span-80 to the oil phase is stronger than

any attractive intermolecular forces with anionic surfactants. This finding is of consequence for oil spill dispersant applications, which rely on mixtures of nonionic and anionic surfactants to lower the surface tension between crude oil and water to disperse the oil spill into the ocean.

Because the systems involved in remediating oil spills through dispersant mixtures contain complex chemical mixtures, future studies investigating the effects salt and various solvents on the surface behavior of these co-surfactant systems will provide further insight to their efficacy as dispersant mixture ingredients. Additionally, if computational costs can be overcome for simulating large systems, computational studies analyzing the behavior of polymer chains in interfacial mixed systems would be beneficial for further understanding the wide variety of structures these polymers can form at the surface, especially in the presence of charged surfactants. Along with the results discussed in these works, studies utilizing other methods to probe the complex behavior of molecules at the oil/water interface together can provide the scientific community with collective insight to the mysteries of surface-specific chemical events.

APPENDIX A:

FIT PARAMETERS FOR SPECTRAL OF WATER STRETCH + LIBRATION COMBINATION BAND SYSTEMS

Table A.1: Fit parameters for VSF spectra in Figure 3.1 of the bare water/CCl₄ interface with aqueous solvents of H₂O and D₂O in the 3600-4000 cm⁻¹ region in SSP polarizations. Spectra were fit individually.

Peak Assignment	Fit Variable	H ₂ O : D ₂ O	
		0 : 1	1 : 0
Free OH	Amplitude	0.03 ± 0.02	0.90 ± 0.03
	Phase	3.14	3.14
	Lorentzian Width	12	12
	Peak Position (cm ⁻¹)	3692 ± 4	3679 ± 0.7
	Gaussian Width	11 ± 9	12 ± 0.7
Coordinated O-H Stretches	Amplitude		0.281 ± 0.008
	Phase		0
	Lorentzian Width		5
	Peak Position (cm ⁻¹)		3470 ± 20
	Gaussian Width		100 ± 20
H ₂ O Stretch + Rotation Combination Band	Amplitude		0.083 ± 0.007
	Phase		3.14
	Lorentzian Width		5
	Peak Position (cm ⁻¹)		3805 ± 8
	Gaussian Width		200 ± 20
Water monomer OH sym. stretch	Amplitude		0.15 ± 0.03
	Phase		0
	Lorentzian Width		5
	Peak Position (cm ⁻¹)		3650 ± 3
	Gaussian Width		21 ± 4
Water monomer OH asym. stretch	Amplitude		0.061 ± 0.005
	Phase		3.14
	Lorentzian Width		5
	Peak Position (cm ⁻¹)		3744 ± 2
	Gaussian Width		26 ± 3
Nonresonant	Amplitude	0.054248	0.054248
	Phase	0	0

Table A.2: Fit parameters for VSF spectra in Figure 3.3 of the isotopic dilutions of the bare water/CCl₄ interface in the 3600-4000 cm⁻¹ region in SSP polarizations. The integrated area of the combination band fit peak under the 0.3:0.7, 0.6:0.4, and 1:0 ratios are 0.04, 0.19, and 0.79, respectively, providing further evidence of the gradual increase in combination mode signal. It is noted that large Gaussian widths are present in the coordinated O-H stretch and the water combination band fit peaks, as the hydrogen bonding network of liquid water creates a complex bonding environment for O-H oscillators, causing large spectral widths in modes dependent on O-H stretch and libration motions. The spectra of isotopic dilution ratios of 0:1 and 0.1:0.9 were fit individually, while those of 0.3:0.7, 0.6:0.4, and 1:0 ratios were globally fit to determine the peak position of the combination band, due to their more prominent spectral features.

Peak Assignment	Fit Variable	H ₂ O : D ₂ O				
		0 : 1	0.1 : 0.9	0.3 : 0.7	0.6 : 0.4	1 : 0
Free OH	Amplitude	0.03 ± 0.02	0.146 ± 0.009	0.31 ± 0.02	0.53 ± 0.02	0.90 ± 0.03
	Phase	3.14	3.14	3.14	3.14	3.14
	Lorentzian Width	12	12	12	12	12
	Peak Position (cm ⁻¹)	3692 ± 4	3669 ± 1	3671 ± 1	3674 ± 0.06	3679 ± 0.7
	Gaussian Width	11 ± 9	20 ± 2	17 ± 1	13 ± 0.5	12 ± 0.7
Coordinated O-H Stretches	Amplitude		0.023 ± 0.005	0.05 ± 0.01	0.121 ± 0.007	0.281 ± 0.008
	Phase		0	0	0	0
	Lorentzian Width		5	5	5	5
	Peak Position (cm ⁻¹)		3190 ± 180	3538 ± 30	3540 ± 8	3470 ± 20
	Gaussian Width		300 ± 100	60 ± 30	60 ± 10	100 ± 20
H ₂ O Stretch + Rotation Combination Band	Amplitude			0.018 ± 0.004	0.041 ± 0.003	0.083 ± 0.007
	Phase			3.14	3.14	3.14
	Lorentzian Width			5	5	5
	Peak Position (cm ⁻¹)			3805 ± 8	3805 ± 8	3805 ± 8
	Gaussian Width			200 ± 100	200 ± 40	200 ± 20
Water monomer OH sym. stretch	Amplitude					0.15 ± 0.03
	Phase					0
	Lorentzian Width					5
	Peak Position (cm ⁻¹)					3650 ± 3
	Gaussian Width					21 ± 4

Table A.2 continued

Water monomer OH asym. stretch	Amplitude					0.061 ± 0.005
	Phase					3.14
	Lorentzian Width					5
	Peak Position (cm ⁻¹)					3744 ± 2
	Gaussian Width					26 ± 3
Nonresonant	Amplitude	0.054248	0.054248	0.054248	0.054248	0.054248
	Phase	0	0	0	0	0

Table A.3: Fit parameters for VSF spectra in Figure 3.4a of the isotopic dilutions of the water/CCl₄ interface in the 3600-4000 cm⁻¹ region with 0.1 mM anionic SDS in SSP polarizations. The integrated area of the combination band fit peak under the 0.1 : 0.9, 0.3 : 0.7, 0.6 : 0.4, and 1 : 0 ratios are 0.005, 0.008, 0.01, and 0.588, respectively, providing further evidence of the gradual increase in signal contribution due to the combination mode. The spectrum of isotopic dilution ratio 0:1 was fit individually, while those of 0.1:0.9, 0.3:0.7, 0.6:0.4, and 1:0 ratios were globally fit to determine the peak position of the combination band, due to their more prominent spectral features.

Peak Assignment	Fit Variable	H ₂ O : D ₂ O				
		0 : 1	0.1 : 0.9	0.3 : 0.7	0.6 : 0.4	1 : 0
Free OH	Amplitude	0.06 ± 0.1	0.15 ± 0.03	0.23 ± 0.02	0.50 ± 0.03	1.2 ± 0.3
	Phase	3.14	3.14	3.14	3.14	3.14
	Lorentzian Width	12	12	12	12	12
	Peak Position (cm ⁻¹)	3692 ± 2	3689 ± 3	3683 ± 2	3674.9 ± 0.5	3675.8 ± 0.4
	Gaussian Width	13 ± 4	20 ± 6	20 ± 3	12 ± 2	5 ± 1
Coordinated O-H Stretches	Amplitude	0.073 ± 0.001	0.229 ± 0.004	0.423 ± 0.003	0.825 ± 0.004	0.819 ± 0.007
	Phase	3.14	3.14	3.14	3.14	3.14
	Lorentzian Width	5	5	5	5	5
	Peak Position (cm ⁻¹)	3510 ± 10	3550 ± 10	3373 ± 4	3188 ± 6	3304 ± 4
	Gaussian Width	120 ± 10	120 ± 10	262 ± 5	300 ± 5	227 ± 3
H ₂ O Stretch + Rotation Combination Band	Amplitude		0.03 ± 0.02	0.037 ± 0.006	0.040 ± 0.004	0.145 ± 0.003
	Phase		3.14	3.14	3.14	3.14
	Lorentzian Width		5	5	5	5
	Peak Position (cm ⁻¹)		3848 ± 3	3848 ± 3	3848 ± 3	3848 ± 3
	Gaussian Width		52 ± 47	55 ± 10	58 ± 9	100 ± 7
Water monomer OH sym. stretch	Amplitude			0.09 ± 0.02	0.105 ± 0.008	0.021 ± 0.009
	Phase			0	0	0
	Lorentzian Width			5	5	5
	Peak Position (cm ⁻¹)			3642 ± 3	3634 ± 5	3628 ± 6
	Gaussian Width			15 ± 4	50 ± 5	18 ± 10
Water monomer OH asym. stretch	Amplitude					0.11 ± 0.009
	Phase					3.14
	Lorentzian Width					5
	Peak Position (cm ⁻¹)					3741 ± 2
	Gaussian Width					38 ± 3
Nonresonant	Amplitude	0.0190261	0.0190261	0.0190261	0.0190261	0.0190261
	Phase	3.14	3.14	3.14	3.14	3.14

Table A.4: Fit parameters for VSF spectra in Figure 3.4b of the isotopic dilutions of the water/CCl₄ interface in the 3600-4000 cm⁻¹ region with 0.1 mM cationic DTAB in SSP polarizations. The integrated areas of the combination band fit peak under the 0.1:0.9, 0.3:0.7, 0.6:0.4, and 1:0 ratios are 0.0108, 0.002, 0.080, 0.445, respectively. It is noted the integrated area under the 0.3:0.7 isotopic dilution ratio is an outlier in the trend of the combination mode's contribution to signal intensity increasing upon addition of O-H modes. This is likely due to the large errors in fitting the combination mode at this isotopic ratio, as the overall VSF intensity is nearly zero due to mode interferences (see Figure 3.4b), proving fitting of this isotopic dilution spectrum very difficult. However, the general trend in the integrated area under the combination mode regardless of this outlier still provides evidence of the gradual increase in signal contribution due to the combination mode. The spectrum of isotopic dilution ratio 0:1 was fit individually, while those of 0.1:0.9, 0.3:0.7, 0.6:0.4, and 1:0 ratios were globally fit to determine the peak position of the combination band, due to their more prominent spectral features.

Peak Assignment	Fit Variable	H ₂ O : D ₂ O				
		0 : 1	0.1 : 0.9	0.3 : 0.7	0.6 : 0.4	1 : 0
Free OH	Amplitude	0.14 ± 0.04	0.14 ± 0.10	0.21 ± 0.04	0.34 ± 0.02	0.79 ± 0.04
	Phase	3.14	3.14	3.14	3.14	3.14
	Lorentzian Width	12	12	12	12	12
	Peak Position (cm ⁻¹)	3689 ± 2	3670 ± 30	3678 ± 3	3671 ± 1	3676 ± 0.6
	Gaussian Width	12 ± 4	24 ± 29	26 ± 6	24 ± 2	12 ± 1
Coordinated O-H Stretches	Amplitude	1 ± 12	0.39 ± 0.02	0.560 ± 0.004	0.97 ± 0.01	1.07 ± 0.03
	Phase	0	0	0	0	0
	Lorentzian Width	5	5	5	5	5
	Peak Position (cm ⁻¹)	3130 ± 300	3177 ± 50	3314 ± 6	3268 ± 9	3434 ± 10
	Gaussian Width	76 ± 900	300 ± 40	280 ± 7	242 ± 7	146 ± 7
H ₂ O Stretch + Rotation Combination Band	Amplitude		0.02 ± 0.01	0.018 ± 0.03	0.10 ± 0.01	0.193 ± 0.006
	Phase		3.14	3.14	3.14	3.14
	Lorentzian Width		5	5	5	5
	Peak Position (cm ⁻¹)		3857 ± 13	3857 ± 13	3857 ± 13	3857 ± 13
	Gaussian Width		95 ± 70	65 ± 130	66 ± 13	78 ± 5
Water monomer OH sym stretch	Amplitude					0.071 ± 0.007
	Phase					3.14
	Lorentzian Width					5
	Peak Position (cm ⁻¹)					3602 ± 1
	Gaussian Width					24 ± 3
Nonresonant	Amplitude	0.19939	0.19939	0.19939	0.19939	0.19939
	Phase	0	0	0	0	0

Table A.5: Fit parameters for VSF spectra in Figure 3.5b of the isotopic dilutions of the D₂O/CCl₄ surface in the presence of 0.01 mM d-SDS with and without 1 M NaCl in SSP polarizations. Spectra were fit individually.

Peak Assignment	Fit Variable	0.01 mM SDS + 1M NaCl in D ₂ O	0.01 mM SDS in D ₂ O
Free OD	Amplitude	0.06 ± 0.01	0.36 ± 0.02
	Phase	3.14	3.14
	Lorentzian Width	12	12
	Peak Position (cm ⁻¹)	2721	2720.7 ± 0.7
	Gaussian Width	16 ± 12	12 ± 2
Coordinated O-D Stretches	Amplitude	0.06 ± 0.01	0.33 ± 0.01
	Phase	0	3.14
	Lorentzian Width	5	5
	Peak Position (cm ⁻¹)	2550	2495 ± 4
	Gaussian Width	100 ± 40	61 ± 1
D ₂ O Stretch + Rotation Combination Band	Amplitude	0.05 ± 0.04	0.042 ± 0.003
	Phase	3.14	3.14
	Lorentzian Width	5	5
	Peak Position (cm ⁻¹)	2855 ± 80	2851 ± 10
	Gaussian Width	100 ± 50	87 ± 10
Water monomer OD sym. stretch	Amplitude	0.02 ± 0.02	0.093 ± 0.008
	Phase	0	0
	Lorentzian Width	5	5
	Peak Position (cm ⁻¹)	2708	2708 ± 2
	Gaussian Width	11 ± 8	57 ± 5
Water monomer OD asym. stretch	Amplitude	0.02 ± 0.07	0.06 ± 0.01
	Phase	3.14	3.14
	Lorentzian Width	5	5
	Peak Position (cm ⁻¹)	2762	2762 ± 7
	Gaussian Width	70 ± 100	45 ± 10
Nonresonant	Amplitude	0.034463	0.017982
	Phase	0	0

Table A.6: Fit parameters for VSF spectra in Figure 3.6 of the bare D₂O/CCl₄ interface, and in the presence of 0.01 mM and 0.1 mM d-SDS in SSP polarizations. Spectra were fit individually.

Peak Assignment	Fit Variable	D ₂ O	0.01 mM SDS in D ₂ O	0.1 mM SDS in D ₂ O
Free OD	Amplitude	0.28 ± 0.03	0.36 ± 0.02	0.47 ± 0.04
	Phase	3.14	3.14	3.14
	Lorentzian Width	12	12	12
	Peak Position (cm ⁻¹)	2721 ± 1	2720.7 ± 0.7	3720.7 ± 0.7
	Gaussian Width	10 ± 1	12 ± 2	16 ± 2
Coordinated O-D Stretches	Amplitude	0.070 ± 0.005	0.33 ± 0.01	0.407 ± 0.007
	Phase	0	3.14	3.14
	Lorentzian Width	5	5	5
	Peak Position (cm ⁻¹)	2560 ± 20	2495 ± 4	2480 ± 4
	Gaussian Width	110 ± 10	61 ± 1	89 ± 1
D ₂ O Stretch + Rotation Combination Band	Amplitude	0.012 ± 0.003	0.042 ± 0.003	0.077 ± 0.007
	Phase	3.14	3.14	3.14
	Lorentzian Width	5	5	5
	Peak Position (cm ⁻¹)	2815 ± 30	2851 ± 10	2856 ± 10
	Gaussian Width	96 ± 31	87 ± 10	100 ± 10
Water monomer OD sym. stretch	Amplitude	0.026 ± 0.008	0.093 ± 0.008	0.22 ± 0.04
	Phase	0	0	0
	Lorentzian Width	5	5	5
	Peak Position (cm ⁻¹)	2697 ± 2	2708 ± 2	2708 ± 2
	Gaussian Width	10 ± 5	57 ± 5	36 ± 1
Water monomer OD asym. stretch	Amplitude	0.008 ± 0.004	0.06 ± 0.01	0.05 ± 0.02
	Phase	3.14	3.14	3.14
	Lorentzian Width	5	5	5
	Peak Position (cm ⁻¹)	2770 ± 5	2762 ± 7	2762 ± 7
	Gaussian Width	15 ± 13	45 ± 10	59 ± 20
Nonresonant	Amplitude	0.03368	0.017982	0.00186515
	Phase	0	0	0

Table A.7: Fit parameters for VSF spectra in Figure 3.7 of the D₂O/CCl₄ interface with 0.02 mM Span-80 + 0.015 mM d-SDS and 0.02 mM Span-80 + 0.015 mM d-DTAB in SSP polarizations. Spectra were fit individually.

Peak Assignment	Fit Variable	15 uM d-SDS + 20 uM Span-80 in D ₂ O	15 uM d-DTAB + 20 uM Span-80 in D ₂ O
CH₂ S.S.	Amplitude	0.24 ± 0.02	0.7 ± 0.1
	Phase	3.14	3.14
	Lorentzian Width	2	2
	Peak Position (cm ⁻¹)	2851 ± 1	2852.6 ± 0.8
	Gaussian Width	8.9 ± 0.6	9.5 ± 0.5
CH₃ S.S.	Amplitude	0.10 ± 0.03	0.32 ± 0.04
	Phase	3.14	3.14
	Lorentzian Width	2	2
	Peak Position (cm ⁻¹)	2871 ± 1	2869 ± 1
	Gaussian Width	4 ± 2	4.0 ± 0.8
CH₂ A.S.	Amplitude	0.2 ± 0.2	0.3 ± 1
	Phase	0	0
	Lorentzian Width	2	2
	Peak Position (cm ⁻¹)	2919 ± 7	2916 ± 5
	Gaussian Width	10 ± 7	16 ± 5
CH₃ F.R.	Amplitude	0.6 ± 1	0.4 ± 0.1
	Phase	0	0
	Lorentzian Width	2	2
	Peak Position (cm ⁻¹)	2933 ± 2	2928 ± 2
	Gaussian Width	8 ± 2	7 ± 2
CH₃ A.S.	Amplitude	0.16 ± 0.07	0.6 ± 0.3
	Phase	0	3.14
	Lorentzian Width	2	2
	Peak Position (cm ⁻¹)	2960 ± 10	2940 ± 7
	Gaussian Width	22 ± 20	14 ± 2
D₂O Stretch + Rotation Combination Band	Amplitude	0.26 ± 0.03	0.14 ± 0.06
	Phase	3.14	0
	Lorentzian Width	5	5
	Peak Position (cm ⁻¹)	2865 ± 60	2825 ± 45
	Gaussian Width	150 ± 70	100 ± 50
Water monomer OD asym. stretch	Amplitude	0.4 ± 0.2	
	Phase	0	
	Lorentzian Width	5	
	Peak Position (cm ⁻¹)	2781 ± 8	
	Gaussian Width	50 ± 10	

APPENDIX B:

FIT PARAMETERS FOR SPECTRA OF POLYACRYLAMIDE- SURFACTANT SYSTEMS

Table B.1: Fit parameters for VSF spectra in Figure 4.12 of the D₂O/CCl₄ with 0.015 mM d-SDS and 0, 0.15, 4.2, and 21 mM PAM in SSP polarizations. Spectra were fit individually.

PAM + 0.015 mM d-SDS (SSP)		0 mM PAM	0.015 mM PAM	4.2 mM PAM	21 mM PAM
Coordinated O-D stretches	Amplitude	0.9 ± 0.2	0.9 ± 0.1	0.7 ± 0.1	0.7 ± 0.2
	Phase	0	0	0	0
	Lorentzian	5	5	5	5
	Peak Position	2480 ± 30	2485 ± 6	2484 ± 25	2486 ± 48
	Gaussian	100 ± 4	80 ± 6	96 ± 4	110 ± 7
Free OD	Amplitude	0.62 ± 0.06	0.5 ± 0.1	0.42 ± 0.08	0.5 ± 0.2
	Phase	0	0	0	0
	Lorentzian	12	12	12	12
	Peak Position	2719	2716 ± 1	2717 ± 2	2719 ± 2
	Gaussian	11 ± 1	8 ± 2	10 ± 2	8 ± 3
Water monomer OD asym. stretch	Amplitude	0.10 ± 0.01	0.09 ± 0.03	0.1 ± 0.04	0.10 ± 0.04
	Phase	0	0	0	0
	Lorentzian	5	5	5	5
	Peak Position	2781	2789 ± 2	2790 ± 3	2791 ± 3
	Gaussian	40 ± 8	40 ± 8	43 ± 10	44 ± 10
D ₂ O Stretch + Rotation Combination Band	Amplitude	0.14 ± 0.2	0.067 ± 0.009	0.07 ± 0.02	0.08 ± 0.03
	Phase	0	0	0	0
	Lorentzian	5	5	5	5
	Peak Position	2880 ± 9	2871 ± 31	2872 ± 47	2878 ± 43
	Gaussian	112 ± 14	111 ± 31	112 ± 46	115 ± 46
CH ₂ symmetric stretch	Amplitude		0.08 ± 0.01	0.09 ± 0.01	0.07 ± 0.01
	Phase		3.14	3.14	3.14
	Lorentzian		2	2	2
	Peak Position		2932 ± 2	2931 ± 2	2928 ± 3
	Gaussian		13 ± 3	16 ± 3	20 ± 5

Table B.2: Fit parameters for VSF spectra in Figure 4.15 of the D₂O/CCl₄ with 0.015 mM d-SDS and 1 M NaCl with and without 4.2 mM PAM in SSP polarizations. Spectra were fit individually.

0.015 mM d-SDS + 1 M NaCl (SSP)		0 mM PAM	4.2 mM PAM
Coordinated O-D stretches peak 1	Amplitude	0.07 ± 0.01	0.080 ± 0.007
	Phase	0	0
	Lorentzian	5	5
	Peak Position	2646 ± 4	2640 ± 8
	Gaussian	60 ± 10	75 ± 22
Coordinated O-D stretches peak 2	Amplitude	0.27 ± 0.01	0.38 ± 0.01
	Phase	0	0
	Lorentzian	5	5
	Peak Position	2488 ± 12	2490 ± 8
	Gaussian	88 ± 11	66 ± 8
Free OD	Amplitude	0.11 ± 0.03	0.1 ± 0.1
	Phase	0	0
	Lorentzian	12	12
	Peak Position	2720 ± 2	2719 ± 4
	Gaussian	11 ± 5	8 ± 11
Water monomer OD asym. stretch	Amplitude	0.03 ± 0.01	0.04 ± 0.02
	Phase	0	0
	Lorentzian	5	5
	Peak Position	2785 ± 8	2790 ± 9
	Gaussian	53 ± 18	43 ± 19
D ₂ O Stretch + Rotation Combination Band	Amplitude	0.067 ± 0.004	0.056 ± 0.004
	Phase	0	0
	Lorentzian	5	5
	Peak Position	2906 ± 18	2909 ± 21
	Gaussian	174 ± 35	123 ± 37

Table B.3: Fit parameters for VSF spectra in Figure 4.16a of the D₂O/CCl₄ with 0.015 mM d-DTAB and 0.15, 4.2, and 21 mM PAM in SSP polarizations. Spectra were fit individually.

PAM + 0.015 mM d-DTAB (SSP)		0.015 mM PAM	4.2 mM PAM	21 mM PAM
C-H Stretch	Amplitude	0.06 ± 0.01	0.096 ± 0.009	0.11 ± 0.01
	Phase	0	0	0
	Lorentzian	2	2	2
	Peak Position	2875 ± 3	2872 ± 2	2871 ± 2
	Gaussian	15 ± 4	15 ± 2	15 ± 3
CH ₂ symmetric stretch	Amplitude	0.319 ± 0.003	0.450 ± 0.003	0.458 ± 0.004
	Phase	0	0	0
	Lorentzian	2	2	2
	Peak Position	2935.5 ± 0.3	2935.7 ± 0.2	2935.2 ± 0.2
	Gaussian	14.4 ± 0.3	14.1 ± 0.2	14.0 ± 0.3

Table B.4: Fit parameters for VSF spectra in Figure 4.16a of the D₂O/CCl₄ with 0.015 mM d-DTAB only in SSP polarizations.

0.015 mM d-DTAB (SSP)		
Coordinated D ₂ O peak 1	Amplitude	0.92 ± 0.02
	Phase	3.14
	Lorentzian	2
	Peak Position	2576 ± 4
	Gaussian	47 ± 3
Coordinated D ₂ O peak 2	Amplitude	0.42 ± 0.02
	Phase	0
	Lorentzian	2
	Peak Position	2719 ± 1
	Gaussian	18 ± 1
Free OD	Amplitude	0.11 ± 0.02
	Phase	0
	Lorentzian	2
	Peak Position	2682 ± 1
	Gaussian	15 ± 3

Table B.5: Fit parameters for VSF spectra in Figure 4.16b of the D₂O/CCl₄ with 0.015 mM d-DTAB and 0.015, 4.2, and 21 mM PAM in SPS polarization. The elevated background in the spectra is fit to a constant background response. Spectra were fit individually.

PAM + 0.015 mM d-DTAB (SPS)		0.015 mM PAM	4.2 mM PAM	21 mM PAM
C-H stretch	Amplitude	1.71 ± 0.09	1.60 ± 0.09	1.47 ± 0.08
	Phase	0	0	0
	Lorentzian	2	2	2
	Peak Position	2875 ± 3	2873 ± 3	2870 ± 3
	Gaussian	63 ± 14	63 ± 13	52 ± 7
CH₂ symmetric stretch	Amplitude	0.12 ± 0.2	1.2 ± 0.2	1.07 ± 0.07
	Phase	0	0	0
	Lorentzian	2	2	2
	Peak Position	2959 ± 2	2957 ± 2	2957 ± 1
	Gaussian	32 ± 3	30 ± 3	28 ± 2
Background	Amplitude	1.09 ± 0.05	1.07 ± 0.05	1.08 ± 0.04
	Phase	3.14	3.14	3.14

Table B.6: Fit parameters for VSF spectra in Figure 4.17 of the D₂O/CCl₄ with 0.015 mM d-DTAB and 0.015, 4.2, and 21 mM PAM in SSP polarizations. Spectra were fit individually.

PAM + 0.015 mM d-DTAB (SSP)		0.015 mM PAM	4.2 mM PAM	21 mM PAM
C=O peak	Amplitude	1.51 ± 0.09	2.2 ± 0.1	1.85 ± 0.08
	Phase	0	0	0
	Lorentzian	5	5	5
	Peak Position	1650.4 ± 0.8	1651.1 ± 0.6	1649.6 ± 0.5
	Gaussian	12 ± 1	10.3 ± 0.8	10.0 ± 0.7

Table B.7: Fit parameters for VSF spectra in Figure 4.17 of the D₂O/CCl₄ with 0.015 mM d-CTAB and 0.015, 4.2, and 21 mM PAM in SSP polarizations. Spectra were fit individually.

PAM + 0.001 mM d-CTAB (SSP)		0.015 mM PAM	4.2 mM PAM	21 mM PAM
C-H stretch	Amplitude	0.051 ± 0.007	0.07 ± 0.008	0.12 ± 0.01
	Phase	0	0	0
	Lorentzian	2	2	2
	Peak Position	2879 ± 3	2875 ± 2	2873 ± 2
	Gaussian	20 ± 4	15 ± 2	12 ± 2
CH₂ symmetric stretch	Amplitude	0.266 ± 0.002	0.413 ± 0.002	0.396 ± 0.004
	Phase	0	0	0
	Lorentzian	2	2	2
	Peak Position	2937.2 ± 0.3	2937.1 ± 0.2	2934.0 ± 0.3
	Gaussian	15.7 ± 0.3	15.4 ± 0.2	15.4 ± 0.3

APPENDIX C:

FIT PARAMETERS FOR SPECTRA OF SPAN-80 CO-SURFACTANT SYSTEMS

Table C.1: Fit parameters for VSF spectra in Figure 4.30 of the D₂O/CCl₄ with 0.01 mM d-AOT at 1 hour and 24 hours after formation of the interface in SSP polarizations. Spectra were fit individually.

d-AOT + Span-80 SSP		1 hour	24 hours
C=O stretch	Amplitude	1.04 ± 0.03	0.88 ± 0.03
	Phase	0	0
	Lorentzian	2	2
	Peak Position	1730 ± 1	1728 ± 1
	Gaussian	13 ± 2	16 ± 1
Background D₂O combination mode	Amplitude	0.56 ± 0.01	0.54 ± 0.01
	Phase	3.14	3.14
	Lorentzian	5	5
	Peak Position	1698 ± 6	1670 ± 10
	Gaussian	230 ± 30	200 ± 30

Table C.2: Fit parameters for VSF spectra in Figure 4.32 of the D₂O/CCl₄ with 0.1 mM Span-80 at 1 hour and 24 hours after formation of the interface in SSP polarizations. Spectra were fit individually.

d-AOT + Span-80 SSP		1 hour	24 hours
C=O stretch	Amplitude	0.37 ± 0.01	0.42 ± 0.01
	Phase	0	0
	Lorentzian	2	2
	Peak Position	1726 ± 1	1726 ± 1
	Gaussian	20 ± 1	22 ± 1

Table C.3: Fit parameters for VSF spectra in Figure 4.34 of the D₂O/CCl₄ with 0.01 mM d-AOT and 0.1 mM Span-80 at 1 hour and 24 hours after formation of the interface in SSP polarizations. Spectra were fit individually.

d-AOT + Span-80 SSP		1 hour	24 hours
C=O stretch	Amplitude	0.43 ± 0.07	0.38 ± 0.06
	Phase	0	0
	Lorentzian	2	2
	Peak Position	1729 ± 2	1738 ± 4
	Gaussian	12 ± 2	17 ± 3
Background D₂O combination mode	Amplitude	0.17 ± 0.03	0.20 ± 0.03
	Phase	3.14	3.14
	Lorentzian	5	5
	Peak Position	1600 ± 200	1600 ± 200
	Gaussian	100 ± 200	100 ± 200

REFERENCES CITED

1. Aloisio, S.; Francisco, J. S., Radical–Water Complexes in Earth's Atmosphere. *Accounts of Chemical Research* **2000**, *33* (12), 825-830.
2. Anglada, J. M.; Martins-Costa, M.; Ruiz-López, M. F.; Francisco, J. S., Spectroscopic signatures of ozone at the air–water interface and photochemistry implications. *Proceedings of the National Academy of Sciences* **2014**, *111* (32), 11618-11623.
3. Deiseroth, M.; Bonn, M.; Backus, E. H. G., Electrolytes Change the Interfacial Water Structure but Not the Vibrational Dynamics. *The Journal of Physical Chemistry B* **2019**, *123* (40), 8610-8616.
4. Doshi, B.; Sillanpaa, M.; Kalliola, S., A review of bio-based materials for oil spill treatment. *Water Res* **2018**, *135*, 262-277.
5. Shamay, E. S.; Valley, N. A.; Moore, F. G.; Richmond, G. L., Staying hydrated: the molecular journey of gaseous sulfur dioxide to a water surface. *Phys Chem Chem Phys* **2013**, *15* (18), 6893-902.
6. Venkataraman, P.; Tang, J.; Frenkel, E.; McPherson, G. L.; He, J.; Raghavan, S. R.; Kolesnichenko, V.; Bose, A.; John, V. T., Attachment of a Hydrophobically Modified Biopolymer at the Oil–Water Interface in the Treatment of Oil Spills. *ACS Applied Materials & Interfaces* **2013**, *5* (9), 3572-3580.
7. Athas, J. C.; Jun, K.; McCafferty, C.; Owoseni, O.; John, V. T.; Raghavan, S. R., An Effective Dispersant for Oil Spills Based on Food-Grade Amphiphiles. *Langmuir* **2014**, *30* (31), 9285-9294.
8. Riehm, D. A.; Rokke, D. J.; McCormick, A. V., Water-in-Oil Microstructures Formed by Marine Oil Dispersants in a Model Crude Oil. *Langmuir* **2016**, *32* (16), 3954-3962.
9. Duong, T. V.; Van Humbeeck, J.; Van den Mooter, G., Crystallization Kinetics of Indomethacin/Polyethylene Glycol Dispersions Containing High Drug Loadings. *Molecular Pharmaceutics* **2015**, *12* (7), 2493-2504.
10. Ruel-Gariépy, E.; Leroux, J.-C., In situ-forming hydrogels—review of temperature-sensitive systems. *European Journal of Pharmaceutics and Biopharmaceutics* **2004**, *58* (2), 409-426.
11. Kawaguchi, M.; Ishikawa, R.; Yamamoto, M.; Kuki, T.; Kato, T., Molecular Weight Dependence of Interfacial Properties of Poly(n-hexyl isocyanate) Films at the Air–Water and Oil–Water Interfaces. *Langmuir* **2001**, *17* (2), 384-387.

12. Gregory, J., *Polymers at interfaces*, by G. J. Fler, M. A. Cohen Stuart, J. M. H. M. Scheutjens, T. Cosgrove and B. Vincent. Chapman and Hall, London, 1993. Pp. xv + 502, price £65.00. ISBN 0-412-58160-4. *Polymer International* **1995**, *36* (1), 102-102.
13. Gordon, B. P.; Moore, F. G.; Scatena, L. F.; Valley, N. A.; Wren, S. N.; Richmond, G. L., Model Behavior: Characterization of Hydroxyacetone at the Air-Water Interface Using Experimental and Computational Vibrational Sum Frequency Spectroscopy. *J Phys Chem A* **2018**, *122* (15), 3837-3849.
14. Morita, A.; Ishiyama, T., Recent progress in theoretical analysis of vibrational sum frequency generation spectroscopy. *Physical Chemistry Chemical Physics* **2008**, *10* (38), 5801-5816.
15. Valley, N. A.; Richmond, G. L., Computational Vibrational Sum Frequency Spectra of Formaldehyde and Hydroxymethanesulfonate at Aqueous Interfaces. *The Journal of Physical Chemistry C* **2016**, *120* (26), 14122-14129.
16. Barnes, T. J.; Prestidge, C. A., PEO-PPO-PEO Block Copolymers at the Emulsion Droplet-Water Interface. *Langmuir* **2000**, *16* (9), 4116-4121.
17. Tucker, I. M.; Petkov, J. T.; Jones, C.; Penfold, J.; Thomas, R. K.; Rogers, S. E.; Terry, A. E.; Heenan, R. K.; Grillo, I., Adsorption of Polymer-Surfactant Mixtures at the Oil-Water Interface. *Langmuir* **2012**, *28* (42), 14974-14982.
18. Lambert, A. G.; Davies, P. B.; Neivandt, D. J., Implementing the Theory of Sum Frequency Generation Vibrational Spectroscopy: A Tutorial Review. *Applied Spectroscopy Reviews* **2005**, *40* (2), 103-145.
19. Bain, C. D., Sum-frequency vibrational spectroscopy of the solid/liquid interface. *Journal of the Chemical Society, Faraday Transactions* **1995**, *91* (9), 1281-1296.
20. Shen, Y. R.; Ostroverkhov, V., Sum-Frequency Vibrational Spectroscopy on Water Interfaces: Polar Orientation of Water Molecules at Interfaces. *Chemical Reviews* **2006**, *106* (4), 1140-1154.
21. G. L. Richmond, Vibrational Spectroscopy of Molecules at Liquid Surfaces and Interfaces. *Anal. Chem.* **1997**, *69*, 536A-543A.
22. Bain, C.; Davies, P.; Ong, T.; Ward, R.; Brown, M., The Structure of Interfaces Probed by Sum-Frequency Spectroscopy. *Surface and Interface Analysis - SURF INTERFACE ANAL* **1991**, *17*, 529-530.
23. Fu, L.; Liu, J.; Yan, E. C. Y., Chiral Sum Frequency Generation Spectroscopy for Characterizing Protein Secondary Structures at Interfaces. *Journal of the American Chemical Society* **2011**, *133* (21), 8094-8097.

24. Wang, J.; Chen, X.; Clarke, M. L.; Chen, Z., Detection of chiral sum frequency generation vibrational spectra of proteins and peptides at interfaces in situ. *Proceedings of the National Academy of Sciences of the United States of America* **2005**, *102* (14), 4978.
25. Hauptert, L. M.; Simpson, G. J., Chirality in Nonlinear Optics. *Annual Review of Physical Chemistry* **2009**, *60* (1), 345-365.
26. Schabes, B. K.; Altman, R. M.; Richmond, G. L., Come Together: Molecular Details into the Synergistic Effects of Polymer–Surfactant Adsorption at the Oil/Water Interface. *The Journal of Physical Chemistry B* **2018**, *122* (36), 8582-8590.
27. Blower, P. G.; Ota, S. T.; Valley, N. A.; Wood, S. R.; Richmond, G. L., Sink or Surf: Atmospheric Implications for Succinic Acid at Aqueous Surfaces. *The Journal of Physical Chemistry A* **2013**, *117* (33), 7887-7903.
28. Bain, C. D.; Davies, P. B.; Ward, R. N., In-Situ Sum-Frequency Spectroscopy of Sodium Dodecyl Sulfate and Dodecanol Coadsorbed at a Hydrophobic Surface. *Langmuir* **1994**, *10* (7), 2060-2063.
29. Casson, B. D.; Bain, C. D., Phase Transitions in Mixed Monolayers of Sodium Dodecyl Sulfate and Dodecanol at the Air/Water Interface. *The Journal of Physical Chemistry B* **1998**, *102* (38), 7434-7441.
30. Ward, R. N.; Davies, P. B.; Bain, C. D., Coadsorption of Sodium Dodecyl Sulfate and Dodecanol at a Hydrophobic Surface. *The Journal of Physical Chemistry B* **1997**, *101* (9), 1594-1601.
31. Javadi, A.; Mucic, N.; Vollhardt, D.; Fainerman, V. B.; Miller, R., Effects of dodecanol on the adsorption kinetics of SDS at the water–hexane interface. *Journal of Colloid and Interface Science* **2010**, *351* (2), 537-541.
32. Joos, P.; Vollhardt, D.; Vermeulen, M., Interfacial tension of sodium dodecyl sulfate solutions at the hexane-water interface. *Langmuir* **1990**, *6* (2), 524-525.
33. Schabes, B. K.; Hopkins, E. J.; Richmond, G. L., Molecular Interactions Leading to the Coadsorption of Surfactant Dodecyltrimethylammonium Bromide and Poly(styrenesulfonate) at the Oil/Water Interface. *Langmuir* **2019**, *35* (22), 7268-7276.
34. Ciszewski, R. K.; Gordon, B. P.; Muller, B. N.; Richmond, G. L., Takes Two to Tango: Choreography of the Coadsorption of CTAB and Hexanol at the Oil-Water Interface. *J Phys Chem B* **2019**, *123* (40), 8519-8531.

35. Scatena, L. F.; Richmond, G. L., Aqueous solvation of charge at hydrophobic liquid surfaces. *Chemical Physics Letters* **2004**, *383* (5), 491-495.
36. Scatena, L. F.; Richmond, G. L., Isolated Molecular Ion Solvation at an Oil/Water Interface Investigated by Vibrational Sum-Frequency Spectroscopy. *The Journal of Physical Chemistry B* **2004**, *108* (33), 12518-12528.
37. Gragson, D. E.; McCarty, B. M.; Richmond, G. L., Ordering of Interfacial Water Molecules at the Charged Air/Water Interface Observed by Vibrational Sum Frequency Generation. *J. Am. Chem. Soc.* **1997**, *119*, 6144-6152.
38. Gragson, D. E.; Richmond, G. L., Investigations of the Structure and Hydrogen Bonding of Water Molecules at Liquid Surfaces by Vibrational Sum Frequency Spectroscopy. *The Journal of Physical Chemistry B* **1998**, *102* (20), 3847-3861.
39. Bonn, M.; Nagata, Y.; Backus, E., Molecular Structure and Dynamics of Water at the Water-Air Interface Studied with Surface-Specific Vibrational Spectroscopy. *Angewandte Reviews* **2015**, *54*, 5560-5576.
40. Morita, A.; Hynes, J. T., A Theoretical Analysis of the Sum Frequency Generation Spectrum of the Water Surface. II. Time-Dependent Approach. *The Journal of Physical Chemistry B* **2002**, *106* (3), 673-685.
41. Nihonyanagi, S.; Yamaguchi, S.; Tahara, T., Water Hydrogen Bond Structure near Highly Charged Interfaces Is Not Like Ice. *Journal of the American Chemical Society* **2010**, *132* (20), 6867-6869.
42. Sulpizi, M.; Salanne, M.; Sprik, M.; Gaigeot, M.-P., Vibrational Sum Frequency Generation Spectroscopy of the Water Liquid-Vapor Interface from Density Functional Theory-Based Molecular Dynamics Simulations. *The Journal of Physical Chemistry Letters* **2013**, *4* (1), 83-87.
43. Gragson, D. E.; Richmond, G. L., Probing the Structure of Water Molecules at an Oil/Water Interface in the Presence of a Charged Soluble Surfactant through Isotopic Dilution Studies. *J. Phys. Chem. B* **1998**, *102*, 569-576.
44. Pavelec, J.; DiGuseppi, D.; Zavlavsky, B. Y.; Uversky, V. N.; Schweitzer-Stenner, R., Perturbation of water structure by water-polymer interactions probed by FTIR and polarized Raman spectroscopy. *Journal of Molecular Liquids* **2019**, *275*, 463-473.
45. Aguiar, H. B. D., Vibrational Sum-Frequency Scattering Studies of Oil-in-Water Emulsions. *ÉCOLE POLYTECHNIQUE FÉDÉRALE DE LAUSANNE* **2011**, *Thesis No 5074*.

46. Altman, R. M.; Richmond, G. L., Coming to Order: Adsorption and Structure of Nonionic Polymer at the Oil/Water Interface as Influenced by Cationic and Anionic Surfactants. *Langmuir* **2020**, *36* (8), 1975-1984.
47. Tran, E.; Carpenter, A. P.; Richmond, G. L., Probing the Molecular Structure of Coadsorbed Polyethylenimine and Charged Surfactants at the Nanoemulsion Droplet Surface. *Langmuir* **2020**, *36* (31), 9081-9089.
48. Allen, H. C.; Raymond, E. A.; Richmond, G. L., Surface Structural Studies of Methanesulfonic Acid at Air /Aqueous Solution Interfaces Using Vibrational Sum Frequency Spectroscopy. *The Journal of Physical Chemistry A* **2001**, *105* (9), 1649-1655.
49. Raymond, E. A.; Tarbuck, T. L.; Richmond, G. L., Isotopic Dilution Studies of the Vapor/Water Interface as Investigated by Vibrational Sum-Frequency Spectroscopy. *The Journal of Physical Chemistry B* **2002**, *106* (11), 2817-2820.
50. Walker, D. S.; Richmond, G. L., Interfacial Depth Profiling of the Orientation and Bonding of Water Molecules across Liquid-Liquid Interfaces. *The Journal of Physical Chemistry C* **2008**, *112* (1), 201-209.
51. Fagiani, M. R.; Knorke, H.; Esser, T. K.; Heine, N.; Wolke, C. T.; Gewinner, S.; Schöllkopf, W.; Gaigeot, M.-P.; Spezia, R.; Johnson, M. A.; Asmis, K. R., Gas phase vibrational spectroscopy of the protonated water pentamer: the role of isomers and nuclear quantum effects. *Physical Chemistry Chemical Physics* **2016**, *18* (38), 26743-26754.
52. Carnegie, P. D.; McCoy, A. B.; Duncan, M. A., IR Spectroscopy and Theory of $\text{Cu}^+(\text{H}_2\text{O})\text{Ar}_2$ and $\text{Cu}^+(\text{D}_2\text{O})\text{Ar}_2$ in the O-H (O-D) Stretching Region: Fundamentals and Combination Bands. *The Journal of Physical Chemistry A* **2009**, *113* (17), 4849-4854.
53. Yeh, L. I.; Okumura, M.; Myers, J. D.; Price, J. M.; Lee, Y. T., Vibrational spectroscopy of the hydrated hydronium cluster ions $\text{H}_3\text{O}^+(\text{H}_2\text{O})_n$ ($n=1, 2, 3$). *The Journal of Chemical Physics* **1989**, *91* (12), 7319.
54. Jiang, J.-C.; Wang, Y.-S.; Chang, H.-C.; Lin, S. H.; Lee, Y. T.; Niedner-Schatteburg, G.; Chang, H.-C., Infrared Spectra of $\text{H}^+(\text{H}_2\text{O})_{5-8}$ Clusters: Evidence for Symmetric Proton Hydration. *Journal of the American Chemical Society* **2000**, *122* (7), 1398-1410.
55. Duong, C. H.; Gorlova, O.; Yang, N.; Kelleher, P. J.; Johnson, M. A.; McCoy, A. B.; Yu, Q.; Bowman, J. M., Disentangling the Complex Vibrational Spectrum of the Protonated Water Trimer, $\text{H}^+(\text{H}_2\text{O})_3$, with Two-Color IR-IR Photodissociation of the Bare Ion and Anharmonic VSCF/VCI Theory. *The Journal of Physical Chemistry Letters* **2017**, *8* (16), 3782-3789.

56. Morawietz, T.; Marsalek, O.; Pattenaude, S. R.; Streacker, L. M.; Ben-Amotz, D.; Markland, T. E., The Interplay of Structure and Dynamics in the Raman Spectrum of Liquid Water over the Full Frequency and Temperature Range. *The Journal of Physical Chemistry Letters* **2018**, *9* (4), 851-857.
57. Walrafen, G. E.; Pugh, E., Raman Combinations and Stretching Overtones from Water, Heavy Water, and NaCl in Water at Shifts to ca. 7000 cm⁻¹. *Journal of Solution Chemistry* **2004**, *33*, 81-97.
58. Doublerly, G. E.; Walters, R. S.; Cui, J.; Jordan, K. D.; Duncan, M. A., Infrared Spectroscopy of Small Protonated Water Clusters, H⁺(H₂O)_n (n = 2–5): Isomers, Argon Tagging, and Deuteration. *The Journal of Physical Chemistry A* **2010**, *114* (13), 4570-4579.
59. Ke, H.; Linde, C. v. d.; Lisy, J. M., Insights into Gas-Phase Structural Conformers of Hydrated Rubidium and Cesium Cations, M⁺(H₂O)_nAr (M = Rb, Cs; n = 3–5), Using Infrared Photodissociation Spectroscopy. *The Journal of Physical Chemistry A* **2014**, *118* (8), 1363-1373.
60. Bandyopadhyay, B.; Reishus, K. N.; Duncan, M. A., Infrared Spectroscopy of Solvation in Small Zn⁺(H₂O)_n Complexes. *The Journal of Physical Chemistry A* **2013**, *117* (33), 7794-7803.
61. Andersen, J.; Heimdal, J.; Wugt Larsen, R., The influence of large-amplitude librational motion on the hydrogen bond energy for alcohol-water complexes. *Phys Chem Chem Phys* **2015**, *17* (37), 23761-9.
62. Khatib, R.; Hasegawa, T.; Sulpizi, M.; Backus, E. H. G.; Bonn, M.; Nagata, Y., Molecular Dynamics Simulations of SFG Librational Modes Spectra of Water at the Water–Air Interface. *The Journal of Physical Chemistry C* **2016**, *120* (33), 18665-18673.
63. Tong, Y.; Kampftrath, T.; Campen, R. K., Experimentally probing the libration of interfacial water: the rotational potential of water is stiffer at the air/water interface than in bulk liquid. *Phys. Chem. Chem. Phys.* **2016**, *18*, 18424--18430.
64. Vinaykin, M.; Benderskii, A. V., Vibrational Sum-Frequency Spectrum of the Water Bend at the Air/Water Interface. *The Journal of Physical Chemistry Letters* **2012**, *3* (22), 3348-3352.
65. de Aguiar, H. B.; Strader, M. L.; de Beer, A. G. F.; Roke, S., Surface Structure of Sodium Dodecyl Sulfate Surfactant and Oil at the Oil-in-Water Droplet Liquid/Liquid Interface: A Manifestation of a Nonequilibrium Surface State. *The Journal of Physical Chemistry B* **2011**, *115* (12), 2970-2978.

66. Tyrode, E.; Hedberg, J., A Comparative Study of the CD and CH Stretching Spectral Regions of Typical Surfactants Systems Using VSFS: Orientation Analysis of the Terminal CH₃ and CD₃ Groups. *The Journal of Physical Chemistry C* **2012**, *116* (1), 1080-1091.
67. Walker, D. S.; Richmond, G. L., Understanding the Effects of Hydrogen Bonding at the Vapor-Water Interface: Vibrational Sum Frequency Spectroscopy of H₂O/HOD/D₂O Mixtures Studied Using Molecular Dynamics Simulations. *J. Phys. Chem. C* **2007**, *111*, 8321-8330.
68. Backus, E. H. G.; Garcia-Araez, N.; Bonn, M.; Bakker, H. J., On the Role of Fresnel Factors in Sum-Frequency Generation Spectroscopy of Metal–Water and Metal-Oxide–Water Interfaces. *The Journal of Physical Chemistry C* **2012**, *116* (44), 23351-23361.
69. Wang, L.; Nihonyanagi, S.; Inoue, K.-i.; Nishikawa, K.; Morita, A.; Ye, S.; Tahara, T., Effect of Frequency-Dependent Fresnel Factor on the Vibrational Sum Frequency Generation Spectra for Liquid/Solid Interfaces. *The Journal of Physical Chemistry C* **2019**, *123* (25), 15665-15673.
70. Hagen, W.; Tielens, A. G. G. M.; Greenberg, J. M., A laboratory study of the infrared spectra of interstellar ices. *Astron. Astrophys. Suppl. Ser.* **1983**, *51*, 389-416.
71. Lindner, J.; Vöhringer, P.; Pshenichnikov, M. S.; Cringus, D.; Wiersma, D. A.; Mostovoy, M., Vibrational relaxation of pure liquid water. *Chemical Physics Letters* **2006**, *421* (4), 329-333.
72. Liu, P.; Harder, E.; Berne, B. J., Hydrogen-Bond Dynamics in the Air–Water Interface. *The Journal of Physical Chemistry B* **2005**, *109* (7), 2949-2955.
73. Liang, C.; Jeon, J.; Cho, M., Ab initio Modeling of the Vibrational Sum-Frequency Generation Spectrum of Interfacial Water. *The Journal of Physical Chemistry Letters* **2019**, *10* (5), 1153-1158.
74. Ataka, K.-i.; Yotsuyanagi, T.; Osawa, M., Potential-Dependent Reorientation of Water Molecules at an Electrode/Electrolyte Interface Studied by Surface-Enhanced Infrared Absorption Spectroscopy. *J. Phys. Chem.* **1996**, *100*, 10664-10672.
75. McWilliams, L. E.; Valley, N. A.; Wren, S. N.; Richmond, G. L., A means to an interface: investigating monoethanolamine behavior at an aqueous surface. *Phys Chem Chem Phys* **2015**, *17* (33), 21458-69.
76. Morita, A.; Hynes, J. T., A theoretical analysis of the sum frequency generation spectrum of the water surface. *Chemical Physics* **2000**, *258*, 371-390.

77. Eisenthal, K. B., Liquid Interfaces Probed by Second-Harmonic and Sum-Frequency Spectroscopy. *Chem. Rev.* **1996**, *96*, 1343-1360.
78. Ohno, P. E.; Wang, H. F.; Geiger, F. M., Second-order spectral lineshapes from charged interfaces. *Nat Commun* **2017**, *8* (1), 1032.
79. Gopalakrishnan, S.; Liu, D.; Allen, H. C.; Kuo, M.; Shultz, M. J., Vibrational Spectroscopic Studies of Aqueous Interfaces: Salts, Acids, Bases, and Nanodrops. *Chemical Reviews* **2006**, *106* (4), 1155-1175.
80. Verma, P. K.; Kundu, A.; Poretz, M. S.; Dhoonmoon, C.; Chegwidan, O. S.; Londergan, C. H.; Cho, M., The Bend+Libration Combination Band Is an Intrinsic, Collective, and Strongly Solute-Dependent Reporter on the Hydrogen Bonding Network of Liquid Water. *The Journal of Physical Chemistry B* **2018**, *122* (9), 2587-2599.
81. Tomobe, K.; Yamamoto, E.; Kojić, D.; Sato, Y.; Yasui, M.; Yasuoka, K., Origin of the blueshift of water molecules at interfaces of hydrophilic cyclic compounds. *Sci Adv* **2017**, *3* (12), e1701400.
82. Miura, N.; Yamada, H.; Kitagawa, T.; Nishikawa, K.; Moon, A. In *Far infrared spectroscopy by portable synchrotron MIRRORCLE 20*, 2005 Joint 30th International Conference on Infrared and Millimeter Waves and 13th International Conference on Terahertz Electronics, 19-23 Sept. 2005; 2005; pp 16-17 vol. 1.
83. De Marco, L.; Carpenter, W.; Liu, H.; Biswas, R.; Bowman, J. M.; Tokmakoff, A., Differences in the Vibrational Dynamics of H₂O and D₂O: Observation of Symmetric and Antisymmetric Stretching Vibrations in Heavy Water. *The Journal of Physical Chemistry Letters* **2016**, *7* (10), 1769-1774.
84. Tyrode, E.; Liljeblad, J. F. D., Water Structure Next to Ordered and Disordered Hydrophobic Silane Monolayers: A Vibrational Sum Frequency Spectroscopy Study. *The Journal of Physical Chemistry C* **2013**, *117* (4), 1780-1790.
85. Chen, Y.; Jena, K. C.; Roke, S., From Hydrophobic to Hydrophilic: The Structure and Density of the Hexadecane Droplet/Alkanol/Water Interface. *The Journal of Physical Chemistry C* **2015**, *119* (31), 17725-17734.
86. Knock, M. M.; Bell, G. R.; Hill, E. K.; Turner, H. J.; Bain, C. D., Sum-Frequency Spectroscopy of Surfactant Monolayers at the Oil–Water Interface. *The Journal of Physical Chemistry B* **2003**, *107* (39), 10801-10814.

87. Rzeźnicka, I. I.; Sovago, M.; Backus, E. H. G.; Bonn, M.; Yamada, T.; Kobayashi, T.; Kawai, M., Duramycin-Induced Destabilization of a Phosphatidylethanolamine Monolayer at the Air–Water Interface Observed by Vibrational Sum-Frequency Generation Spectroscopy. *Langmuir* **2010**, *26* (20), 16055-16062.
88. Carpenter, W. B.; Fournier, J. A.; Biswas, R.; Voth, G. A.; Tokmakoff, A., Delocalization and stretch-bend mixing of the HOH bend in liquid water. *The Journal of Chemical Physics* **2017**, *147* (8), 084503.
89. Chieffo, L.; Shattuck, J.; Amsden, J. J.; Erramilli, S.; Ziegler, L. D., Ultrafast vibrational relaxation of liquid H₂O following librational combination band excitation. *Chemical Physics* **2007**, *341* (1), 71-80.
90. Kuo, C.-H.; Hochstrasser, R. M., Two dimensional infrared spectroscopy and relaxation of aqueous cyanide. *Chemical Physics* **2007**, *341* (1), 21-28.
91. McCoy, A. B.; Guasco, T. L.; Leavitt, C. M.; Olesen, S. G.; Johnson, M. A., Vibrational manifestations of strong non-Condon effects in the H₃O⁺·X₃ (X = Ar, N₂, CH₄, H₂O) complexes: A possible explanation for the intensity in the “association band” in the vibrational spectrum of water. *Physical Chemistry Chemical Physics* **2012**, *14* (20), 7205-7214.
92. McCoy, A. B., The Role of Electrical Anharmonicity in the Association Band in the Water Spectrum. *The Journal of Physical Chemistry B* **2014**, *118* (28), 8286-8294.
93. Duan, M.; Song, X.; Zhao, S.; Fang, S.; Wang, F.; Zhong, C.; Luo, Z., Layer-by-Layer Assembled Film of Asphaltenes/Polyacrylamide and Its Stability of Water-in-Oil Emulsions: A Combined Experimental and Simulation Study. *The Journal of Physical Chemistry C* **2017**, *121* (8), 4332-4342.
94. Kim, D.; Karns, K.; Tia, S. Q.; He, M.; Herr, A. E., Electrostatic Protein Immobilization Using Charged Polyacrylamide Gels and Cationic Detergent Microfluidic Western Blotting. *Analytical Chemistry* **2012**, *84* (5), 2533-2540.
95. Wang, Y.-Y.; Dai, Y.-H.; Zhang, L.; Luo, L.; Chu, Y.-P.; Zhao, S.; Li, M.-Z.; Wang, E.-J.; Yu, J.-Y., Hydrophobically Modified Associating Polyacrylamide Solutions: Relaxation Processes and Dilational Properties at the Oil–Water Interface. *Macromolecules* **2004**, *37* (8), 2930-2937.
96. Péron, N. M., R.; Varga, I.; Gilányi, T., Competitive adsorption of sodium dodecyl sulfate and polyethylene oxide at the air/water interface. *Journal of Colloid and Interface Science* **2007**, *313* (2), 389-397.

97. Sacchetti, C.; Motamedchaboki, K.; Magrini, A.; Palmieri, G.; Mattei, M.; Bernardini, S.; Rosato, N.; Bottini, N.; Bottini, M., Surface Polyethylene Glycol Conformation Influences the Protein Corona of Polyethylene Glycol-Modified Single-Walled Carbon Nanotubes: Potential Implications on Biological Performance. *ACS Nano* **2013**, *7* (3), 1974-1989.
98. Xu, Y.; Wu, J.; Dabros, T.; Hamza, H., Optimizing the Polyethylene Oxide and Polypropylene Oxide Contents in Diethylenetriamine-Based Surfactants for Destabilization of a Water-in-Oil Emulsion. *Energy & Fuels* **2005**, *19*, 916-921.
99. Akanno, A.; Guzman, E.; Fernandez-Pena, L.; Llamas, S.; Ortega, F.; Rubio, R. G., Equilibration of a Polycation-Anionic Surfactant Mixture at the Water/Vapor Interface. *Langmuir* **2018**, *34* (25), 7455-7464.
100. Beaman, D. K.; Robertson, E. J.; Richmond, G. L., From Head to Tail: Structure, Solvation, and Hydrogen Bonding of Carboxylate Surfactants at the Organic–Water Interface. *The Journal of Physical Chemistry C* **2011**, *115* (25), 12508-12516.
101. Bonincontro, A.; Michiotti, P.; La Mesa, C., Structure and Dynamics of Polymer–Surfactant Complexes: Dielectric Relaxation Studies. *The Journal of Physical Chemistry B* **2003**, *107* (51), 14164-14170.
102. Hensel, J. K.; Carpenter, A. P.; Ciszewski, R. K.; Schabes, B. K.; Kittredge, C. T.; Moore, F. G.; Richmond, G. L., Molecular characterization of water and surfactant AOT at nanoemulsion surfaces. *Proceedings of the National Academy of Sciences* **2017**, *114* (51), 13351-13356.
103. Mafi, A.; Hu, D.; Chou, K. C., Complex Formations between Surfactants and Polyelectrolytes of the Same Charge on a Water Surface. *Langmuir* **2017**, *33* (32), 7940-7946.
104. Mahdavi, S. Z.; Aalaie, J.; Miri, T.; Razavi, S. M. R.; Rahmani, M. R., Study of polyacrylamide-surfactant system on the water–oil interface properties and rheological properties for EOR. *Arabian Journal of Chemistry* **2017**, *10* (8), 1136-1146.
105. Robertson, E. J.; Beaman, D. K.; Richmond, G. L., Designated Drivers: The Differing Roles of Divalent Metal Ions in Surfactant Adsorption at the Oil–Water Interface. *Langmuir* **2013**, *29* (50), 15511-15520.
106. Chen, Z., Polyacrylamide and its derivatives for oil recovery. *Scholars' Mine - Doctoral Dissertations* **2016**, 2532.

107. Corredor, L.; Husein, M.; Maini, B., Impact of PAM-Grafted Nanoparticles on the Performance of Hydrolyzed Polyacrylamide Solutions for Heavy Oil Recovery at Different Salinities. *Industrial & Engineering Chemistry Research* **2019**, *58*.
108. Jongwon Jung, J. J. a. J. A., Characterization of a Polyacrylamide Solution Used for Remediation of Petroleum Contaminated Soils. *Materials* **2016**, *9* (16), 1-13.
109. Li, X. e.; Xu, Z.; Yin, H.; Feng, Y.; Quan, H., Comparative Studies on Enhanced Oil Recovery: Thermoviscosifying Polymer Versus Polyacrylamide. *Energy & Fuels* **2017**, *31* (3), 2479-2487.
110. Narasimha, V. R.; Rao, B. S.; Reddy, N. V., Dielectric Properties of Polyacrylamide Polymer Films. *Nuovo Cimento* **1992**, *14* (3), 253-260.
111. Smithson, R. L. W.; Evans, D. F.; Monfils, J. D.; Guire, P. E., Ultrathin film characterization: photoreactive polyacrylamide. *Colloids and Surfaces B: Biointerfaces* **1993**, *1* (6), 349-355.
112. Yang, T.-H., *Recent Applications of Polyacrylamide as Biomaterials*. 2008; Vol. 100.
113. Edler, K. J.; Wasbrough, M. J.; Holdaway, J. A.; O'Driscoll, B. M. D., Self-Assembled Films Formed at the Air–Water Interface from CTAB/SDS Mixtures with Water-Soluble Polymers. *Langmuir* **2009**, *25* (7), 4047-4055.
114. Li, X.; Prukop, S. L.; Biswal, S. L.; Verduzco, R., Surface Properties of Bottlebrush Polymer Thin Films. *Macromolecules* **2012**, *45* (17), 7118-7127.
115. Singh, A.; Edler, K. J.; Holdaway, J. A.; Wasbrough, M. J., Mesostructure in functionalised polymer-surfactant films. *ESRF* **2009**, *SC-2707*.
116. Yang, B.; Holdaway, J. A.; Edler, K. J., Robust Ordered Cubic Mesostructured Polymer/Silica Composite Films Grown at the Air/Water Interface. *Langmuir* **2013**, *29* (12), 4148-4158.
117. Chen, S.; Li, Y.; Guo, C.; Wang, J.; Ma, J.; Liang, X.; Yang, L.-R.; Liu, H.-Z., Temperature-Responsive Magnetite/PEO–PPO–PEO Block Copolymer Nanoparticles for Controlled Drug Targeting Delivery. *Langmuir* **2007**, *23* (25), 12669-12676.
118. Gil, E. S.; Hudson, S. M., Stimuli-reponsive polymers and their bioconjugates. *Progress in Polymer Science* **2004**, *29* (12), 1173-1222.
119. Hamidi, M.; Azadi, A.; Rafiei, P., Hydrogel nanoparticles in drug delivery. *Advanced Drug Delivery Reviews* **2008**, *60* (15), 1638-1649.

120. Saaka, Y.; Allen, D. T.; Luangwitchajaroen, Y.; Shao, Y.; Campbell, R. A.; Lorenz, C. D.; Lawrence, M. J., Towards optimised drug delivery: structure and composition of testosterone enanthate in sodium dodecyl sulfate monolayers. *Soft Matter* **2018**, *14* (16), 3135-3150.
121. Slaughter, B. V.; Khurshid, S. S.; Fisher, O. Z.; Khademhosseini, A.; Peppas, N. A., Hydrogels in regenerative medicine. *Advanced materials (Deerfield Beach, Fla.)* **2009**, *21* (32-33), 3307-3329.
122. Beaman, D. K.; Robertson, E. J.; Richmond, G. L., Metal Ions: Driving the Orderly Assembly of Polyelectrolytes at a Hydrophobic Surface. *Langmuir* **2012**, *28* (40), 14245-14253.
123. Bromberg, L.; Temchenko, M.; Colby, R. H., Interactions among Hydrophobically Modified Polyelectrolytes and Surfactants of the Same Charge. *Langmuir* **2000**, *16* (6), 2609-2614.
124. Comert, F.; Nguyen, D.; Rushanan, M.; Milas, P.; Xu, A. Y.; Dubin, P. L., Precipitate-Coacervate Transformation in Polyelectrolyte-Mixed Micelle Systems. *J Phys Chem B* **2017**, *121* (17), 4466-4473.
125. Ge, A.; Matsusaki, M.; Qiao, L.; Akashi, M.; Ye, S., Salt Effects on Surface Structures of Polyelectrolyte Multilayers (PEMs) Investigated by Vibrational Sum Frequency Generation (SFG) Spectroscopy. *Langmuir* **2016**, *32* (16), 3803-3810.
126. Iakovides, I. C.; Pantziaros, A. G.; Zagklis, D. P.; Paraskeva, C. A., Effect of electrolytes/polyelectrolytes on the removal of solids and organics from olive mill wastewater. *Journal of Chemical Technology & Biotechnology* **2016**, *91* (1), 204-211.
127. Kuznetsov, V. M.; Akentiev, A. V.; Noskov, B. A.; Toikka, A. M., Spread films of synthetic polyelectrolyte-surfactant complexes: Dilational viscoelasticity and effect on water evaporation. *Colloid Journal* **2009**, *71* (2), 202-207.
128. Ma, M.; Zhu, S., Grafting polyelectrolytes onto polyacrylamide for flocculation 1. Polymer synthesis and characterization. *Colloid and Polymer Science* **1999**, *277* (2), 115-122.
129. Plazzotta, B.; Fegyver, E.; Meszaros, R.; Pedersen, J. S., Anisometric Polyelectrolyte/Mixed Surfactant Nanoassemblies Formed by the Association of Poly(diallyldimethylammonium chloride) with Sodium Dodecyl Sulfate and Dodecyl Maltoside. *Langmuir* **2015**, *31* (26), 7242-50.
130. Valley, N. A.; Robertson, E. J.; Richmond, G. L., Twist and Turn: Effect of Stereoconfiguration on the Interfacial Assembly of Polyelectrolytes. *Langmuir* **2014**, *30* (47), 14226-14233.

131. Wang, Y. K., K.; Dubin, P.L.; Jaeger, W., Polyelectrolyte-Micelle Coacervation: Effects of Micelle Surface Charge Density, Polymer Molecular Weight, and Polymer/Surfactant Ratio. *Macromolecules* **2000**, *33*, 3324-3331.
132. Wilts, E. M.; Herzberger, J.; Long, T. E., Addressing water scarcity: cationic polyelectrolytes in water treatment and purification. *Polymer International* **2018**, *67* (7), 799-814.
133. Zhao, Z.; Shi, S.; Cao, H.; Li, Y.; Van der Bruggen, B., Layer-by-layer assembly of anion exchange membrane by electrodeposition of polyelectrolytes for improved antifouling performance. *Journal of Membrane Science* **2018**, *558*, 1-8.
134. Nyankson, E.; Olasehinde, O.; John, V. T.; Gupta, R. B., Surfactant-Loaded Halloysite Clay Nanotube Dispersants for Crude Oil Spill Remediation. *Industrial & Engineering Chemistry Research* **2015**, *54* (38), 9328-9341.
135. Shuang Cindy Cao, B. B., Jong Wan Hu and Jongwon Jung, Engineering Behavior and Characteristics of Water-Soluble Polymers: Implication on Soil Remediation and Enhanced Oil Recovery. *Sustainability* **2016**, *8* (3), 205.
136. Tewari, S.; Sirvaiya, A., *OIL SPILL REMEDIATION AND ITS REGULATION*. 2015; Vol. 1, p 2394-8299.
137. Dai, S. T., K. C., Isothermal titration calorimetry studies of binding interactions between polyethylene glycol and ionic surfactants. *The Journal of Physical Chemistry B* **2001**, *105* (44), 10759-10763.
138. Peng, L.; Chang, L.; Liu, X.; Lin, J.; Liu, H.; Han, B.; Wang, S., Antibacterial Property of a Polyethylene Glycol-Grafted Dental Material. *ACS Applied Materials & Interfaces* **2017**, *9* (21), 17688-17692.
139. Casford, M. T. L.; Davies, P. B.; Neivandt, D. J., Study of the Coadsorption of an Anionic Surfactant and an Uncharged Polymer at the Aqueous Solution/Hydrophobic Surface Interface by Sum Frequency Spectroscopy. *Langmuir* **2003**, *19* (18), 7386-7391.
140. R. Murugan, S. M., A. Bigotto, FTIR and Polarised Raman Spectra of Acrylamide and Polyacrylamide. *Journal of the Korean Physical Society* **1998**, *32* (4), 505~512.
141. Biggs, S.; Selb, J.; Candau, F., Effect of surfactant on the solution properties of hydrophobically modified polyacrylamide. *Langmuir* **1992**, *8* (3), 838-847.

142. Zana, R.; Binana-Limbele, W.; Kamenka, N.; Lindman, B., Ethyl(hydroxyethyl)cellulose-cationic surfactant interactions: electrical conductivity, self-diffusion and time-resolved fluorescence quenching investigations. *The Journal of Physical Chemistry* **1992**, *96* (13), 5461-5465.
143. Bu, H. T.; Yang, Z. Z.; Zhang, Y. X., Experimental characterization of fluorocarbon-modified polyacrylamide/surfactant aqueous solutions. *Chinese Journal of Polymer Science (English Edition)* **2003**, *21*, 297-302.
144. Ghoreishi, S. M.; Fox, G. A.; Bloor, D. M.; Holzwarth, J. F.; Wyn-Jones, E., EMF and Microcalorimetry Studies Associated with the Binding of the Cationic Surfactants to Neutral Polymers. *Langmuir* **1999**, *15* (17), 5474-5479.
145. Brackman, J.; Engberts, J., Interactions between water-soluble nonionic polymers and surfactant aggregates. *ACS Symposium Series: Structure and Flow in Surfactant Solutions* **1994**, *578*, 337-349.
146. Robertson, E. J.; Richmond, G. L., Molecular Insights in the Structure and Layered Assembly of Polyelectrolytes at the Oil/Water Interface. *The Journal of Physical Chemistry C* **2014**, *118* (49), 28331-28343.
147. Bae, K. H.; Lee, Y.; Park, T. G., Oil-Encapsulating PEO-PPO-PEO/PEG Shell Cross-Linked Nanocapsules for Target-Specific Delivery of Paclitaxel. *Biomacromolecules* **2007**, *8* (2), 650-656.
148. Kujawinski, E. B.; Kido Soule, M. C.; Valentine, D. L.; Boysen, A. K.; Longnecker, K.; Redmond, M. C., Fate of Dispersants Associated with the Deepwater Horizon Oil Spill. *Environmental Science & Technology* **2011**, *45* (4), 1298-1306.
149. Zhang, Z.; Avij, P.; Perkins, M. J.; Liyana-Arachchi, T. P.; Field, J. A.; Valsaraj, K. T.; Hung, F. R., Combined Experimental and Molecular Simulation Investigation of the Individual Effects of Corexit Surfactants on the Aerosolization of Oil Spill Matter. *The Journal of Physical Chemistry A* **2016**, *120* (30), 6048-6058.
150. Judson, R. S.; Martin, M. T.; Reif, D. M.; Houck, K. A.; Knudsen, T. B.; Rotroff, D. M.; Xia, M.; Sakamuru, S.; Huang, R.; Shinn, P.; Austin, C. P.; Kavlock, R. J.; Dix, D. J., Analysis of Eight Oil Spill Dispersants Using Rapid, In Vitro Tests for Endocrine and Other Biological Activity. *Environmental Science & Technology* **2010**, *44* (15), 5979-5985.
151. Owoseni, O.; Nyankson, E.; Zhang, Y.; Adams, S. J.; He, J.; McPherson, G. L.; Bose, A.; Gupta, R. B.; John, V. T., Release of Surfactant Cargo from Interfacially-Active Halloysite Clay Nanotubes for Oil Spill Remediation. *Langmuir* **2014**, *30* (45), 13533-13541.

152. Kirby, S. M.; Anna, S. L.; Walker, L. M., Sequential Adsorption of an Irreversibly Adsorbed Nonionic Surfactant and an Anionic Surfactant at an Oil/Aqueous Interface. *Langmuir* **2015**, *31* (14), 4063-4071.
153. Perrine, S. A.; Whitehead, T. L.; Hicks, R. P.; Szarek, J. L.; Krause, J. E.; Simmons, M. A., Solution Structures in SDS Micelles and Functional Activity at the Bullfrog Substance P Receptor of Ranatachykinin Peptides. *Journal of Medicinal Chemistry* **2000**, *43* (9), 1741-1753.
154. Liu, W.; Guo, R., Interaction between Morin and Sodium Dodecyl Sulfate (SDS) Micelles. *Journal of Agricultural and Food Chemistry* **2005**, *53* (8), 2890-2896.
155. Su, G.; Zhang, H.; Geng, T.; Yuan, S., Effect of SDS on Reducing the Viscosity of Heavy Oil: A Molecular Dynamics Study. *Energy & Fuels* **2019**, *33* (6), 4921-4930.
156. Zhong, D.-L.; Ding, K.; Yan, J.; Yang, C.; Sun, D.-J., Influence of Cyclopentane and SDS on Methane Separation from Coal Mine Gas by Hydrate Crystallization. *Energy & Fuels* **2013**, *27* (12), 7252-7258.
157. Tran, C.; Yasir, M.; Dutta, D.; Eswaramoorthy, N.; Suchowerska, N.; Willcox, M.; McKenzie, D. R., Single Step Plasma Process for Covalent Binding of Antimicrobial Peptides on Catheters To Suppress Bacterial Adhesion. *ACS Applied Bio Materials* **2019**, *2* (12), 5739-5748.
158. Posocco, P.; Perazzo, A.; Preziosi, V.; Laurini, E.; Pricl, S.; Guido, S., Interfacial tension of oil/water emulsions with mixed non-ionic surfactants: comparison between experiments and molecular simulations. *RSC Advances* **2016**, *6* (6), 4723-4729.
159. Vu, T. V.; Papavassiliou, D. V., Oil-water interfaces with surfactants: A systematic approach to determine coarse-grained model parameters. *The Journal of Chemical Physics* **2018**, *148* (20), 204704.
160. Maréchal, Y., Infrared spectra of water. I. Effect of temperature and of H/D isotopic dilution. *The Journal of Chemical Physics* **1991**, *95* (8), 5565-5573.
161. Bodis, P.; Larsen, O. F. A.; Woutersen, S., Vibrational Relaxation of the Bending Mode of HDO in Liquid D₂O. *The Journal of Physical Chemistry A* **2005**, *109* (24), 5303-5306.
162. Lu, R.; Gan, W.; Wu, B.-h.; Zhang, Z.; Guo, Y.; Wang, H.-f., C-H Stretching Vibrations of Methyl, Methylene and Methine Groups at the Vapor/Alcohol (n = 1-8) Interfaces. *The Journal of Physical Chemistry B* **2005**, *109* (29), 14118-14129.

163. Thavorn, J.; Hamon, J. J.; Kitiyanan, B.; Striolo, A.; Grady, B. P., Competitive Surfactant Adsorption of AOT and TWEEN 20 on Gold Measured Using a Quartz Crystal Microbalance with Dissipation. *Langmuir* **2014**, *30* (37), 11031-11039.